Multi-focus image fusion using local variability

Ias Sri Wahyuni

SPIM

Thèse de Doctorat

école doctorale **sciences pour l'ingénieur et microtechniques**

UNIVERSITÉ DE BOURGOGNE

Multi-focus image fusion using local variability

IAS SRI WAHYUNI

SPIM

Thèse de Doctorat

école doctorale **sciences pour l'ingénieur et microtechniques**

UNIVERSITÉ DE BOURGOGNE

N° | X | X | X |

THÈSE présentée par

IAS SRI WAHYUNI

pour obtenir le

Grade de Docteur de
l'Université de Bourgogne

Spécialité : **Instrumentation et informatique de l'image**

Multi-focus image fusion using local variability

Unité de Recherche :
Laboratoire Électronique, Informatique et Image

Soutenue publiquement le 28 Février 2018 devant le Jury composé de :

JOCELYN CHANUSSOT	Rapporteur	Professeur à Institut Polytechnique de Grenoble
CHRISTIAN GERMAIN	Rapporteur	Professeur à Bordeaux Sciences Agro
EL-BAY BOURENNANE	Examinateur	Professeur à l'Université Bourgogne Franche-Comté
FRÉDÉRIC COINTAULT	Examinateur	Maître de Conferences (HDR) à Agrosup Dijon
VIRGINIE FRESSE	Examinatrice	Maître de Conferences (HDR) à Université Jean Monnet Saint-Etienne
RACHID SABRE	Directeur de thèse	Maître de Conferences (HDR) à Agrosup Dijon

ACKNOWLEDGEMENTS

First and foremost I would like to express my sincerest gratitude to my supervisor, Dr. Rachid Sabre, who has supported me thoughout my thesis with his patience and knowledge and given me a lot of guidance during my doctoral study and research.

I would like to thank the referees: Professor Jocelyn Chanussot and Professor Christian Germain for their time, interest, and helpful comments. I would also like to thank to all the jury members for their time, insightful questions, review and constructive suggestions on my oral defense.

I gratefully acknowledge the funding sources that made my study possible: the Directorate General of Higher Education (DIKTI), Ministry of Research and Technology Republic of Indonesia and Gunadarma University, Indonesia.

I would like to thank Ecole Doctoral SPIM, the laboratory LE2I, and Agrosup Dijon that have provided the support and equipment I have needed to produce and complete my thesis.

I would also like to thank my parents and family for their support and counsel . I thank my friends for supporting me throughout all my studies. Finally, I would like to thank all people who made this thesis possible.

Ias Sri Wahyuni
Université Bourgogne Franche Comté
Dijon, February 2018

CONTENTS

I

Problems and Context

1

INTRODUCTION

Now a days numerous criteria that define the characteristics of a high quality image such as sharp, focus, be properly exposed, having correct color balance, and not having too much noise have been proposed and discussed extensively in image processing literature. Image quality has as much to do with user applications and requirements as it does with perceived visual quality in general. There are many techniques to get a good image or a high quality image. One of them is image fusion technique. Image fusion is an important research topic in many related areas such as computer vision, automatic object detection, remote sensing, image processing, robotics, and medical imaging [56]. The need for image fusion in current image processing systems is increasing mainly due to the increased number and variety of image acquisition techniques. Multi-focus image fusion is the process of combining relevant information from several images into one image. The final output image can provide more information than any of the single images. In Section 1.1, we detail the objectif behind this thesis along with its related research objectives. Next, we formulate these objectives into a problem statement and summarize the solution, provided by this thesis, in Section 1.2. Technical contributions for each application in Section 1.3.

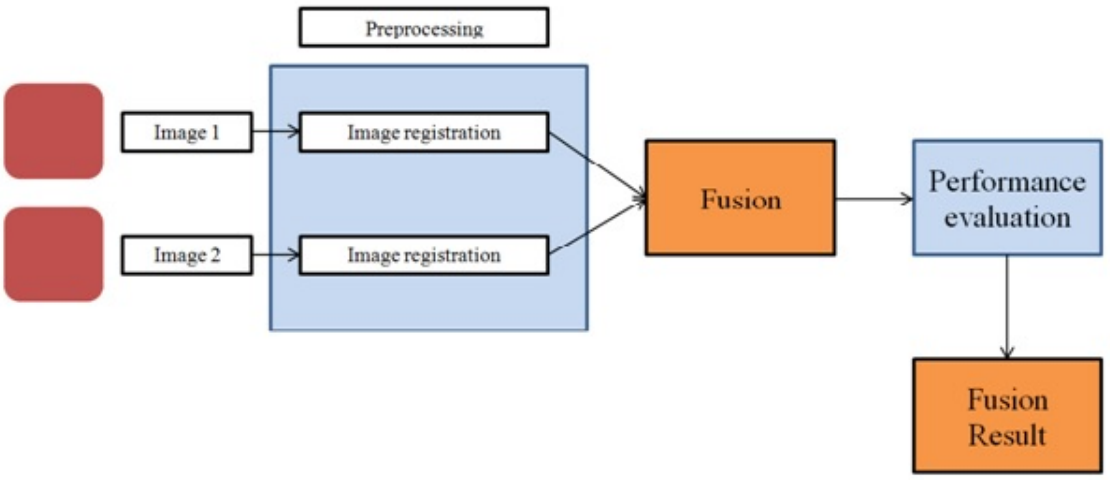

Figure 1.1: Image fusion process

1.1/ OBJECTIVES OF THE WORK

Image fusion, an important branch of data fusion, is the process of combining relevant information from two or more images into a single image where the resulting image will be more informative than any of the input images. The result image should be more suitable for visual perception and machine perception or computer processing. The goal of image fusion is to reduce uncertainty and minimize redundancy in the output as well maximize relevant information particular to an application or task [25]. The key of image fusion lies on choosing one reliable and effective fusion method to determine fusion coefficient [21]. Now a days, with rapid advancements in technology, it is now possible to obtain information from multi sources images to produce a high quality information from a set of images. However, due to the limited depth-of-focus of optical lenses in camera devices, it is often not possible to get an image with contains all relevant object 'in focus' so that one scene of image can be taken into set of images with different focus settings of every image. Besides solutions making use of specialized optics [14],[46] and computational imaging [6],[17], the way to solve this problem is multi-focus image fusion. Multi-focus image fusion is a branch of image fusion which integrate the source of multiple images with different focus settings at the same scene into a composite image that contain all object in focus. The objective of multi-focus image fusion is to produce an image that contains all relevant objects in focus by extracting and synthesizing the focused objects of source images. The basic assumption of the multi-focus image fusion is that the focused object is sharper than the unfocused object, and the sharpness is linked to some computed information measures. During the last decade, a number of sharpness measures for multi-focus image fusion have been proposed. The objective of the work is to develop multi-focus image fusion techniques that result high precision fused image which is more suitable for human or machine perception and for further image-processing tasks.

1.2/ PROBLEM STATEMENT

Up to now, many multi-focus images fusion methods have been developed. The simplest fusion method is to take average of the source images pixel by pixel but this method usually leads to undesirable effect such as reduction in the contrast of fused image [40]. Generally, the method of multi-focus image fusion can be classified into spatial domain and transform domain [86]. The technique for multi-focus image fusion that results high precision fused image usually are complicated and high consuming in time, which are of vital importance to fusion quality. In this thesis we develop some techniques of multi-focus image fusion that are low cost and not time consuming however it results a high quality fused image.

1.3/ AREA CONTRIBUTION

Motivated towards addressing the needs in the applications mentioned in Section 1.1, our research demonstrates the pixel-level image fusion technology towards a multi-focus imaging system. We list the following contributions:

- **Multi-focus image fusion algorithm:**

1. Wavelet decomposition in Laplacian Pyramid for image fusion.
2. Multi-focus image fusion using Dempster Shafer Theory based on local variability.
3. Pixel level multi-focus image fusion based on neighbor local variability.

- **Implementation and testing the methods:**
  We implement the multi-focus image fusion algorithms using MATLAB.

1.4/ DOCUMENT ORGANIZATIONS

After Introduction in the current chapter, the rest of the thesis is presented in the following outline.
Chapter 2 gives some introductions to image fusion, in context of our research.
Chapter 3 presents our results on Multi-focus image fusion using combination Laplacian pyramid (LP) and the discrete wavelet transform (DWT) image fusion. In this technique, we decompose the source images into different level of Laplacian pyramid and we fuse the images of each level using DWT method. The final fused image is obtained after reconstruction Laplacian pyramid.
Chapter 4 presents our results on multi-focus image fusion using Dempster Shafer Theory based on local variability. We perform multi-focus image fusion by exploiting pixels surrounding a pixel to be fused and using Dempster Shafer Theory to decide which pixel that we take as the final fused image.
Chapter 5 presents our results on pixel level multi-focus image fusion based on neighbor local variability. This method takes into consideration the information in the surrounding region of pixels. The wide of the neighborhood or the kernel size depends on the quality of the blurring area that is represented by the variance and the kernel size of the blurring filter, assumed that the blurring filter is Gaussian [48], [55]. The fusion is done by weighting each pixel by the exponential of the local variability.

2

STATE OF THE ART

2.1/ IMAGE FUSION

Initially, the main aim of fusion was restricted to human observation and decision making. The first form of fusion is pixel averaging; this method can be mathematically expressed as

$$f(x,y) = \frac{1}{N}\sum_{i=1}^{N} I_i(x,y), \tag{2.1}$$

where $f(x,y)$ is a fused image, $I_i(x,y)$'s are the source images, $i = 1,2,\cdots,N$. This method is simple, easily to implement, and low cost computationally, by using this method all information content within images are treated the same. However the result of this method is unsatisfactory because this method introduces artifacts, causes pattern cancellation and contrast reduction [53]. In mid-eighties, Burt and Adelson introduced a novel method of image fusion based on hierarchical image decomposition, namely Laplacian pyramid [25].

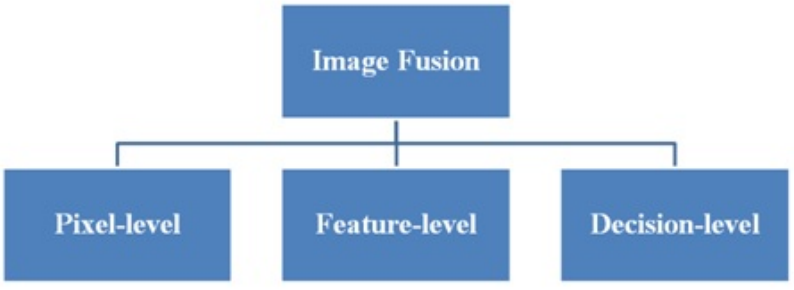

Figure 2.1: Image fusion categorization

Image fusion process can be divided into three categories [35]:

- **Pixel-level:** Pixel-level is the lowest level of the image fusion process. It deals directly with the pixels. The advantages of this level are to detect unwanted noise, to provide detail information, less complexity, and ease of implementation. However, these methods do not handle mis-registration and can cause blocking artefact.

- **Feature-level:** In feature level process, features are extracted from input images. Image is segmented in continuous regions and fuse them using fusion rule. Features of images are combined such as size, shape, contrast, pixel intensities, edge and texture.

- **Decision-level:** Decision level consists of merging information at a higher level of abstraction, combines the results from multiple algorithms to yield a final fused decision.

Input images are processed individually for information extraction. The obtained information is then combined applying decision rules to reinforce common interpretation.

Based on domain, image fusion methods can be categorized into two domains [86]:

- spatial domain
  Spatial domain deals directly with pixel to integrate relevant information. Some of the spatial domain techniques include Averaging, select maximum/minimum method, Bovey transforms, Intensity hue saturation method (IHS), High pass filtering method (HPF), Principal component analysis method (PCA). Drawbacks of Spatial domain fusion include spatial distortion in new fused image. This spatial distortion problem is solved in frequency domain.

- frequency domain
  In frequency domain, image is transformed in frequency domain and frequency coefficients are combined to get fused image. Some of the transform domain fusion techniques include discrete wavelet transform, stationary wavelet transform.

Based on the input data and the purpose [36], image fusion methods are classified as:

- Multi-view fusion
  Multi-view fusion combines the images taken by a sensor from different view- points at the same time. Multi-view fusion provides an image with higher resolution and also recovers the $3-D$ representation of a scene.

- Multi-temporal fusion
  Multi-temporal fusion integrates several images taken at various interval time to detect changes among them or to produce accurate images of objects.

- Multi-focus fusion
  It is impossible for the optical lens to capture all the objects at various focal lengths. Multi-focus image fusion integrates the images of various focal lengths from the imaging equipment into a single image of better quality.

- Multi-modal fusion
  Multi-modal fusion refers the combination of images from different sensors and is often referred as multi-sensor fusion which is widely used in applications like medical diagnosis, security, surveillance, etc.

2.2/ MULTI-FOCUS IMAGE FUSION

Multi-focus image fusion is a branch of image fusion. Optical lenses suffer from the problem of limited depth of field. So, it is almost impossible to obtain an image which is in focus everywhere. To solve this problem, several pictures of the same scene are taken by a camera with different focal lengths and the focused parts of the images are then fused to form a single image. The fused image becomes the focused image of the scene. The methods that we use in this work are called multi-focus image fusion. The general principle of these methods is from two images of the same scene with different focus to give an image with in focus everywhere (without blurring). There are numerous methods with different aims. In the following we study a large number of multi-focus methods, particularly the most recent methods and widely used.

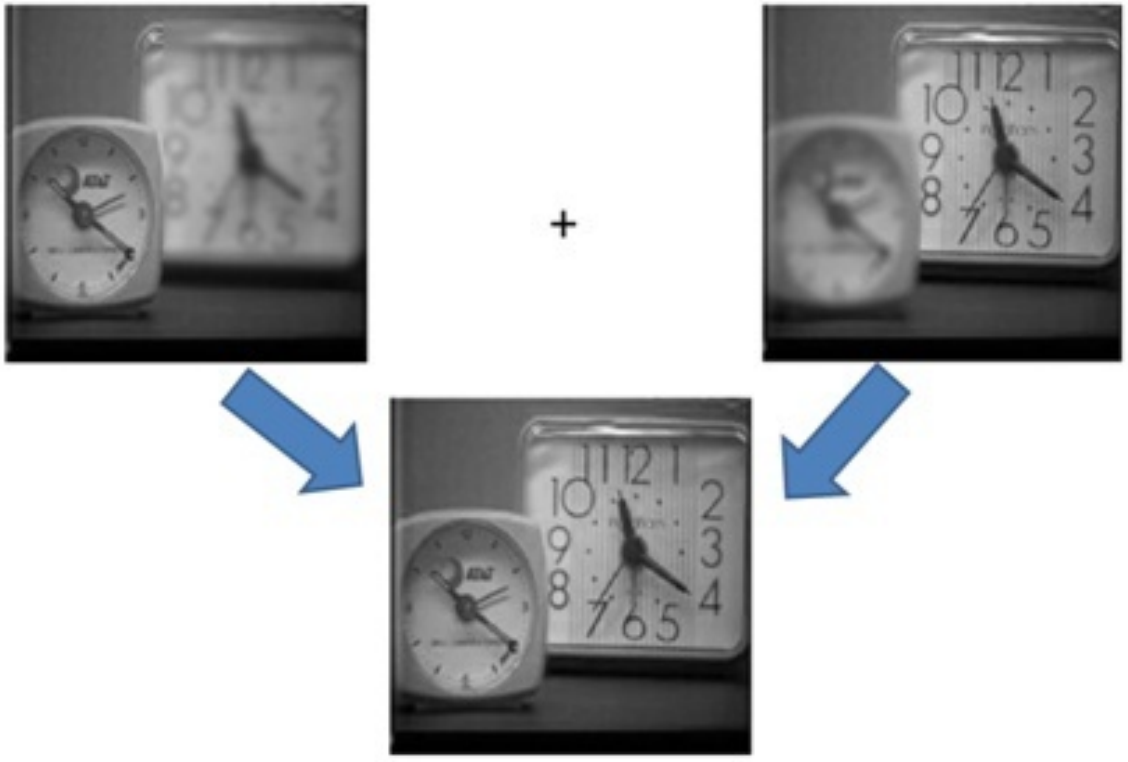

Figure 2.2: multifocus mage fusion

2.2.1/ LAPLACIAN PYRAMID IMAGE FUSION

The Laplacian pyramid was proposed by [4]. Each level of the Laplacian pyramid is recursively constructed from its lower level by applying the following four basic steps: blurring (low-pass filtering), sub-sampling (reduce size), interpolation (expand), and differencing (to subtract two images pixel by pixel). In the LP, the lowest level of the pyramid is constructed from the original image.

2.2.1.1/ Gaussian Pyramid Decomposition

We assume that the source image g_0 with size $R \times C$ columns is equal to the zero level of the pyramid, which on the bottom of the pyramid, and denoted the l-th level of Gaussian pyramid which can be obtained by the following equation

$$g_l = \text{REDUCE}\,(g_{l-1}) \tag{2.2}$$

which means, for level $l \in \{1, 2, \cdots, p\}$ and nodes (x, y) such that $0 < x < C_l$, $0 < y < R_l$

$$g_l(x, y) = \sum_{m=-2}^{2} \sum_{n=-2}^{2} w'(m, n) g_{l-1}(2x + m, 2y + n), \tag{2.3}$$

where $p + 1$ refers to the number of levels in the pyramid and $C_l \times R_l$ is the size of the lth level image. $w'(m, n)$ is generating kernel which is separable: $w'(m, n) = w(m)w(n)$ and satisfies some conditions, explained in Chapter 3.
Through recursive use equation (2.3) we can obtain $p + 1$ levels of Gaussian pyramid, $g_0, g_1, \cdots, g_p$. Due to the source image g_0 at the bottom level of Gaussian pyramid, so the total levels of Gaussian pyramid is $p + 1$, and the top level is g_p.
A function *EXPAND* is the reverse of function *REDUCE*. Its effect is to expand an $(M_1 + 1) \times (M_2 + 1)$ array into a $(2M_1 + 1) \times (2M_2 + 1)$ array by interpolating new node values between the given values. Thus, expand applied to array g_l of the *Gaussian pyramid* would yield an array $\hat{g}_l$ which is the same size as g_{l-1}.

$$\hat{g}_l = \text{EXPAND}(g_l), \tag{2.4}$$

by expand it means, for level $l \in \{1, 2, \cdots, p\}$ and pixel (x, y),

$$\hat{g}_l(x, y) = 4 \sum_{m=-2}^{2} \sum_{n=-2}^{2} w'(m, n) g_l\left(\frac{x - m}{2}, \frac{y - n}{2}\right), \tag{2.5}$$

where

$$g_l\left(\frac{x - m}{2}, \frac{y - n}{2}\right) = \begin{cases} g_l\left(\frac{x-m}{2}, \frac{y-n}{2}\right), & \text{if } \frac{x-m}{2}, \frac{y-n}{2} \text{ integer} \\ 0, & \text{otherwise.} \end{cases}$$

2.2.1.2/ Laplacian Pyramid Generation

The Laplacian pyramid is a sequence of error images $L_0, L_1, L_2, \cdots, L_p$. Each is the difference between two levels of the Gaussian pyramid

$$L_l = \begin{cases} g_l - \hat{g}_{l+1}, \text{if } l = 0, 1, 2, \cdots, p - 1 \\ g_p, \text{if } l = p. \end{cases} \tag{2.6}$$

The reconstruction of image from Laplacian pyramid is a inverse process of decomposition, and in the reverse direction, from the top to the bottom level with the definition as follows. The original image, g_0, can be obtained by expanding then summing all the levels of LP:

$$\begin{cases} g_p = L_p \\ g_l = L_l + \hat{g}_{l+1} \text{ if } l = p - 1, p - 2, \cdots, 0. \end{cases} \tag{2.7}$$

2.2.1.3/ IMAGE FUSION USING LAPLACIAN PYRAMID

Based on [1], Laplacian pyramid can be used for multi-focus image fusion. It started with two or more images focused on different distances and fuse them in a way that retains the sharp regions of each. Let L_A and L_B be Laplacian pyramids for the two original images. Thus, in focus image components can be selected pixel-by-pixel in the pyramid. A pyramid L_C is constructed for the composite image:

$$L_C(x,y) = \begin{cases} L_A(x,y), & \text{if } |L_A(x,y)| > |L_B(x,y)|, \\ L_B(x,y), & \text{otherwise.} \end{cases} \tag{2.8}$$

The composite image is then obtained simply by expanding and summing the levels of L_C's as in (2.7).
The other way of image fusion using Laplacian pyramid is by taking average for each level of Laplacian pyramid, as follows

$$L_C(x,y) = \frac{L_A(x,y) + L_B(x,y)}{2} \tag{2.9}$$

and again the composite image is obtained by expanding and summing L_C's .

2.2.2/ IMAGE FUSION USING DISCRETE WAVELET TRANSFORM (DWT)

The DWT is obtained by applying a low or high pass filter along the rows of the source image and down sampling, then applying a low or high pass filter along the columns of the intermediate image and down sampling once more. The low frequency subbands corresponds to approximation part, which contains average information of the entire image and is represented as (LL) subband. Whereas, the high frequency subbands are considered as detail parts containing the sharp information of images. The detail parts consist of three high frequency subbands (LH, HL and HH). DWT can be applied in performing image fusion. The coefficients of frequency subbands preserved the image transformation. Such coefficients that come from different images can be combined to get new coefficients where the information in the new or fused coefficients is also preserved. Once the coefficients are merged, the final fused image is obtained by performing the inverse discrete wavelet transform (IDWT).

2.2.3/ IMAGE FUSION USING PRINCIPAL COMPONENT ANALYSIS (PCA)

[50] proposed image fusion using PCA. PCA is a mathematical tool which transforms a number of correlated variables into a reduced number of uncorrelated variables. The fusion using PCA method is achieved by weighted average of images to be fused. The weights for each source image are obtained from the eigen vector corresponding to the largest eigenvalue of the covariance matrices of each source.
Let X be a d-dimensional random vector and assume it to have zero empirical mean. Orthonormal projection matrix V would be such that $Y = V^T X$ with the following constraints: covariance of Y, $\mathrm{cov}(Y)$ is a diagonal and the inverse of V is equal to its transpose

($V^{-1} = V^T$). Using matrix algebra

$$\begin{aligned} \text{cov}(Y) &= E(YY^T) \\ &= E\left((V^T X)(V^T X)^T\right) \\ &= E\left((V^T X)(X^T V)\right) \\ &= V^T E(XX^T)V \\ &= V^T \text{cov}(X)V. \end{aligned} \tag{2.10}$$

Multiplying both sides by V, it is obtained

$$V\text{cov}(Y) = VV^T \text{cov}(X)V = \text{cov}(X)V, \tag{2.11}$$

where

$$V = [V_1, V_2, \cdots, V_d] \text{ and } \text{cov}(Y) = \begin{bmatrix} \lambda_1 & 0 & \dots & 0 & 0 \\ 0 & \lambda_2 & \dots & 0 & 0 \\ \vdots & \vdots & \vdots & \ddots & \vdots \\ 0 & 0 & \dots & \lambda_{d-1} & 0 \\ 0 & 0 & \dots & 0 & \lambda_d \end{bmatrix}. \tag{2.12}$$

by substituting the equation (2.11) into the equation (2.12), we get

$$\begin{aligned} [\lambda_1 V_1, \lambda_2 V_2, \cdots, \lambda_d V_d] &= [\text{cov}(X)V_1, \text{cov}(X)V_2, \cdots, \text{cov}(X)V_d] \\ \lambda_i V &= \text{cov}(X)V_i, \end{aligned} \tag{2.13}$$

where $i = 1, 2, \cdots, d$ and V_i is eigenvector of $\text{cov}(X)$.

In the [50], let the source images (I_1 and I_2 images to be fused) be arranged in two-column vectors. The fused image is

$$I_f(x, y) = P_1 I_1(x, y) + P_2 I_2(x, y). \tag{2.14}$$

where P_1 and P_2 are eigenvalues corresponding to the larger eigenvalue of covariance matrix of X.

The disadvantage of this method is that this method is sensitive to the area to be sharpen and produces fusion result that may vary depending on the selected image subset. The PCA produces the fused image with high spatial quality. However, it causes spectral degradation in the fused image.

2.2.4/ IMAGE FUSION USING COMBINATION LAPLACIAN PYRAMID AND PCA (LP-PCA)

[66] uses combination of Laplacian Pyramid and PCA techniques. Different levels of an input image are created using Laplacian Pyramid method, the top level are fused using PCA algorithm given in [50] and for other levels are fused using traditional image fusion method (DWT-based method). Resultant fused image is reconstructed by the pyramid

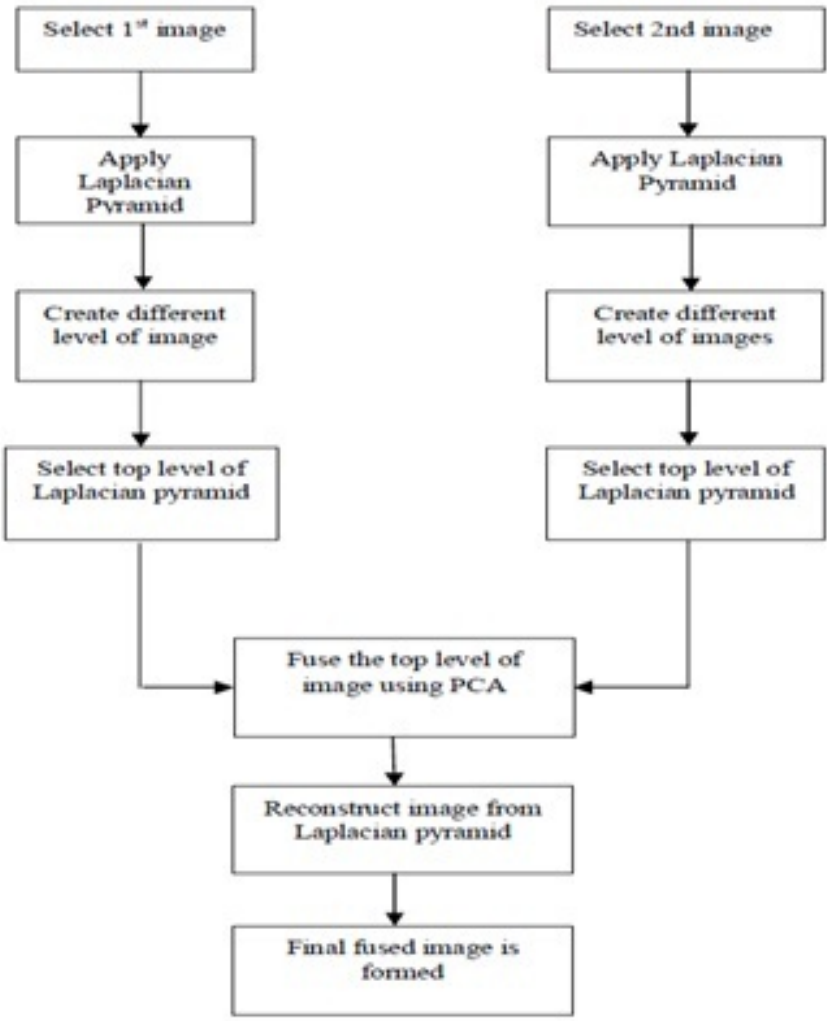

Figure 2.3: Flowchart of image fusion based using combination Laplacian pyramid and PCA method.

2.2.5/ MULTI-FOCUS IMAGE FUSION BASED ON VARIANCE CALCULATED IN DISCRETE COSINE TRANSFOM (DCT) DOMAIN (DCT+VAR)

[30] has explained that the image fusion is a technique to combine information from multiple images of the same scene in order to deliver only the useful information. The discrete cosine transformation based methods of image fusion are more suitable and time-saving in real time system. In this paper an efficient approach for fusion of multi-focus images based on variance calculated in DCT domain is presented. Two dimensional DCT transform of an $N \times N$ block of an image $I(x, y)$ is defined as

$$d(k,l) = \frac{2\alpha(k)\alpha(l)}{N} \sum_{x=0}^{N-1} \sum_{y=0}^{N-1} I(x,y) \cos\left[\frac{(2x+1)\pi k}{2N}\right] \cos\left[\frac{(2y+1)\pi k}{2N}\right], \tag{2.15}$$

where $k, l = 0, 1, \cdots, N-1$ and

$$\alpha(k) = \begin{cases} \frac{1}{\sqrt{2}}, \text{ if } k = 0, \\ 1, \text{ otherwise.} \end{cases}$$

The inverse DCT(IDCT) is also defined as

$$I(x,y) = \frac{2\alpha(k)\alpha(l)}{N} \sum_{k=0}^{N-1} \sum_{l=0}^{N-1} d(k,l) \cos\left[\frac{(2x+1)\pi k}{2N}\right] \cos\left[\frac{(2y+1)\pi k}{2N}\right], \tag{2.16}$$

where $m, n = 0, 1, \cdots, N-1$. The normalized transform coefficient $\hat{d}(k,l)$'s are defined as below:

$$\hat{d}(k,l) = \frac{d(k,l)}{N}. \tag{2.17}$$

Mean value, μ, and variance, σ^2, of $N \times N$ block in spatial domain are calculated as:

$$\mu = \frac{1}{N^2} \sum_{x=0}^{N-1} \sum_{y=0}^{N-1} I(x,y) \tag{2.18}$$

and

$$\sigma^2 = \frac{1}{N^2} \sum_{x=0}^{N-1} \sum_{y=0}^{N-1} I^2(x,y) - \mu^2. \tag{2.19}$$

It is known that mean value $\mu = \hat{d}(0,0)$ and for variance

$$\begin{aligned} \sum_{x=0}^{N-1} \sum_{y=0}^{N-1} I^2(x,y) &= \sum_{x=0}^{N-1} \sum_{y=0}^{N-1} I(x,y) I(x,y) \\ &= \sum_{x=0}^{N-1} \sum_{y=0}^{N-1} I(x,y) \left(\frac{2\alpha(k)\alpha(l)}{N} \sum_{k=0}^{N-1} \sum_{l=0}^{N-1} d(k,l) \cos\left[\frac{(2x+1)\pi k}{2N}\right] \cos\left[\frac{(2y+1)\pi k}{2N}\right] \right) \\ &= \sum_{k=0}^{N-1} \sum_{l=0}^{N-1} \frac{2\alpha(k)\alpha(l)}{N} d(k,l) \sum_{x=0}^{N-1} \sum_{y=0}^{N-1} I(x,y) \cos\left[\frac{(2x+1)\pi k}{2N}\right] \cos\left[\frac{(2y+1)\pi k}{2N}\right] \\ &= \sum_{k=0}^{N-1} \sum_{l=0}^{N-1} \frac{2\alpha(k)\alpha(l)}{N} d(k,l) \frac{N d(k,l)}{2\alpha(k)\alpha(l)} \\ &= \sum_{k=0}^{N-1} \sum_{l=0}^{N-1} d^2(k,l) \end{aligned} \tag{2.20}$$

then

$$\sigma^2 = \sum_{k=0}^{N-1} \sum_{l=0}^{N-1} \frac{d^2(k,l)}{N^2} - \hat{d}^2(0,0). \tag{2.21}$$

In multi-focus images, the focus area contains more information. This information corresponds to the high variance. Suppose there are two source image I_A and I_B. The steps of the fusion images with this method as follows.

Step 1: Divide the source images into 8×8 block partitions and compute the DCT coefficients for each block.

Step 2: Calculate the variances of the corresponding blocks from source images as the activity measures.

Step 3: Determine the block with high activity level as the appropriate one from source image either I_A or I_B.

It is observed that fusion performance is not good while using the algorithms with block size less than 8×8 and also the block size equivalent to the image size itself. It is also able to generates all in focus image but not generate desirable focused image.

2.2.6/ MULTI-FOCUS IMAGE FUSION USING A BILATERAL GRADIENT-BASED CRITERION (BILATERAL GRADIENT)

This method [64] assesses the local content (sharp) information of the input image by using a bilateral sharpness criterion that exploits both the strength and the phase coherence that are calculated using gradient information of the images. The statistics of image's gradient is used to propose a new sharpness measurement criterion, that utilize bilateral statistics of image's gradient information. Image structure can be measure effectively by using image gradients. Consider an image $I(x, y)$.

Step1: Calculate the gradient covariance matrix of a region within $M \times N$ local window

$$\begin{pmatrix} \sum_w I_x^2(x,y) & \sum_w I_x(x,y)I_y(x,y) \\ \sum_w I_x(x,y)I_y(x,y) & \sum_w I_y^2(x,y) \end{pmatrix}, \tag{2.22}$$

where $I_x(x, y)$ and $I_y(x, y)$ represents image's gradient at the row and column direction respectively.

Step2: Decompose the gradient covariance matrix as

$$C = VDV^T = \begin{pmatrix} v_1 & v_2 \end{pmatrix} \begin{pmatrix} \lambda_1 & 0 \\ 0 & \lambda_2 \end{pmatrix} \begin{pmatrix} v_1^T \\ v_2^T \end{pmatrix}. \tag{2.23}$$

where V denotes a 2x2 matrix whose column vectors are eigen vector v_1 and v_2 and D represents a 2x2 diagonal matrix whose diagonal elements are eigenvalues λ_1 and λ_2 ($\lambda_1 > \lambda_2$) that correspond to eigenvectors v_1 and v_2, respectively, and the superscript T represents the transpose. The geometrical structure at pixel in an image can be described by eigenvalues λ_1 and λ_2 the above gradient covariance matrix above.

Step3: Compute the first criterion, the strength of the image's gradient, which is defined as

$$A(x, y) = \lambda_1 - \lambda_2. \tag{2.24}$$

Step4: Calculate the second criterion, the phase coherence of image's gradient, that is

$$P(x, y) = -\cos\left(\theta(x, y) - \bar{\theta}(x, y)\right), \tag{2.25}$$

where $\theta(x, y)$ is the phase information at the position (x, y) determined by eigenvector v_1 associated with the largest eigenvalue λ_1. $\overline{\theta}(x, y)$ is the average of phases of the neighboring position.

Step5: From the first criterion and the second criterion, develop a bilateral sharpness criterion as

$$S_{BSC} = A^{\alpha}(x, y)P^{\beta}(x, y), \tag{2.26}$$

where α and β are two factors to adjust contributions of two criterions.

The proposed criterion is exploited to develop a weighted aggregation approach to perform image fusion.

2.2.7/ MULTI-FOCUS IMAGE FUSION USING THE ENERGY OF LAPLACIAN (EOL), MAJORITY FILTER AND GUIDED IMAGE FILTER (EOL)

The method is developed by [85]. The energy of Laplacian is evaluated in order to find the most suitable region from multi-focused images. It is then followed by the majority filters that offers a means spreading the focused regions to neighborhood and a guided image filter to overcome blocking artefacts. The EOL focus measure, M_p , of source images I_A and I_B as follows.

$$M_p = (I * L)^2 \tag{2.27}$$

where $*$ denotes the convolution, I is an input image, L is the Laplacian operator,

$$L = \frac{4}{1+\alpha}\begin{bmatrix} \frac{\alpha}{4} & \frac{1-\alpha}{4} & \frac{\alpha}{4} \\ \frac{1-\alpha}{4} & -1 & \frac{1-\alpha}{4} \\ \frac{\alpha}{4} & \frac{1-\alpha}{4} & \frac{\alpha}{4} \end{bmatrix}.$$

where α is a proportion coefficient. The majority filter is utilized in window-based consistency verification and is given by

$$D_b = \begin{cases} 1, \text{ if } D * W_l > \frac{l^2}{2}, \\ 0, \text{ otherwose,} \end{cases} \tag{2.28}$$

where D is the input decision map, D_b is the filtered decision map, W is a sliding $l \times l$ matrix in which all values are set to 1, the term $\frac{l^2}{2}$ can be obtained by the term $0.5 * W_l$.

image fusion.jpg image fusion.jpg

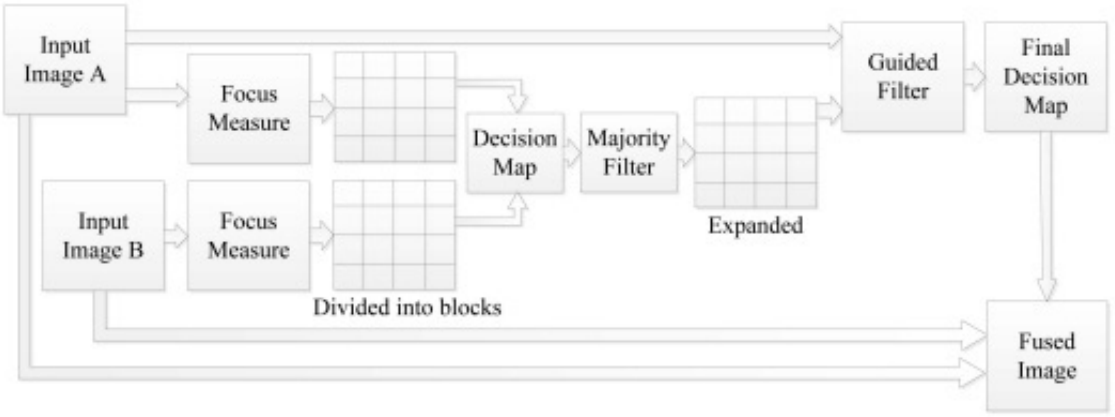

Figure 2.4: Schematic diagram for the multi-focus image fusion using energy of Laplacian and guided filter.

Step 1. Normalize the grayscale intensity of I_A and I_B so that they lie within the range $[0, 1]$.

Step 2. Calculate the EOL focus measure of the input images are computed to obtain M_p, respectively.

Step 3. Divide EOL, the matrix M_p, into non-overlapping 8×8 blocks. The focus measure of each block is the sum of the values in the block

$$M_b(m,n) = \sum M_p(x,y), \tag{2.29}$$

where x and y are pixel indexes, m and n are block indexed, and $M_b(m,n)$ is the focus bmeasure for each block.

Step 4. Compare the focus measures in the matrix M_b to obtain a binary decision map by

$$D(m,n) = \begin{cases} 1, \text{ if } M_b^1(m,n) > M_b^2(m,n), \\ 0, \text{ otherwise} \end{cases} \tag{2.30}$$

where $M_b^1(m,n)$ is focus measure for image I_A and $M_b^2(m,n)$ is focus measure for image I_B. The focused image area yield larger EOL metrices.

Step 5. To modify the majority filter, and the decision map D is filtered twice to obtain D_b by the modified majority filter. The decision map D_b is expanded to D_p by

$$D_p = D_b \otimes W_8 \tag{2.31}$$

where $\otimes$ denotes the Kronecker product and W_8 is an 8×8 matrix in which every value is 1.

Step 6. The fused result under the decision map D_p has block effect and lose edge and texture pinformation from input images, the guided filter is applied to optimize the decision map. To set the image I_A and decision map D_p to guidance image and the fimtering image of the guided filter respectively, and the filtered result is denoted by D_2. Therefore, the fused image is obtained from original input images using decision map D_2,

$$I_f(x,y) = D_2(x,y)I_1(x,y) + (1 - D_2)(x,y)I_2(x,y), \tag{2.32}$$

where I_f is the fused image.
Even though this image fusion algorithms provide significant results, there is still place for some improvement in spatial and spectral quality.

2.2.8/ MULTI-FOCUS METHOD BASED ON SALIENCY DETECTION AND MULTI-SCALE AVERAGE FILTERING (MSSF)

The method [5] exploits maximum surround saliency detection algorithm for the purpose fusion and designs an optimal weight construction based on visual saliency with simple normalization process, which is capable of identifying focused and defocused regions. The steps of this method as follow.

Step 1. Decompose the input image into approximation and detail layers by using an average filter.
Consider the input images $\{I_n(x,y)\}_{n=1}^{N}$ of the same size $N_1 \times N_2$ which are co-registered pixel by pixel. These N-images are decomposed into approximation layers and detail layers as follows:

$$B_n^{k+1} = B_n^k * A, \tag{2.33}$$

where $k = 0, 1, 2, \cdots, K$, K is the number of levels. A is an average filter..
B_n^{k+1} is the approximation layer of n-th source image at level $k+1$ which depend on its previous level approximation layer B_n^k. B_n^0 represents the n-th input image I_n. $*$ denote the convolution operation. The detail layer D_n^{k+1} at level $k+1$ are obtained by subtracting approximation layers B at previous level k from approximation layers B_n^{k+1} at present level $k+1$.

$$D_n^{k+1} = B_n^{k+1} - B_n^k. \tag{2.34}$$

Step 2. Calculate the saliencies of input image at different levels by using maximum surround saliency detection method.
The saliency map defined for an image I of width w and height h:

$$S(u,v) = \left\| I_\mu(u,v) - I_f(u,v) \right\| \tag{2.35}$$

where $I_\mu(u,v)$ is the mean of the sub image centered at pixel (u,v) is denoted as follows

$$\begin{aligned} I_\mu(u,v) &= \sum_{i=u-u_0}^{u+u_0} \sum_{j=v-v_0}^{v+v_0} I(i,j) \\ u_0 &= \min(u, w-u) \\ v_0 &= \min(v, h-v) \\ A &= (2u_0+1)(2v_0+1) \end{aligned}$$

I_f is the Gaussian blurred version of the image I.
This saliency detection process is denoted as follows:

$$S = MSSS(I). \tag{2.36}$$

The process of saliency extraction from the approximation layer B_n^{k+1} at level k is represented as follow

$$S_n^{k+1} = MSSS(B_n^k). \tag{2.37}$$

Step 3. Determine weight maps w_i^{k+1} from the extracted saliency maps by normalizing them as

$$w_i^{k+1} = \frac{S_i^{k+1}}{\sum_{i=1}^{n} S_i^{k+1}}. \tag{2.38}$$

Step 4. Multiply detail layers with the weight maps and fuse weighted detail layers to obtain a final detail layer $\overline{D}$

$$\overline{D} = \sum_{K=1}^{N} \sum_{k=1}^{N} w_n^k D_n^k. \tag{2.39}$$

Step 5. Compute the final approximation layer, $\overline{B}$,

$$\overline{B} = \frac{1}{NK} \sum_{k=1}^{N} \sum_{n=1}^{N} B_n^k. \tag{2.40}$$

Step 6. Sum final approximation and final detail layers to obtain the fused image F

$$F = \overline{B} + \overline{D}. \tag{2.41}$$

2.3/ DEMPSTER-SHAFER THEORY

Let Θ represent a finite set of hypotheses for a problem domain, called frame of discernment. Define a function m from 2^Θ to $[0, 1]$ where 2^Θ be the set of all subsets of Θ

$$2^\Theta = \{A | A \subseteq \Theta\}. \tag{2.42}$$

The function m is called a basic probability assignment whenever

$$m(\varnothing) = 0 \text{ and } \sum_{A \subseteq \Theta} m(A) = 1. \tag{2.43}$$

$m(A)$ is the measure of the belief that is committed exactly to A. According to [34], $m(A)$ is the degree of evidence supporting the claim that a specific element of Θ belongs to the set A, but not to any special subset of A. Each A of Θ such that $m(A) > 0$ are called the focal element of m. By applying the basic assignment function, several evidential functions can be created. A belief measure is given by the function $Bel : 2^\Theta \mapsto [0, 1]$:

$$Bel(A) = \sum_{B \subseteq A} m(B). \tag{2.44}$$

The plausibility measure $Pl : 2^\Theta \mapsto [0, 1]$ is defined by [62] as follows:

$$Pl(A) = \sum_{A \cap B \neq \varnothing} m(B) = 1 - Bel(\overline{A}). \tag{2.45}$$

where $\overline{A}$ is complement of A or doubt of A. Doubt of A is represented by $1 - Pl(A)$. $Bel(A)$ measures the degree of evidence that the element in question belongs to the set A as well as to the various special subsets of A. As stated in [80], the crucial aspect of DST

concerns the aggregation of evidence provided by different sources. If two mass function m_1 and m_2 are from distinct items of evidence such that $m_1(B) > 0$ and $m_2(C) > 0$ for some non disjoint subsets B and C of Θ, then they are combinable by means of Dempster's rule. DST [18], [19], [62] suggested a rule of combination that permits that the basic probability assignments are combined. The combination (joint mass) of two sets of masses m_1 and m_2 is defined as follows

$$m_1 \oplus m_2(\varnothing) = 0 \tag{2.46}$$

$$m_1 \oplus m_2(A) = \frac{\sum_{B \cap C = A} m_1(B) m_2(C)}{1 - \sum_{B \cap C = \varnothing} m_1(B) m_2(C)}. \tag{2.47}$$

The numerator represents the accumulated evidence for the sets B and C, which supports the hypothesis A and the denominator sum quantifies the amount of conflict between the two sets. Equation (2.47) can be written as

$$m_1 \oplus m_2(A) = \frac{\sum_{B \cap C = A} m_1(B) m_2(C)}{\sum_{B \cap C \neq \varnothing} m_1(B) m_2(C)}. \tag{2.48}$$

As stated in [10], having a zero mass on a subset A does not mean that his set is impossible, simply that we are not capable of assigning a level precisely to A, since we could have non-zero masses on subsets of A, which would lead us to $Bel(A) \neq 0$.

One of application of Dempster-Shafer theory is image fusion. The image fusion using Dempster-Shafer theory is described in chapter 4.

2.4/ CONCLUSION

The conclusion of this part is given as a table where we give advantages and disadvantages of the existing fusion methods mentioned above.

Method	Advantage	Disadvantage
Laplacian Pyramid image fusion [Adelson and Burt,1984]	It well preserves edge information in image.	Pyramid decomposition does not provide the information about sudden intensity changes in the spatial resolution of the input images. Adelson and Burt used maximum selection as a selection rule, it produces a high contrast in the fused image.
DWT method [Pajares, 2004]	The DWT fusion method may outperform pixel based approach fusion in terms of minimizing the spectral distortion. It also provide better signal to noise ratio than pixel based approach.	The final fused image have a less spatial resolution. This method is complex in fusion algorithm. Required good fusion technique for better result.

PCA method [Naidu, 2008]	PCA is a tools which transforms number of correlated variables into number of uncorrelated variables, this property can be used in image fusion. It is computationally efficient.	It may produce spectral degradation.
LP-PCA [Verma, 2016]	Multi level fusion where the image undergoes fusion twice using efficient fusion technique provide improved result	It is reduced in contrast
DCT+Var [Haghighat, 2010]	It is able to generate all-in focus images.	It are not generating desirable focused image. It is computationally expensive. It is observed that fusion performance is not good while using the algorithms with block size less than 8x8 and also the block size equivalent to the image size itself.
Bilateral Gradient [Tian, 2011]	It measures the local sharpness of image.	There are some erroneous selections of some blocks in the focus region due to noise or undesired effects
EOL [Zhan, 2015]	It well preserves the detail information without distortions.	It suffers from blur artifact. It is complicated and suffers from being time-consuming as it is based upon the spatial domain.
MSSF [Bavirisetti, 2016]	It produces fused images with more sharpened regions.	It does not well preserve the edge. It is difficult to determine the level of the multi-scale method.

Table 2.1: Comparison of different multi-focus image fusion methods

To overcome the drawbacks from the existing fusion methods mentioned above, we propose several methods. Our methods exploit local variability to evaluate the blur of each source image. The local variability on the blurred area is smaller than the local varibility on the focus area. With this idea, we develop methods to optimize the choice of pixel of the source images. So that we obtain the fused image without blocking artifact and spatial distortion.

II

CONTRIBUTION

3

Wavelet Decomposition in Laplacian Pyramid for Image Fusion

In this chapter we discuss about image fusion using Laplacian pyramid where we propose discrete wavelet transform as a selection rule.

3.1/ Introduction

Many methods exist to perform image fusion. In this work, we propose a new method for fusing images, where we use combination Laplacian pyramid (LP) and the discrete wavelet transform (DWT). As explained in chapter 2, the LP image fusion integrates multi-source information at the basic level and can provide more abundant, accurate and reliable detail information. The quality of fusion images by LP method is depending on the selection rule used. This selection rule allows to fuse the images at each level of the pyramid. Among the selections rules used in the literature we have: The averaging selection, maximum selection [1], saliency and match measure [7], and combination of averaging and maximum energy selection [70] . Recently, [83] used PCA as selection rule in LP image fusion.

As we know that LP is good in preserving the edge. The LP image fusion with average selection rule often leads to undesirable side effects such as reduced contrast. While the LP with maximum selection rule tends to have the higher contrast and brightness. On the other hand, As explained in the chapter 2, the wavelet fusion transformation (DWT) method allows the image decomposition in different kind of coefficients subbands see [24], [41], [54], [78]. [24] showed that the modulus maximum in DWT fusion gives better preservation of both edge features and component information of the object in new fused image preserving the detail image information . A maximum absolute value rule effectively retains the coefficients of in focus regions within the image.

In this thesis, we proposed a new method fusion using Laplacian Pyramid (LP) where the selection rule is DWT with modulus maximum for high frequency subbands and average for low frequency subband. Thus, DWT is used in each level of LP before undergoing fusion. This proposed method gives improvement significantly in the resulting fused image developed in section 3.4.

In the following section we give more details about Laplacian Pyramid and DWT methods.

3.2/ LAPLACIAN PYRAMID AND DISCRETE WAVELET TRANSFORM

3.2.1/ LAPLACIAN PYRAMID

The Laplacian pyramid was first introduced by [4] as a model for binocular fusion in human stereo vision, where the implementation used a Laplacian pyramid and a maximum selection rule at each point of the pyramid transform. Essentially, the procedure involves a set of band-pass copies of an image is referred to as the Laplacian pyramid due to its similarity to a Laplacian operator. Each level of the Laplacian pyramid is recursively constructed from its lower level by applying the following four basic steps: blurring (low-pass filtering), sub-sampling (reduce size), interpolation (expand), and differencing (to subtract two images pixel by pixel). In the LP, the lowest level of the pyramid is constructed from the original image.

3.2.1.1/ GAUSSIAN PYRAMID DECOMPOSITION

In this section we develop the pyramidal construction that we use in the sequel. For that we consider g_0 is the original image with size $R \times C$. This image becomes the bottom or zero level of pyramid. Pyramid level 1 contains image g_1, which is reduce and low-pass filtered version of g_0. Pyramid level 2, g_2, is obtained by applying reduce and low-pass filtered version of g_1. The level-to-level process is as followed

$$g_l = \text{REDUCE}\,(g_{l-1})$$

which means, for level $l \in \{1, 2, \cdots, p\}$ and nodes (x, y) such that $0 < x < C_l, 0 < y < R_l$.

$$g_l(x, y) = \sum_{m=-2}^{2} \sum_{n=-2}^{2} w'(m, n) g_{l-1}(2x + m, 2y + n) \tag{3.1}$$

we denote (3.1) as

$$g_l = w' * g_{l-1} \tag{3.2}$$

N refers to the number of levels in the pyramid and $R_l \times C_l$ is the size of the lth level image (it is known that the size of image in the lth level is half of the size of image in the l-1th level). $w'(m, n)$ is generating kernel which is separable: $w'(m, n) = w(m)w(n)$. The one dimensional $w(m)$, length 5, is

(i) Normalized: $\sum_{m=-2}^{2} w(m) = 1$

(ii) Symmetric: $w(-i) = w(i)$ for $i = 0, 1, 2$

(iii) Equal contribution: all nodes at a given level l must contribute the same total weight to nodes at the next higher level $l + 1$.

Let $w(0) = a$, $w(-1) = w(1) = b$, and $w(-2) = w(2) = c$. It is easy to show that the three constraints are satisfied [4] when

$$\begin{aligned} w(0) &= a, \\ w(-1) = w(1) &= \frac{1}{4}, \\ w(-2) = w(2) &= \frac{1}{4} - \frac{a}{2}. \end{aligned}$$

Hence, we can write that $w = \left[\frac{1}{4} - \frac{a}{2}; \frac{1}{4}; a; \frac{1}{4}; \frac{1}{4} - \frac{a}{2}\right]$.
Usually the value of a is $[0.3, 0.6]$ as in [4] and [31].
The sequence images $g_0, g_1, g_2, \cdots, g_p$ form a pyramid of $p + 1$ levels where the bottom level is g_0 and the top level is g_p. The image at a higher level l is reduced a half both in resolution and size of the image at the predecessor level $l - 1$.
Iterative pyramid generation is equivalent to convolving the image g_0 with a set of 'equivalent weighting functions' h_l defined as follows:

$$g_l = h_l \oplus g_0 \tag{3.3}$$

Thus,

$$\begin{aligned} g_1 &= w' * g_0 \triangleq h_1 \oplus g_0 \\ g_2 &= w' * g_1 = w' * (w' * g_0) \triangleq h_2 \oplus g_0 \\ g_3 &= w' * g_2 = w' * (w' * (w' * g_0)) \triangleq h_3 \oplus g_0 \\ g_4 &= w' * g_3 = w' * (w' * (w' * (w' * g_0))) \triangleq h_4 \oplus g_0 \\ &\vdots \\ g_l &= w' * g_{l-1} = \underbrace{w' * (w' * (\cdots (w' * (w'}_{l\ w'\text{'s}} * g_0)) \cdots)) \triangleq h_l \oplus g_0 \end{aligned}$$

So that, we can write

$$g_l(x, y) = \sum_{m=-N_l}^{N_l} \sum_{n=-N_l}^{N_l} h_l(m, n) g_0(x2^l + m, y2^l + n) \tag{3.4}$$

The value of N_l doubles from one level to next level.
To clarify (3.4), we develop h_l given in (3.4) from (3.1) only for $l = 2$.

$$g_1(x, y) = \sum_{m'=-2}^{2} \sum_{n'=-2}^{2} w'(m', n') g_0(2x + m', 2y + n') \tag{3.5}$$

$$\begin{aligned} g_2(x, y) &= \sum_{m''=-2}^{2} \sum_{n''=-2}^{2} w'(m'', n'') g_1(2x + m'', 2y + n'') \\ &= \sum_{n''=-2}^{2} \sum_{n''=-2}^{2} w'(m'', n'') \sum_{m'=-2}^{2} \sum_{n'=-2}^{2} w'(m', n') g_0\left(2(2x + m'') + m', 2(2y + n'') + n'\right) \\ &= \sum_{n''=-2}^{2} \sum_{n''=-2}^{2} w'(m'', n'') \sum_{m'=-2}^{2} \sum_{n'=-2}^{2} w'(m', n') g_0\left(2^2 x + 2m'' + m', 2^2 y + 2n'' + n'\right) \end{aligned} \tag{3.6}$$

Let $m = 2m'' + m'$ and $n = 2n'' + n'$, we have $m' = m - 2m''$ and $n' = n - 2n''$, by substituting m' and n' in (3.6), we get

$$\begin{aligned}
g_2(x,y) &= \sum_{n''=-2}^{2}\sum_{n''=-2}^{2} w'(m'',n'') \sum_{m'=-2}^{2}\sum_{n'=-2}^{2} w'(m',n') g_0\left(2^2x + 2m'' + m', 2^2y + 2n'' + n'\right) \\
&= \sum_{n''=-2}^{2}\sum_{n''=-2}^{2} w'(m'',n'') \sum_{m=2m''-2}^{2m''+2}\sum_{n=2n''-2}^{2n''+2} w'(m-2m'', n-2n'') g_0\left(2^2x + m, 2^2y + n\right) \\
&= \sum_{n''=-2}^{2}\sum_{n''=-2}^{2} w'(m'',n'') \sum_{m=-6}^{6}\sum_{n=-6}^{6} \chi_{[2m''-2,2m''+2]\times[2n''-2,2n''+2]}(m,n) \\
&\times w'(m-2m'', n-2n'') g_0\left(2^2x + m, 2^2y + n\right) \\
&= \sum_{m=-6}^{6}\sum_{n=-6}^{6}\sum_{n''=-2}^{2}\sum_{n''=-2}^{2} w'(m'',n'') \chi_{[2m''-2,2m''+2]\times[2n''-2,2n''+2]}(m,n) \\
&\times w'(m-2m'', n-2n'') g_0\left(2^2x + m, 2^2y + n\right) \qquad (3.7)
\end{aligned}$$

where

$$\chi_(m,n) = \begin{cases} 1, & \text{if } (m,n) \in [2m''-2, 2m''+2] \times [2n''-2, 2n''+2] \\ 0, & \text{otherwise} \end{cases} .$$

From (3.7), we denote

$$h_2(m,n) = \sum_{m''=-2}^{2}\sum_{n''=-2}^{2} w'(m'',n'') \chi_{[2m''-2,2m''+2]\times[2n''-2,2n''+2]}(m,n) w'(m-2m'', n-2n'') \qquad (3.8)$$

To calculate $g_2(x,y)$,

$$g_2(x,y) = \sum_{m=-6}^{6}\sum_{n=-6}^{6} h_2(m,n) g_0(x2^2 + m, y2^2 + n)$$

so we have the formula (3.4), with $N_2 = 6$.
[4] has shown that the case where $a = 0.4$, the shape of equivalent functions closely resemble to Gaussian probability density function. So the sequence image $g_0, g_1, g_2, \cdots, g_N$ is called *Gaussian pyramid*.
On the other hand, the function *EXPAND* is defined as the reverse of function *REDUCE*. Its effect is to expand an $(M_1 + 1) \times (M_2 + 1)$ array into a $(2M_1 + 1) \times (2M_2 + 1)$ array by interpolating new node values between the given values. Thus, expand applied to array g_l of the *Gaussian pyramid* would yield an array $g_{l,1}$ which is the same size as g_{l-1}.

$$g_{l,0} = g_l \quad \text{and } g_{l,k} = \text{EXPAND}(g_l, k-1).$$

By expanding it means, for level $l \in \{1, 2, \cdots, p\}$ and $0 \le k$ and nodes $(x,y), 0 < x < C_{l-k}, 0 < y < R_{l-k}$

$$g_{l,k}(x,y) = 4 \sum_{m=-2}^{2}\sum_{n=-2}^{2} w'(m,n) g_{l,k-1}\left(\frac{x-m}{2}, \frac{y-n}{2}\right), \qquad (3.9)$$

where

$$g_{l,k-1}\left(\frac{x-m}{2},\frac{y-n}{2}\right)=\begin{cases}g_{l,k-1}\left(\frac{x-m}{2},\frac{y-n}{2}\right), & \text{if } \frac{x-m}{2},\frac{y-n}{2} \text{ integer,}\\ 0, & \text{otherwise.}\end{cases}$$

In the following we expand g_l for one time ($k = 1$). We denote

$$\hat{g}_l = g_{l,1}(x,y) = 4\sum_{m=-2}^{2}\sum_{n=-2}^{2} w'(m,n)g_l\left(\frac{x-m}{2},\frac{y-n}{2}\right), \tag{3.10}$$

3.2.1.2/ LAPLACIAN PYRAMID GENERATION

The Laplacian pyramid is a sequence of error images $L_0, L_1, L_2, \cdots, L_p$. Each is the difference between two levels of the Gaussian pyramid

$$L_l = \begin{cases} g_l - \hat{g}_{l+1}, & \text{for } l = 0,1,2,\cdots,p-1,\\ g_p. \end{cases} \tag{3.11}$$

The original image, g_0, can be obtained by expanding then summing all the levels of LP:

$$g_l = L_l + \hat{g}_{l+1} \quad \text{for } l = p-1, p-2, \cdots, 0, \text{ and as we know } g_p = L_p. \tag{3.12}$$

3.2.2/ LAPLACIAN PYRAMID IMAGE FUSION

Laplacian pyramid (LP) is used as image fusion technique in [1] where the key step is how to choose selection rule (SR) in merging the images at each level of LP. This selection is important in order to obtain the best quality of the fused image. Denote the fused image using LP method with selection rule SR as follows: F = LP(SR),

For example: Let L_A and L_B be Laplacian pyramids as defined in Chapter 2 for the two original image A and image B respectively. $F = LP(\text{Average})$ means that we use average method as selection rule in merging images at each level of LP as follows:

$$L_C(x,y) = \frac{L_A(x,y) + L_B(x,y)}{2} \tag{3.13}$$

The final composite image, F, is achieved by using the EXPAND function on L_C's as in (3.11).

3.2.3/ DISCRETE WAVELET TRANSFORM

Discrete Wavelet Transform (DWT) that we use in this thesis is based on Haar wavelet transform. The DWT fusion method allows the image decomposition in different kind of coefficient subbands. In decomposition levels, the DWT gives directional information decomposition levels and contains unique information at different resolutions [43]. The DWT separately filters and downsamples images in the horizontal direction and vertical directions. This produces four coefficient subbands at each scale. As the development of the wavelet theory, DWT has been paid much attention due to its good time-frequency characteristics.

As presented in [54], consider an image $I(x,y)$ of size $R \times C$ and denote the horizontal frequency first by using $1-D$ low pass filter $L = \frac{1}{\sqrt{2}}[1 \quad 1]$ and highpass filter $H = \frac{1}{\sqrt{2}}[1 \quad -1]$ produces the coefficient matrices and and then followed the vertical frequency second by using lowpass filter L and highpass filter H to each column in $I_L(x,y)$ and $I_H(x,y)$, it produces produces four subimages, $I_{LL}(x,y)$, $I_{LH}(x,y)$, $I_{HL}(x,y)$, and $I_{HH}(x,y)$ for one level decomposition. By recursively applying the same scheme to the low-low subband a multiresolution decomposition can be achieved. The algorithm can be expressed as follows: $l(i)$ the analysis lowpass coefficients of a specific wavelet basis, $i = 0,1,2,\cdots N_l - 1$, where N_l is the support length of the filter L. $h(j)$ the analysis lowpass coefficients of a specific wavelet basis, $j = 0,1,2,\cdots N_h - 1$, where N_h is the support length of the filter H. Then,

$$I_L(x,y) = \frac{1}{N_l}\sum_{i=0}^{N_l-1} l(i).I\left((2x+i)\text{mod } R, y\right), \tag{3.14}$$

where $a = b \bmod R$, the modulo, is an operation to find the remainder a of Euclidian division of b by R.

$$I_H(x,y) = \frac{1}{N_h}\sum_{j=0}^{N_h-1} h(j).I\left((2x+j)\text{mod } R, y\right) \tag{3.15}$$

for $x = 0,1,2,\cdots,\frac{R}{2}-1$ and $y = 0,1,2,\cdots,C-1$.

$$I_{LL}(x,y) = \frac{1}{N_l}\sum_{i=0}^{N_l-1} l(i).I_L\left(x,(2y+i)\text{mod } C\right) \tag{3.16}$$

$$I_{LH}(x,y) = \frac{1}{N_h}\sum_{i=0}^{N_h-1} h(j).I_L\left(x,(2y+j)\text{mod } C\right) \tag{3.17}$$

$$I_{HL}(x,y) = \frac{1}{N_l}\sum_{i=0}^{N_l-1} l(i).I_H\left(x,(2y+i)\text{mod } C\right) \tag{3.18}$$

$$I_{HH}(x,y) = \frac{1}{N_h}\sum_{i=0}^{N_h-1} h(i).I_H\left(x,(2y+j)\text{mod } C\right) \tag{3.19}$$

for $x = 0,1,2,\cdots,\frac{R}{2}-1$ and $y = 0,1,2,\cdots,\frac{C}{2}-1$. The algorithm can iterate on the subimage $I_{LL}(x,y)$ to obtain four coefficient matrices in the next decomposition level and so on.

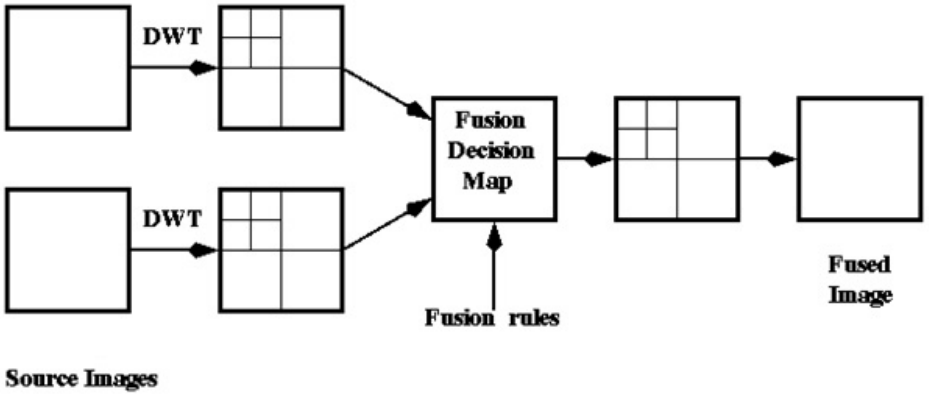

Figure 3.1: DWT image fusion

Fig. 3.1 shows 2-level discrete wavelet decomposition and fusion image using wavelet transform. In the DWT, only coefficients of the same level and representation can be fused. The fused coefficient can be achieved by various strategies. The process of fused coefficients in this work is described in Section 3.3. After the new fused multiscale coefficients then by using Inverse Discrete Wavelet Transform (IDWT) as described in [54], the final fused image is obtained.

3.3/ THE PROPOSED METHOD

The image fusion methods keep progressing to get the better result of fused image. A Laplacian pyramid can be used for compaction of images. To decrease the large number of unwanted information from Gaussian pyramid, it is required to calculate the difference between the adjoining two pictures (images) and receive the bandpass filtered pictures, this set/process is the Laplacian Pyramid (LP) technique. LP takes the advantage of integrating the details at each Laplacian level by retaining large amount of information as well as reducing maximum redundant details from images. On the other hand, The DWT is a mechanism that differentiates data into different frequency components, and then analyzes each component with constancy related to its scale. This hierarchical structure makes very useful because it contains the local information and the global information of images [49]. The DWT technique gives detail information of source images into one fused image. The main benefit of DWT is that it gives results with low cost. The DWT gives fine resolution in time as well as frequency. The other benefits of DWT are edge detection, energy compaction and multi resolution analysis.

In this work, we fuse images using combination LP and DWT fusion method where we decompose each source image by LP at first and then apply wavelet decomposition as selection rule at each level of LP. Indeed, we fuse LP images in wavelet decomposition by merging the DWT coefficient of every corresponding frequency subband. We used a maximum absolute value of high frequency bands (HH, HL, LH) that effectively retains the coefficients of in focus regions, and we take average of the coefficients bands LL in contrary of the work [24] where they use maximum absolute for all coefficients. Because wavelet transform theory shows that the high-frequency coefficients of a clear image are much larger than those of a blurred image. But the low-frequency coefficients are roughly equal [13].

The steps of image fusion in this work as follows. Suppose there are two original source images, image A and image B, with different focus to be fused:

Step 1: To perform Laplacian pyramid decomposition for each source image;

Step 2: To perform discrete wavelet decomposition to every level of Laplacian pyramid for each image in different kinds of coefficient;

Step 3: To merge an appropriate coefficient of the corresponding subband to obtain new coefficients by using maximum absolute for high frequency bands and taking average for low frequency subband. The fused wavelet image is achieved through the inverse discrete wavelete transform (IDWT);

Step 4: The final fused image is obtained by performing LP reconstruction using EXPAND function and summing as in (3.6) on the all level fused wavelet images.

The process of pyramid image fusion can be seen in Fig. 3.2 which the fusion LP for four levels is obtained by applying DWT image fusion. It can be extended for more than two source images.

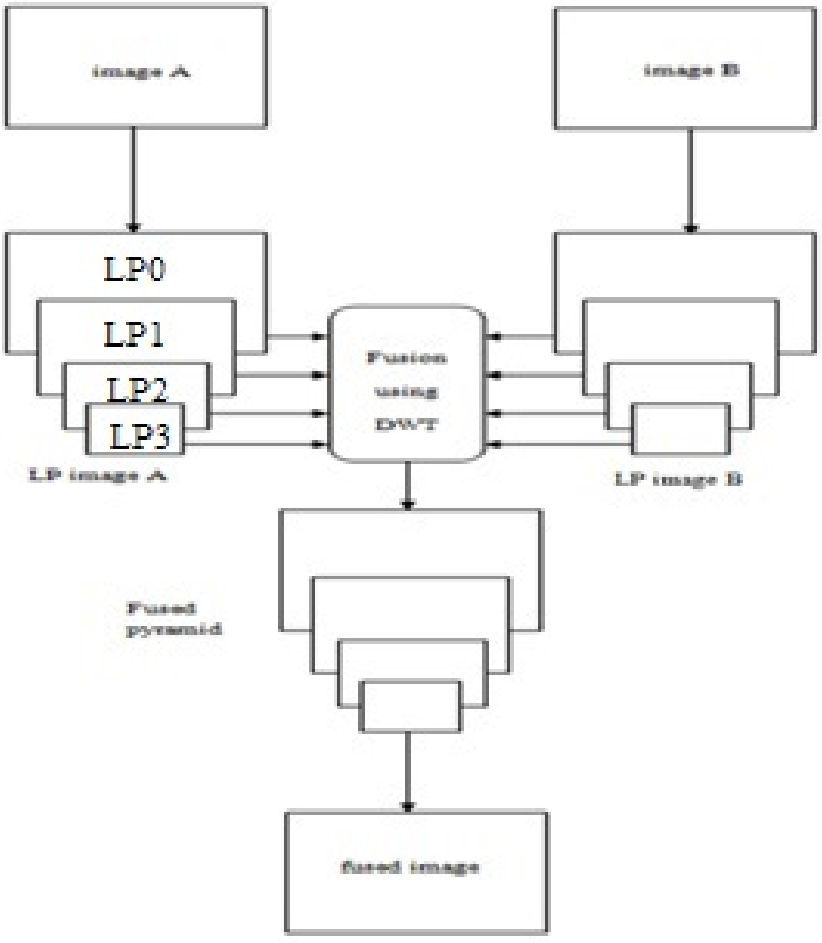

Figure 3.2: The proposed method

3.4/ COMPARISON BETWEEN METHODS

In order to compare our proposed method with other methods, we provide the performance evaluation metrics that we will use from this chapter onwards. In this chapter we do not use all mentioned evaluation metrics in the following however we use root mean square in all methods in this thesis. As we know there are two type of the analysis to evaluate the fused image: qualitative (subjective) analysis and quantitative analysis. Qualitative methods involve visual comparison between a reference image and the fused image. The advantage of this evaluation is easier to interpret. However, it also has some disadvantages such as: it is subjective and depends heavily on the experience of the respective interpreter as well it cannot be represented by mathematical models, and their technique mainly visual.

In this section, we discuss some quantitative analysis that will be used to evaluate the performance of the result fused image. Let $F(x, y)$ be the gray level intensity of pixel (x, y)

of the fused image and $I(x, y)$ be the gray level intensity of pixel (x, y) of the reference image.

3.4.1/ Root Mean Square Error (RMSE)

RMSE gives the information how the pixel values of fused image deviate from the reference image. RMSE between the reference image and fused image is computed as:

$$RMSE = \sqrt{\frac{1}{RC}\sum_{x=1}^{R}\sum_{y=1}^{C}[I(x,y) - F(x,y)]^2}, \tag{3.20}$$

where RxC is the size of the reference image and the fused image, (x, y) represents to the pixel locations. A smaller value of RMSE shows good fusion result. If the value of RMSE is 0 then it means the fused image is exactly the same as reference image.

3.4.2/ Peak Signal to Noise Ratio

PSNR is the ratio between the signal (image data) and the noise. In image processing, PSNR is calculated between two images. We find the peak signal to ratio between the fused image F and the reference image I. PSNR is computed as

$$PSNR = 10\log\left[\frac{255^2}{\frac{1}{RC}\sum_{x=1}^{R}\sum_{y=1}^{C}[I(x,y) - F(x,y)]^2}\right], \tag{3.21}$$

where RxC is the size of the reference image and the fused image. A higher value of PSNR gives better fusion results and this value shows how alike the fused and reference image are.

3.4.3/ Entropy

Image entropy is to evaluate the richness of image information; it represents the property of combination entropy of an image. The entropy on an image is:

$$H = -\sum_{l=0}^{L-1} p(l)\log p(l), \tag{3.22}$$

where L is the number of possible gray levels, $p(l)$ is probability of gray level l.The larger the combination entropy of an image, the richer the information contained in the image. If the entropy of used image is higher than the reference image or input images then it indicates that the fused image contains more information.

3.4.4/ Average Gradient

Average gradient, G, reflects the contrast between the detail variation of pattern on the image. The larger value of G, the clearer of image. In image fusion, the larger average

gradient means a higher spatial resolution

$$G = \frac{1}{(R-1)(C-1)} \sum_{x=1}^{R-1} \sum_{y=1}^{C-1} \sqrt{\left(\left(\frac{\partial F(x,y)}{\partial x}\right)^2 + \left(\frac{\partial F(x,y)}{\partial y}\right)^2\right)/2}. \tag{3.23}$$

where RxC is the size of the reference image and the fused image. $\frac{\partial F(x,y)}{\partial x}$ and $\frac{\partial F(x,y)}{\partial y}$ are one-order differential of pixel (x,y) in x and y direction respectively.

3.4.5/ Normalized Cross Correlation (NCC)

NCC is used as a measure for calculationg the degree of similarity between two images.

$$NCC = \frac{\left(\sum_{x=1}^{R} \sum_{y=1}^{C} \left(I(x,y) - \bar{I}(x,y)\right)\right)\left(\sum_{x=1}^{R} \sum_{y=1}^{C} \left(F(x,y) - \bar{F}(x,y)\right)\right)}{\sqrt{\sum_{x=1}^{R} \sum_{y=1}^{C} \left(I(x,y) - \bar{I}(x,y)\right)^2} \sqrt{\sum_{x=1}^{R} \sum_{y=1}^{C} \left(F(x,y) - \bar{F}(x,y)\right)^2}}. \tag{3.24}$$

where RxC is the size of the reference image and the fused image. $\bar{I}$ and $\bar{F}$ are mean of I and F respectively.

3.4.6/ Structural SIMilarity (SSIM)

SSIM that is developed by [68] measure the similarity between two images where quality assessment based on the degradation of structural information. The SSIM index can be viewed as a quality measure of one of the images being compared, provided the other image is regarded as of perfect quality.

$$SSIM = \frac{(2\mu_I\mu_F + c_1)(\sigma_{IF} + c_2)}{\left(\mu_I^2 + \mu_F^2 + c_1\right)\left(\sigma_I^2 + \sigma_F^2 + c_2\right)} \tag{3.25}$$

where μ_I and μ_F are mean of *I* and *F* respectively, $\sigma_I^2$and σ_F^2 are variance of *I* and *F* respectively, $\sigma_{IF}$is covariance of *I* and *F*, c_1 and c_2 are variables to stabilize the division with weak denominator, see in [68]. The SSIM value is a decimal value between -1 and 1, and value 1 is only reachable in the case of two identical sets of data.

3.4.7/ Mutual Information (MI)

MI was introduced as a similarity measure between two images simoultaneously by [42] and [67]. MI assumes no prior functional relationship between the images. It also assumes that a statistical relationship that can be captured by analyzing the images joint entropy. Joint entropy H can be calculated as follow:

$$H(F,I) = -\sum_{f,i} p_{FR}(f,i) \log p_{FI}(f,i) \tag{3.26}$$

MI considers both joint entropy and individual entropy $H(F)$ and $H(I)$,

$$H(A) = -\sum_{a} p_A(a) \log p_A(a) \tag{3.27}$$

for $A = F$ or I. And MI is calculated as follow

$$MI = H(F) + H(I) - H(F, I) \tag{3.28}$$

MI measures the reduction in uncertainty about the reference image due to the knowledge of the fused image, and so a larger MI is preferred.

3.5/ EXPERIMENTAL RESULT

In the literature, it is known that the blurred area can be obtained by doing low pass filtering on the clear image [27]. The low pass filtering on the clear image is convolution between low pass filter g and clear image I.

$$f(x, y) = \sum_{m,n=-s}^{s} g(m, n)I(x - m, y - n), \tag{3.29}$$

where s is the size of the window and the filter satisfies: $g(-m, -n) = g(m, n)$ and

$$\sum_{m,n=-s}^{s} g(m, n) = 1.$$

In this experiment, to generate sets of multi-focus images we blur clear image or reference image by using low pass filter (Gaussian filter) because it is shown that all blurred area can be simulated by convolution between Gaussian filter and clear image. Gaussian formula:

$$g(m, n) = \frac{1}{2\pi\sigma^2} \exp\left(-\frac{m^2 + n^2}{2\sigma^2}\right) \tag{3.30}$$

The parameters of Gaussian filter (s and σ) influence the quality of the blurred. The illustration of Gaussian convolution can be seen on Fig. 3.3 below. Blurring filter with size "$s = 2$" represents a blurring mask with size $(2s + 1) \times (2s + 1) = 5 \times 5$.

Figure 3.3: Gaussian convolution process

To perfom our proposed method, for 150 images on dataset [57] we apply low pass filtering using Gaussian filter with variance = 10 and filter size = 5 to get sets of multi-focus images. All images have size 256x256 pixels and are assumed registered. We fuse the images using four different methods: the proposed method, LP(average), LP(maximum) and DWT method. To compare the different methods we use four evaluation metrics: RMSE, PSNR, entropy, and average gradient. The fused images using the proposed method show improvement visually and quantitatively. We conclude that the proposed method is the best among the methods (LP(average), LP(maximum), DWT, and the proposed method), see on appendix A.1. To ilustrate this result, we present only two examples: first, a set multi-focus image consists of two images and the second, the set consists of three images.

3.5.1/ EXAMPLE OF TWO BLURRED IMAGES

The first set consist of two images with different focus. One image has focus on the small clock and the other image has focus on the bigger clock as shown in Fig. 3.4 where Fig. 3.4 (a) focuses on the smaller clock and Fig. 3.4(b) focuses on the bigger clock.

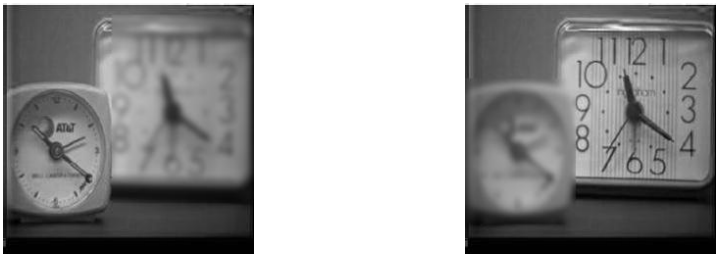

(a) (b)

Figure 3.4: Source images ‘clock’: (a) image with focus on the small clock, (b) image with focus on the big clock

The result of proposed image Fig. 3.5(d) is more obvious in details comparing with the result of wavelet method, Fig. 3.5(c). It is also can be seen that the proposed method has a smaller RMSE, 2.3223, than the DWT does, 3.4539. Fig. 3.5(d) has greater value in average gradient than Fig. 3.5(c), the larger of average gradient indicates the clearer of image.

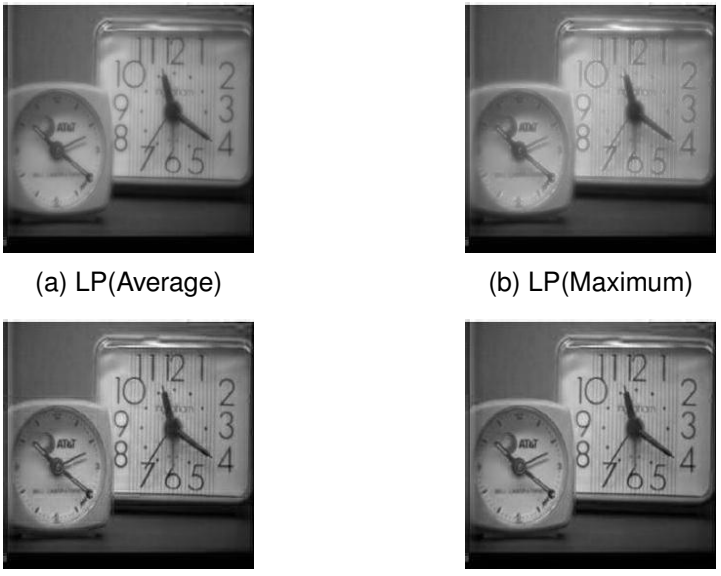

(a) LP(Average) (b) LP(Maximum)

(c) DWT (d) Proposed method

Figure 3.5: The ‘clock’ fusion results

We also can see that the fused image of LP fusion based average method, Fig. 3.5(a), has lower contrast than the result of proposed method Fig. 3.5(d). As we know that one of the disadvantage of average method, it reduces the contrast. Comparing with the result of the proposed method, the fused image of the proposed result gives more clarity.

The more contrast is obtained in the fused image by the proposed method, Fig. 3.5(d), compared with the result of LP fusion based on maximum selection, as shown in Fig. 3.5(b). Again, the RMSE and average gradient of the proposed method have the larger values the RMSE and average gradient of LP with maximum selection as we see in Fig. 3.6 and Fig. 3.8, respectively.

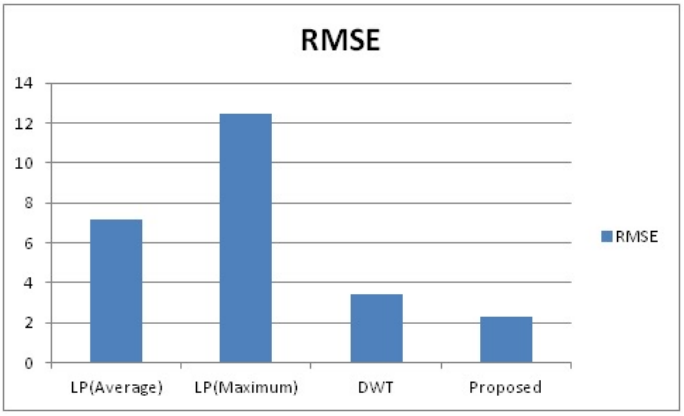

Figure 3.6: RMSE of the LP(average), LP(maximum), DWT, and proposed method

Fig. 3.6 shows that the proposed method gives the best fusion result, it has the lowest value of RMSE. The lower value of RMSE, the more similar the fuse image with the reference image.

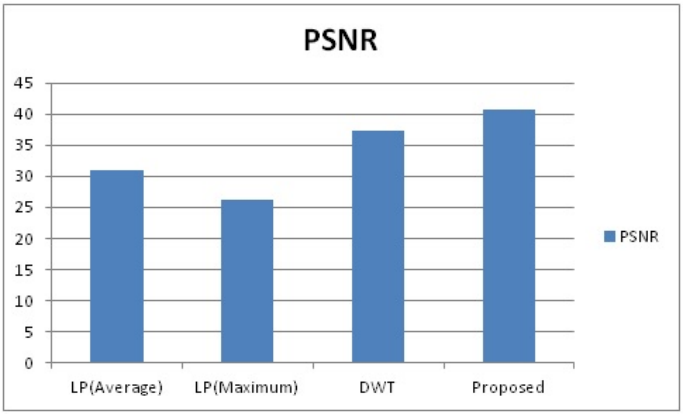

Figure 3.7: PSNR of the LP(average), LP(maximum), DWT, and proposed method

PSNR measures how alike the fused image with the reference image. The fused image is the most alike to reference image if it has high value of PSNR. In the Fig. 3.7, again the proposed method results the best performance with its highest value of PSNR followed by DWT, LP(average), and LP(maximum). For the clarity of image, it is shown by average gradient. The larger average gradient means a higher spatial resolution. It can be seen on chart from Fig. 3.8 that the average gradient value of the proposed method is the largest and the average gradient value of the LP maximum method is the smallest.

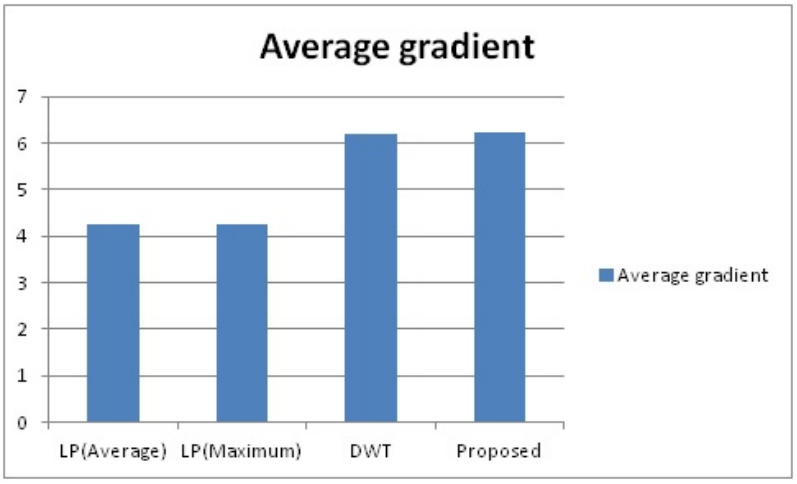

Figure 3.8: Average gradient of the LP(average), LP(maximum), DWT, and proposed method

The result of proposed method has obvious advantages in the details of information. It also gives the better both in visual clarity and quantitative performance evaluation in comparison to other methods. It is clear that the proposed method produce better quality fusion image than the other methods that are performed in this experiment. It can be seen in Table 3.1.

Evaluation	LP(Average)	LP(Maximum)	DWT	Proposed
RMSE	6.3602	6.4383	6.4685	17.0732
PSNR	32.0615	31.9553	31.9147	23.4845
Entropy	7.7500	7.7495	7.7486	7.7690
Average Gradient	12.5887	12.5662	12.5565	10.2972

Table 3.1: Performance evaluation of the fused image ‘bottle’.

3.5.2/ EXAMPLE OF THREE BLURRED IMAGES

In the previous experiment, the proposed method gives the best result among the methods presented. Hence, we will use the proposed method in this experiment for the fusion of three images. Three images in the second dataset show three different object focuses. The first image focuses on the small bottle, the left back of the image. The focus on gear is the second image. And the third image has focus on the big bottle. These images are shown in the Fig. 3.9, respectively Fig. 3.9(a), Fig. 3.9(b) and Fig. 3.9(c).

(I_1) (I_2) (I_3)

Figure 3.9: Multi-focus images:(I_1) in focus on the small bottle, (I_2) in focus on the gear and (I_3) in focus on the big bottle

We found something interesting while fused these images using different steps combination of images. We fuse these images with several combinations: all three images are fused once at the same time and to fuse every two images firstly then the result to be fused with another image. In the fusing of not all image together at the same time, we fuse two image at first using LP based on wavelet, we decompose two source images using Laplacian pyramid, then decompose images at each level by DWT, and to fuse them by Choose-max and mean method of wavelet coefficients,
We apply inverse wavelet on the fused coefficients then to reconstruct them by inverse pyramid to get the fused image. We applied again LP based on wavelet on the first fused image with another image to get all three fused image. Four combination rules are used in this fusion:

- The first combination, F_{123}
  We do the laplacian pyramid decomposition for all three images then we fusel images together at the same time. The result fused images is F_{123}.

- The second combination, $F_{(1,2),3}$
  The laplacian pyramid decomposition is applied to all images. We fuse first two images, image (I_1) and image (I_2), then we reconstruct the fused laplacian pyramid $(F_{1,2})$. The result fused $F_{1,2}$ we fuse with image (I_3) to get th fused image $F_{(1,2),3}$.

- The third combination, $F_{(2,3),1}$
  $F_{(2,3),1}$ is obtained by using similar way with $F_{(1,2),3}$ but the first fusion is image (I_2) and image (I_3). The result of first fusion $(F_{2,3})$, image (I_2) and image (I_3), is fused with image (I_1) to get the fused image $F_{(2,3),1}$.

- The fourth combination, $F_{(1,3),2}$ By fusing image (I_1) and image (I_3) to get the fused image $F_{1,3}$ and then to combine $F_{1,3}$ and image (I_2) to get the fused image $F_{(1,3),2}$.

In this experiment, there is evident that the focus area of image has correlation with the step of combination. The focus areas of image (I_1), the focus areas of image (I_2), and the focus of areas image (I_3) are 8077 units, 15639 units, and 38307 units, respectively.

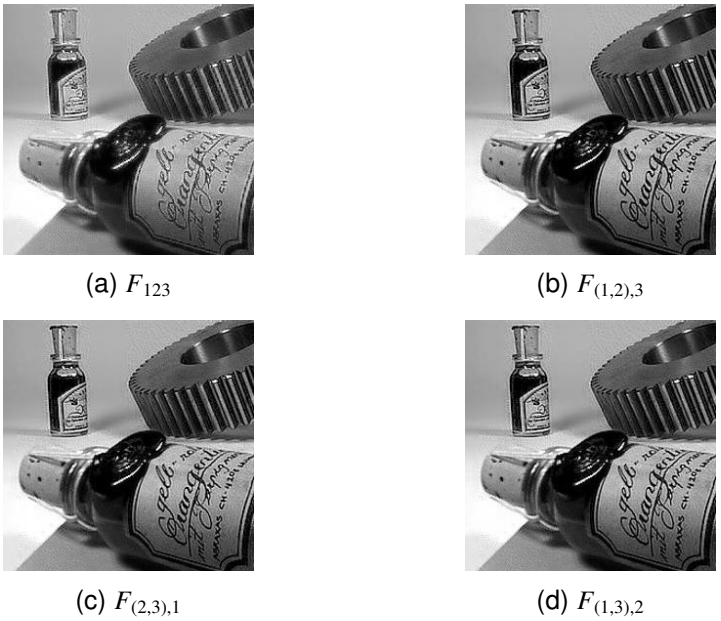

(a) F_{123} (b) $F_{(1,2),3}$

(c) $F_{(2,3),1}$ (d) $F_{(1,3),2}$

Figure 3.10: The results of combination fusion

Fig. 3.10 shows the result of the proposed method in various combination steps. In this case, the fusion of two images at first and followed fusion with another image gives much better result than to fuse all three images together at once. The fusion result of three images together at once, Fig. 3.10(a), produces the fused image with the lowest in contrast among the combinations. Visually, $F_{(1,2),3}$ gives the better result than $F_{(2,3),1}$ and $F_{(1,3),2}$. The contrast on the object 'gear' in the image $F_{(1,2),3}$ is the nearest to the contrast of object 'gear' on the source image (I_2), where the object 'gear' is focus object of it. $F_{(1,2),3}$ also has the sharper brightness for the object 'big bottle' compared with $F_{(2,3),1}$ and $F_{(1,3),2}$. It is also can be seen that the RMSE of $F_{(1,2),3}$, 6.3602, is the smallest, although not very different from $F_{(2,3),1}$, 6.4685, and $F_{(1,3),2}$, 6.4383.

From Table 3.2, in comparing $F_{(1,2),3}$, $F_{(2,3),1}$, and $F_{(1,3),2}$, $F_{(1,2),3}$ has the highest PSNR that $F_{(1,2),3}$ is the best result followed $F_{(1,3),2}$ and $F_{(2,3),1}$, as we know that PSNR show how alike the result image and the reference image are. The clear of image can be measured by average gradient, the clearer of image the higher the value of average gradient. Again, $F_{(1,2),3}$ has the highest value of average gradient, the second is $F_{(1,3),2}$, and followed by $F_{(2,3),1}$. From these performance evaluation values, $F_{(1,2),3}$ is better than $F_{(1,3),2}$ and $F_{(2,3),1}$.

image	$F_{(1,2),3}$	$F_{(1,3),2}$	$F_{(2,3),1}$	F_{123}
RMSE	6.3602	6.4383	6.4685	17.0732
PSNR	32.0615	31.9553	31.9147	23.4845
Entropy	7.7500	7.7495	7.7486	7.7690
Average Gradient	12.5887	12.5662	12.5565	10.2972

Table 3.2: Performance evaluation of the fused image 'bottle'.

Related to the focus areas, from the result, by combining one by one, it is better to combine from the first two smallest focus area, then the result is combined with the third

smaller and so on to the bigger. In this experiment, we see that the first two smallest is combination image (I_1) and image (I_2) first, $F_{1,2}$, then fused with image (I_3) that produced $F_{(1,2),3}$, and followed with $F_{1,3}$ that yields $F_{(1,3),2}$, and $F_{2,3}$ that resulted $F_{(2,3),1}$. It is because when we fuse from the smallest focus area to the bigger focus area, the loss of originality of the focus areas on the big focus image is not as big as others since it is proceed at last time.

3.6/ CONCLUSION

In the this work, we propose image fusion method using combination Laplacian Pyramid and DWT. We decompose source images into different levels of Laplacian Pyramid and fuse them at each level of LP using DWT as selection rule then we reconstruct the result of fused image at each level to get the final fused image. The result of experiment shows that the proposed method gives improved result in both visually and quantitatively in comparison with the other fusion methods: LP(average), LP(maximum), and DWT method. The fusion of more than two images is better done one by one from the smallest focus image to the bigger focus image. It gives better result than other combinations.

4

MULTI-FOCUS IMAGE FUSION USING DEMPSTER SHAFER THEORY BASED ON LOCAL VARIABILITY

4.1/ INTRODUCTION

The framework of the study of fusion in this chapter is the same as in the previous chapter, from several images representing the same object with different focus. The intended application is always general way of detecting possible ”blurred” present in the images with respect to ”clear” images.

As stated in [80], from the evidence point of view, fusion degrades the imprecision and uncertainty by making use of redundancy and complementary information of the source image. That means the weakness evidences from inputs are utilized to give the best estimation . Evidence theory was first proposed by Shafer in 1970s, which is based on Dempster research. The advantage of Dempster-Shafer Theory (DST) is that it allows coping with absence of preference, due to limitations of the available information, which results in indeterminacy, as in [20] and [69].

In this thesis, we propose multi-focus image fusion using the evidence functions of images that derived from one information: local variability. Local variability as the activity measure can detect the abrupt image intensity such as edge. This method also takes into consideration the information in the surrounding region of pixels and preserves the edge. We develop a decision fusion using Dempster-Shafer Theory (DST) method. Experiments are performed on different kinds of images and results are compared with other methods in Chapter 2. As the first step, we detail the main elements of the evidence theory of Dempster-Shafer.

4.2/ DEMPSTER-SHAFER THEORY

As in [61], Dempster-Shafer Theory (DST) is the significant work on this topic is [62], which is an extension of [18]. DST is a generalization of probability theory in a finite discrete space. In DST, the probabilities are assigned to sets in opposition to mutually exclusive singletons. The probability theory deals with evidence which is associated with only one possible event. On the contrary to the probability theory, DST deals with evi-

dence that can be associated with multiple possible events. There are three important functions in Dempster-Shafer theory: the *basic probability assignment* function (bpa or m), the *Belief* function (Bel), and the *Plausibility* function (Pl).

4.2.1/ BASIC PROBABILITY ASSIGNMENT

As in [80], let Θ represent a finite set of hypotheses for a problem domain, called frame of discernment. Defined as a function m from 2^Θ to $[0,1]$ where 2^Θ be the set of all subsets of Θ.

$$2^\Theta = \{A | A \subseteq \Theta\} \tag{4.1}$$

A piece of evidence that influences our belief concerning these hypotheses induces a mass function m, that satisfies:

$$m(\varnothing) = 0 \text{ and } \sum_{A \subseteq \Theta} m(A) = 1 \tag{4.2}$$

The function m is called a basic assignment. $m(A)$ can be interpreted as the belief that one is willing to commit to hypothesis A (and to none of its subsets) given the available evidence. According to [34], $m(A)$ is the degree of evidence supporting the claim that a specific element of Θ belongs to the set A, but not to any special subset of A. Each A of Θ such that $m(A) > 0$ are called the focal element of m. From the basic probability assignment, the upper and lower bounds of an interval can be defined. This interval contains the precise probability of a set of interest (in the classical sense) and is bounded by two nonadditive continuous measures called Belief and Plausibility.

4.2.2/ BELIEF FUNCTION

As in [77], the lower bound *Belief* for a set A is defined as the sum of all the basic probability assignments of the proper subsets (B) of the set of interest (A) $(B \subseteq A)$. A belief measure is given by the function $Bel : 2^\Theta \mapsto [0,1]$:

$$Bel(A) = \sum_{B \subseteq A} m(B) \tag{4.3}$$

A real function over the subsets $Bel : 2^\Theta \mapsto [0,1]$ is called a belief function if and only if it satisfies the following three axioms as defined by [62]:

1. $Bel(\varnothing) = 0$
2. $Bel(\Theta) = 1$
3. For any whole number n and subsets $A_1, A_2, \cdots, A_n \subseteq \Theta$,

$$Bel\left(\bigcup_{i=1}^{n} A_i\right) \geq \sum_{\substack{I \subset \{1,2,\cdots,n\} \\ I \neq \varnothing}} (-1)^{|I|+1} Bel\left(\bigcap_{i \in I} A_i\right)$$

where $|I|$ is the cardinality of I. $Bel(A)$ measures the degree of evidence that the element in question belongs to the set A as well as to the various special subsets of A. It is possible to obtain the basic probability assignment from the *Belief* measure with the following inverse function, by using Mobius transformation [77]:

$$m(A) = \sum_{B \subseteq A} (-1)^{|A-B|} Bel(B) \tag{4.4}$$

where $|A - B|$ is the cardinality of $A \cap \bar{B}$, and $\bar{B}$ is the complement of B.

4.2.3/ PLAUSIBILITY FUNCTION

The upper bound, *Plausibility*, is the sum of all the basic probability assignments of the sets (B) that intersect the set of interest (A) $(B \cap A \neq \varnothing)$. The plausibility measure $Pl : 2^{\Theta} \mapsto [0, 1]$:

$$Pl(A) = \sum_{A \cap B \neq \varnothing} m(B) = 1 - Bel(\overline{A}) \tag{4.5}$$

where $\overline{A}$ is complement of A or doubt of A. Doubt of A is represented by $1 - Pl(A)$.

4.2.4/ RULES FOR COMBINATION OF THE EVIDENCES

As stated in [80], the crucial aspect of DST concerns the aggregation of evidence provided by different sources. If two mass function m_1 and m_2 are from distinct items of evidence such that $m_1(B) > 0$ and $m_2(C) > 0$ for some non disjoint subsets B and C of Θ, then they are combinable by means of Dempster's rule. DST [18], [19], [62] suggested a rule of combination that permits that the basic probability assignments are combined. The combination (joint mass) of two sets of masses m_1 and m_2 is defined as follows

$$m_1 \oplus m_2(\varnothing) = 0 \tag{4.6}$$

$$m_1 \oplus m_2(A) = \frac{\sum_{B \cap C = A} m_1(B) m_2(C)}{1 - \sum_{B \cap C = \varnothing} m_1(B) m_2(C)} \tag{4.7}$$

DST may be successfully used in some situations, such as in cases where all information regarding to the problem is known and when a source provides information concerning only a few of several classes as stated in [9]. The advantages of DST, as stated in [80], are that it distinguishes between lack of belief and disbelief and allows the probability to be assigned to the union of the propositions in the frame of discernment. Such lack of belief typically arises in image fusion problems where a 'real scene' image is to be estimated from incomplete and unreliable observations. DST has been successful in many applications in image processing including image segmentation [45], [60], pattern classification [38], [81], object recognition [29], medical imaging [8], sensor fusion [74].

4.3/ THE PROPOSED METHOD: DEMPSTER-SHAFER THEORY - LOCAL VARIBILITY (DST-LV)

The crucial problem of image fusion using Dempster-Shafter Theory is to construct the evidence that represents the images. In this thesis, we propose one information as the evidential representation images based on the measure at each pixel that we call local variability.

4.3.1/ SOURCE: LOCAL VARIABILITY

Our method takes into consideration the information in the surrounding region of pixels. Indeed, at each pixel $I(x,y)$, the method exploits the local variability calculated from quadratic difference between the value of pixel $I(x,y)$ and the value of all pixels that belong to its neighborhood. The idea comes from the fact that the variation of the value in blurred region is smaller than the variation of the value in focused region that we proved in Chapter 5. Furthermore, the local variability expresses the detail information of image. For image with size (RxC), we use in this work the neighbor of a pixel (x,y) with the size "a" defined as follows:

$(x+i, y+j)$ where $i = -a, -a+1, \cdots, a-1, a$, $j = -a, -a+1, \cdots, a-1, a$, $x+i \in \{1,2,\cdots,R\}$, and $y+j \in \{1,2,\cdots,C\}$

For example the neighbor with the small size ("a" $= 1$) contains: $(x-1, y-1)$, $(x-1, y)$, $(x-1, y+1)$, $(x, y-1)$, $(x, y+1)$, $(x+1, y-1)$, $(x+1, y)$, $(x+1, y+1)$ as we can see in Fig. 4.1.

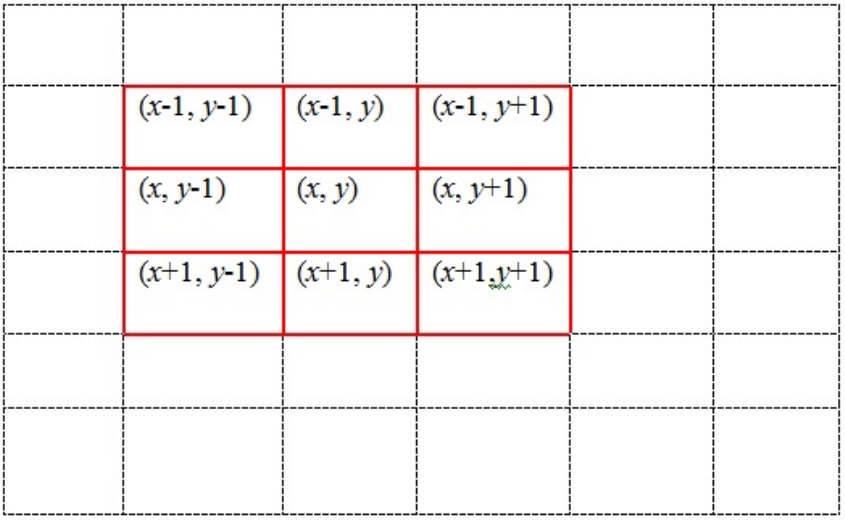

Figure 4.1: Pixel at (x, y) within its neighborhood, a = 1

We consider p source images $(I_1, I_2, \cdots, I_p)$ where each image has size $(R \times C)$. Variability of every source image at pixel (x,y):

$$v_{a,k}(x,y) = \sqrt{\frac{1}{T} \sum_{m=-a}^{a} \sum_{n=-a}^{a} \left| I_k(x,y) - I'_k(x+m, y+n) \right|^2} \tag{4.8}$$

where k is the index of k^{th} source image $(k = 1, 2, \cdots, p)$, a is the size of the neighborhood.

$$I'_k(x+m, y+n) = \begin{cases} I_k(x+m, y+n), \text{if } 1 \leq x+m \leq R \text{ and } 1 \leq y+n \leq C, \\ I_k(x, y), \text{otherwise} \end{cases}$$

$$T = (2a+1)^2 - card(S)$$
$$S = \left\{(m, n) \in \left([-a, a]^2 - \{(0, 0)\}\right) | I_k(x+m, y+n) = I_k(x, y)\right\}$$

The variability of image expresses the behavior of pixel relative to all pixels belong to its neighborhood. The variability preserves edge feature because it detects the abrupt image intensity.

4.3.2/ THE FUSION OF IMAGES

In this thesis, we consider two classes in the Dempster-Shafer theory of evidence. Either a pixel belongs to blurred part ω or it belong to the focus part $\overline{\omega}$. There is also uncertainty θ inherent in the theory of evidence. All this constitute the frame of discernment is Θ in our case [45].

$$\Theta = \{\omega, \overline{\omega}, \theta\} \tag{4.9}$$

For each pixel one value of evidence for information will be obtained, m.

$$\{m(\omega), m(\overline{\omega}), m(\theta)\} \tag{4.10}$$

with the condition $m(\omega) + m(\overline{\omega}) + m(\theta) = 1$.

The precision of this fusion is depending on the size of the neighborhood, "a". For each image we try with different values of "a" in the set $\{1, 2, ..., 10\}$ and we get the value of "a" that corresponds to the minimum of root mean square error (RMSE). This operation is repeated for set of multi-focus images in database [57].

Our method DST-LV consists of the following steps

Suppose there are p original source images, $I_1, I_2, \cdots, I_p$, where each image has size (RxC) with different focus to be fused. The general principle of making fusion rules is

Step 1: To calculate mass function:
for each image where we use different values of size of neighborhood, $a \in \{1, 2, \cdots, 10\}$, we define: $d'_{a,k}(x, y)$

$$d'_{a,k}(x, y) = 1 - \frac{v_{a,k}(x, y) - \min\limits_{(x', y')} (v_{a,k}(x', y'))}{\max\limits_{(x', y')} (v_{a,k}(x', y')) - \min\limits_{(x', y')} (v_{a,k}(x', y'))} \tag{4.11}$$

where k is the k^{th} source image, $k \in \{1, 2, \cdots, p\}$ and a is size of neighborhood of local variability. We set the standard deviation of $d'_{a,k}(x, y) = \sigma_{a,k}(x, y)$
for (x, y) belongs to ω, we calculate:

$$m_{a,k}(\omega) = (1 - \sigma_{a,k}(x, y))\, d'_{a,k}(x, y) \tag{4.12}$$

for (x, y) belongs to θ, we calculate:

$$m_{a,k}(\theta) = \sigma_{a,k}(x, y) \tag{4.13}$$

for (x, y) belongs to $\overline{\omega}$, we calculate:

$$m_{a,k}(\overline{\omega}) = 1 - \left(1 - d'_{a,k}(x, y)\right)\sigma_{a,k}(x, y) - \sigma_{a,k}(x, y) = \left(1 - d'_{a,k}(x, y)\right)(1 - \sigma_{a,k}(x, y)) \tag{4.14}$$

To give the final result of the multi-focus image is obtained by showing which pixels belong to focus area or which do not, we use concept plausibility. In our case the plausibility of ω is the sum of the masses of the evidence for ω and the uncertainty θ:

$$Pl_{a,k}(\omega) = m_{a,k}(\omega) + m_{a,k}(\theta)$$

and for fusion image of the pixel (x, y), due to ω is a set of pixel on blurred area, we take pixel (x, y) from image k_0 that assigned to minimum $Pl_k(\omega)$, $k = 1, 2, \cdots, p$.

Step 2: For (x, y), we take F_a as fused image with size of neighborhood = a

$F_a(x, y) = I_{k_0}(x, y)$, where $k_0 \in \{1, 2, \cdots, p\}$ and $Pl_{a,k_0}(\omega)(x, y) = \min_{k\in\{1,2,\cdots,p\}} (Pl_{a,k}(\omega)(x, y))$.

Step 3: For the proposed method, we use different values of size of neighborhood, $a \in \{1, 2, \cdots, 10\}$, and choose the value of a that corresponds to the minimum value of RMSE, such that our final fused image

$F = F_{a_0}$ where $a_0 \in \{1, 2, \cdots, 10\}$ and $RMSE(F_{a_0}) = \min_{a\in\{1,2,\cdots,10\}} (RMSE(F_a))$

4.4/ EXPERIMENTAL RESULT

We generated numerous sets multi-focus image from reference image on dataset [57] using Gaussian filter, all blurred images with the various values of variance and size of blurring filter and we performed the DST-LV method image fusion on those sets of multi-focus images using Matlab2013a. All images of database given the same conclusion except ten images of 150 images where RMSE of LP(DWT) is smaller than RMSE of the proposed method however the RMSE difference is very small, see appendix A.2. In this thesis, we choose to present only two multi-focus sets in this experimental section, as shown in Fig. 4.2., with size 256x256 $(R = C = 256)$ where the blurred images are obtained by performing low pas filtering using Gaussian filter with variance = 10 and filter size = 5. The first, image 'People' and the second image 'Bottle', all sets of image consist of different focus and one reference image. In this experiment, for the image 'People', we get the value of a = 7 and a = 9 for image 'Bottle'.

(a) reference image 'People' (b) in focus on the left (c) in focus on the right

(d) reference image 'Bottle' (e) in focus on the left (f) in focus on the right

Figure 4.2: Reference image and multi-focus images.

For comparison purposes, we compare the proposed method (DST-LV) with methods in the state of the art: PCA method, Discrete Wavelet Transform (DWT) method, Laplacian Pyramid (LP)-DWT, LP-PCA, DCT+Var, Bilateral gradient, MSSF, and EOL . Four evaluation measures are used: Root Mean Square Error (RMSE), Normalized Cross Correlation (NCC), Structural Similarity (SSIM), and Mutual Information.

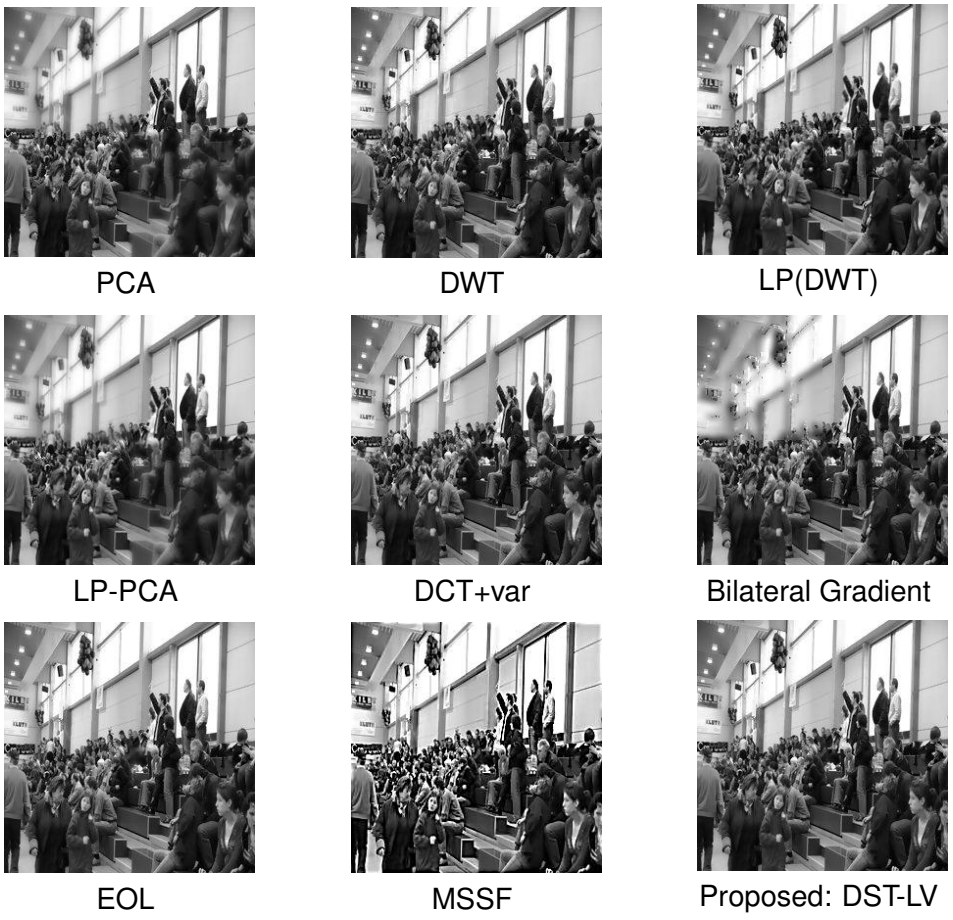

Figure 4.3: Comparison of visual quality of fused images various methods for image 'People'.

From the result figures (Fig 4.3 and Fig 4.4), we can see that the fused images produced by the PCA method and the bilateral gradient method are not so clear. It can be found that the results of the PCA method, and the bilateral gradient method have a poor contrast compared to other methods, while the MSSF method produces a high visual contrast fused image and not good at preserving the edge.

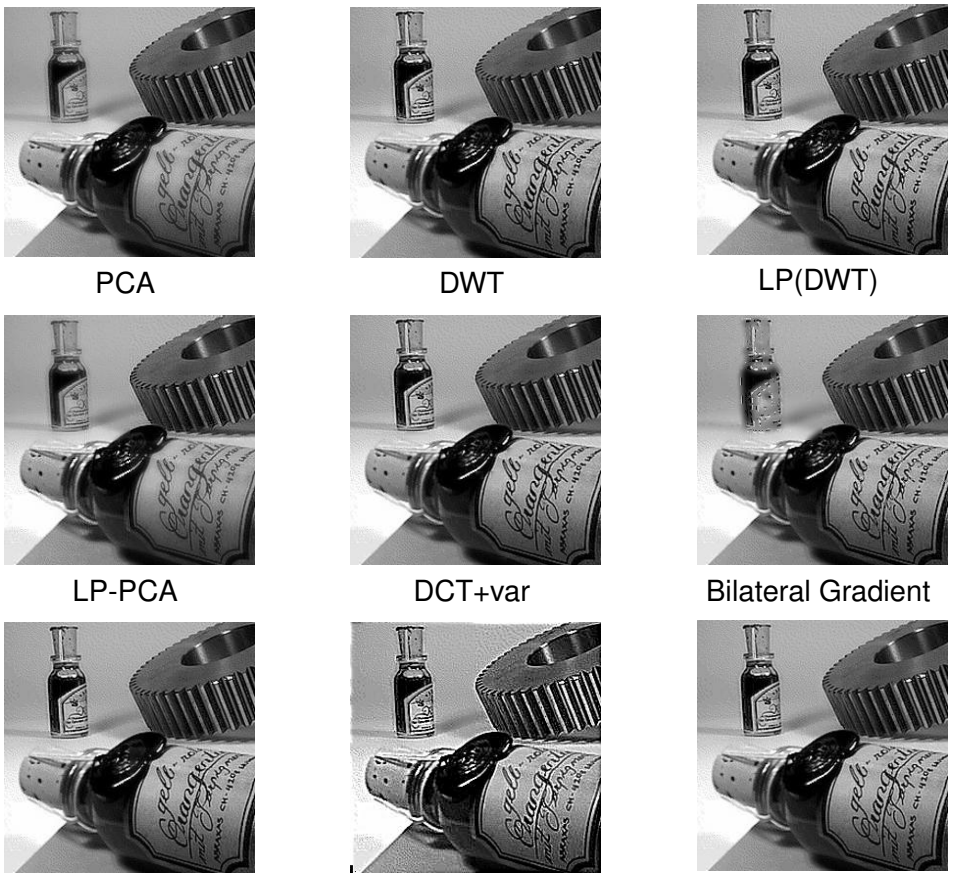

Figure 4.4: Comparison of visual quality of fused images various methods for image 'Bottle'.

However, it is difficult for us to perceive the difference among the results of the DWT method, LP(DWT) method, LP PCA method, DCT+Var method, EOL method and the proposed method according to the subjective evaluation. Therefore, to objectively evaluate these fusion methods, quantitative measures of the fusion results are needed. The results of the quantitative measures are shown in Table 4.1. According to the four evaluation measures, the comparison results are shown in Table 4.1., the proposed method gives the best result among the other methods.

Image	Evaluation	PCA	DWT	LP (DWT)	LP PCA	DCT +var	Bilateral Gradient	EOL	MSSF	DST-LV
People	RMSE	9.4592	3.9258	2.6621	2.5962	2.0286	12.6216	1.6241	26.7263	**0.3819**
a = 7	Mutual information	4.6241	5.1307	5.4237	5.4778	7.3794	6.1377	7.5192	2.4742	**7.6603**
	NCC	0.9930	0.9988	0.9994	0.9995	0.9997	0.9870	0.9998	0.9587	**1.0000**
	SSIM	0.9467	0.9808	0.9957	0.9959	0.9942	0.9121	0.9986	0.8436	**0.9996**
Bottle	RMSE	3.6392	12.1574	2.0605	2.0337	1.5442	12.6469	1.5593	25.0387	**0.5958**
a = 9	Mutual information	5.5539	4.6841	5.9879	6.0142	7.6391	6.4657	7.5768	2.5036	**7.6999**
	NCC	0.9987	0.9857	0.9996	0.9996	0.9998	0.9837	0.9998	0.9529	**1.0000**
	SSIM	0.9856	0.9332	0.9945	0.9964	0.9966	0.9225	0.9983	0.8259	**0.9990**

Table 4.1: Performance evaluation measures of fused images.

4.5/ CONCLUSION

Multi-focus image fusion using Dempster-Shafer theory based on local variability (DST-LV) has been proposed in this Chapter. The method calculates the local variability for each pixel of each image and determines the mass function from local variability. The decision of fusion is obtained by pixels that correspond to minimum plausibility. The fused image produced by DST-LV method is basically a combination of the good-focus parts in the source images.The proposed method was compared to PCA,LP-PCA, DWT, LP(DWT), LP-PCA, DCT+Var, Bilateral gradient, MSSF, and EOL. Experimental results show that the proposed method has better performance in terms of both visual quality and objective evaluation.

5

PIXEL-LEVEL MULTI FOCUS IMAGE FUSION BASED ON NEIGHBOR LOCAL VARIABILITY

5.1/ INTRODUCTION

Due to the limited depth-of-focus of optical lenses, it is often difficult to capture an image that contains all relevant objects in focus. Only the objects within the depth-of-field are in focus, while other objects are blurred. Multi-focus image fusion is developed to solve this problem. There are various approaches have been performed in the literatures.

In this thesis we propose pixel level multi focus image fusion based on the neighbor local variability (NLV). This method takes into consideration the information in the surrounding region of pixels. Indeed, at each pixel $I(x, y)$, the method exploits the local variability calculated from quadratic difference between the value of pixel $I(x, y)$ and the value of all pixels that belong to its neighborhood. It expresses the behavior of pixel relative to all pixels belong to its neighborhood. The variability preserves edge feature because it detects the abrupt image intensity. The fusion of each pixel (x, y) is done by weighting each pixel by the exponential of the local variability. The precision of this fusion depends on the size of the neighborhood. Firstly, we study the optimal size for having the minimum error for that we show that the size of neighborhood depends on the blurring characterized by the variance and its size of blurring filter. We construct a model that give the value of the size of neighborhood from the variance and the size of blurring filter.

We compare our method with other methods exist in the literature as described in Capter 2, we show that our method gives the best result by using Root Mean Square Error (RMSE). In this work, the experimental for fusion image and compare to other methods. This part is organized as follows: Section 2 gives explanation about the idea of NLV and steps of the proposed method fusion process and a model that give the size of neighborhood from parameter of blurring used are described. The experimental results are shown in section 3.

5.2/ NEIGHBOR LOCAL VARIABILITY

5.2.1/ THE IDEA OF THE PROPOSED METHOD

Consider the fusion of two multi-focus images, I_1 and I_2, that have respectively blurred parts B_1 and B_2. These images have the same size: $R \times C$. We study the case where B_1 and B_2 are disjoint. The idea of the NLV fusion method that is to sum the pixel values of the two images weighted by the neighbor local variability of each picture. This neighbor local variability at (x, y) is defined in the previous chapter, equation (4.8).

$$v_{a,k}(x,y) = \sqrt{\frac{1}{T}\sum_{m=-a}^{a}\sum_{n=-a}^{a}\left|I_k(x,y) - I'_k(x+m, y+n)\right|^2} \tag{5.1}$$

where k is the index of k^{th} source image $(k = 1, 2)$, a is the size of the neighborhood.

$$I'_k(x+m, y+n) = \begin{cases} I_k(x+m, y+n), \text{if } 1 \le x+m \le R \text{ and } 1 \le y+n \le C, \\ I_k(x,y), \text{otherwise} \end{cases}$$

$$T = (2a+1)^2 - card(S)$$
$$S = \left\{(m,n) \in \left([-a,a]^2 - \{(0,0)\}\right) \text{ such that } I_k(x+m, y+n) = I_k(x,y)\right\}$$

We show in the following that this local variability is small enough where the location is on the blurred area (B_1 or B_2). Indeed, we consider, without loss the generality, that we have a focus pixel (x, y) in image I_1 and blurred in image I_2 $\quad((x,y) \in B_2)$

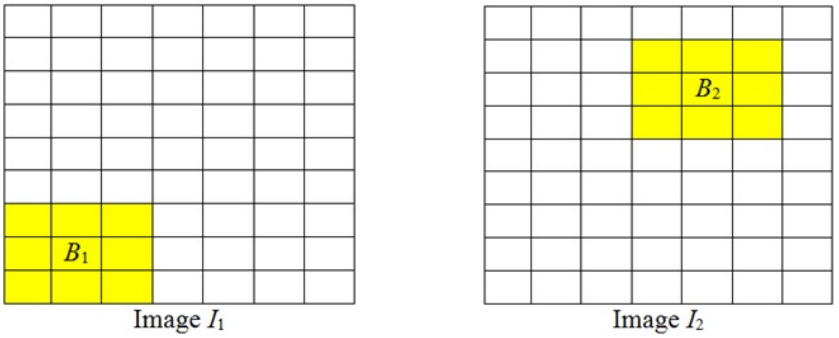

Figure 5.1: Two multi focus images, the yellow part is blurred area. And the white part is clear(focused) area.

The local variability of image I_1 and image I_2 are respectively: $\sqrt{\frac{1}{T}r_1(x,y)}$ and $\sqrt{\frac{1}{T}r_2(x,y)}$, where $r_1(x,y)$ and $r_2(x,y)$ can be written as follow:

$$r_1(x,y) = \sum_{m=0}^{2a}\sum_{n=0}^{2a}|I_1(x,y) - I_1(x+(m-a), y+(n-a))|^2 \tag{5.2}$$

$$r_2(x,y) = \sum_{m=0}^{2a}\sum_{n=0}^{2a} |I_2(x,y) - I_2\left(x+(m-a), y+(n-a)\right)|^2 \tag{5.3}$$

Let I_R is the reference image of multi-focus images I_1 and I_2. Moreover, it is shown in [48] and [55] that the blurred image can be seen as the product convolution between the reference image and a Gaussian filter. Let w_1 and w_2 are Gaussian filter, thus

$$I_1(x,y) = \begin{cases} w_1 * I_R(x,y), & (x,y) \in B_1 \\ I_R(x,y), & (x,y) \notin B_1. \end{cases}, \quad I_2(x,y) = \begin{cases} w_2 * I_R(x,y), & (x,y) \in B_2 \\ I_R(x,y), & (x,y) \notin B_2. \end{cases}, \tag{5.4}$$

The product convolution is defined as

$$w_1 * I_R(x,y) = \sum_{k=-s_1}^{s_1}\sum_{l=-s_1}^{s_1} w_1(k,l) I_R(x-k, y-l),$$
$$w_2 * I_R(x,y) = \sum_{k=-s_2}^{s_2}\sum_{l=-s_2}^{s_2} w_2(k,l) I_R(x-k, y-l),$$

where s_1 and s_2 are the size of Gaussian filter and

$$w_1(k,l) = \frac{\exp\left(-\frac{k^2+l^2}{2\sigma_1^2}\right)}{\sum_{k=-s_1}^{s_1}\sum_{l=-s_1}^{s_1}\exp\left(-\frac{k^2+l^2}{2\sigma_1^2}\right)}, \quad (k,l) \in [-s_1, s_1]^2.$$
$$w_2(k,l) = \frac{\exp\left(-\frac{k^2+l^2}{2\sigma_2^2}\right)}{\sum_{k=-s_2}^{s_2}\sum_{l=-s_2}^{s_2}\exp\left(-\frac{k^2+l^2}{2\sigma_2^2}\right)}, \quad (k,l) \in [-s_2, s_2]^2.$$

Put

$$r_1(x,y) = \sum_{m=0}^{2a}\sum_{n=0}^{2a} \left|D^1_{(m,n)}(x,y)\right|^2 \text{ and } r_2(x,y) = \sum_{m=0}^{2a}\sum_{n=0}^{2a} \left|D^2_{(m,n)}(x,y)\right|^2 \tag{5.5}$$

where

$$D^1_{(m,n)}(x,y) = I_1(x,y) - I_1\left(x+(m-a), y+(n-a)\right) \tag{5.6}$$
$$D^2_{(m,n)}(x,y) = I_2(x,y) - I_2\left(x+(m-a), y+(n-a)\right). \tag{5.7}$$

We will show that the local variability on blurred part is smaller than the local variability on focused part. So that we suppose without loss the generality that $(x,y) \in B_2$ (the blurred part of I_2) and we show that $(r_2(x,y) \leq r_1(x,y))$. For that, we use the Plancherel theorem:

$$\sum_{m=0}^{2a}\sum_{n=0}^{2a} \left|D^1_{(m,n)}(x,y)\right|^2 = \frac{1}{(2a+1)^2}\sum_{p=0}^{2a}\sum_{q=0}^{2a} \left|\hat{D}^1_{(p,q)}(x,y)\right|^2, \tag{5.8}$$

where $\hat{D}^1_{(p,q)}(x,y)$ is the Fourier Transform of $D^1_{(m,n)}(x,y)$.

$$\begin{aligned} \hat{D}^1_{(p,q)}(x,y) &= FT[D^1_{(m,n)}(x,y))] \\ &= FT\left[I_1(x,y) - I_1\left(x+(m-a), y+(n-a)\right)\right], \end{aligned} \tag{5.9}$$

As $(x, y) \in B_2$ therefore $(x, y) \notin B_1$, from (5.4), equation (5.9) can be written as follows

$$\hat{D}^1_{(p,q)}(x, y) = FT\left[I_R(x, y) - I_R\left(x + (m - a), y + (n - a)\right)\right]. \tag{5.10}$$

and

$$I_2(x, y) = \sum_{k=-s_2}^{s_2} \sum_{l=-s_2}^{s_2} w_2(k, l) I_R(x - k, y - l). \tag{5.11}$$

By using the definition of convolution, eq (5.11) can be written as:

$$I_2(x, y) = \sum_{k=-\infty}^{\infty} \sum_{l=-\infty}^{\infty} w_2(k, l) \chi_{[-s_2,s_2]^2} I_R(x - k, y - l) \tag{5.12}$$

and

$$I_2(x, y) = \left(w_2 \chi_{[-s_2,s_2]^2}\right) * I_R(x, y) \tag{5.13}$$

where

$$\chi_{[-s_2,s_2]^2}(k, l) = \begin{cases} 1, & \text{if } (k, l) \in [-s_2, s_2]^2 \\ 0, & \text{otherwise} \end{cases},$$

The Fourier transform of $D^2_{(m,n)}(x, y)$ is

$$\begin{aligned}
\hat{D}^2_{(p,q)}(x, y) &= FT[D^2_{(m,n)}(x, y)] \\
&= FT\left[I_2(x, y) - I_2\left(x + (m - a), y + (n - a)\right)\right] \quad \text{as } (x, y) \in B_2 \text{ we have} \\
\hat{D}^2_{(p,q)}(x, y &= FT\left[w_2 \chi_{[-s_2,s_2]^2} * I_R(x, y) - w_1 \chi_{[-s_2,s_2]^2} * I_R\left(x + (m - a), y + (n - a)\right)\right] \\
&= FT\left[w_2 \chi_{[-s_2,s_2]^2} * \left(I_R(x, y) - I_R\left(x + (m - a), y + (n - a)\right)\right)\right] \\
&= FT\left[w_2 \chi_{[-s_2,s_2]^2}\right] FT\left[I_R(x, y) - I_R\left(x + (m - a), y + (n - a)\right)\right]
\end{aligned} \tag{5.14}$$

Substitute (5.10) into (5.14), we get

$$\begin{aligned}
\hat{D}^2_{(p,q)}(x, y) &= FT\left[w_2 \chi_{[-s_2,s_2]^2}\right] \hat{D}^1_{(p,q)}(x, y) \\
&= \left(\sum_{k=-\infty}^{\infty} \sum_{l=-\infty}^{\infty} w_2(k, l) \chi_{[-s_2,s_2]^2}(k, l) e^{-i2(kp+lq)}\right) \hat{D}^1_{(p,q)}(x, y) \\
&= \left(\sum_{k=-s_2}^{s_2} \sum_{l=-s_2}^{s_2} \frac{e^{\left(-\frac{k^2+l^2}{2\sigma_2^2}\right)}}{\sum_{k'=-s_2}^{s_2} \sum_{l'=-s_2}^{s_2} e^{\left(-\frac{k'^2+l'^2}{2\sigma_2^2}\right)}} e^{-i2(kp+lq)}\right) \hat{D}^1_{(p,q)}(x, y).
\end{aligned} \tag{5.15}$$

Hence from eq. (5.15), we can obtain

$$\begin{aligned}\left|\hat{D}^2_{(p,q)}(x,y)\right| &= \left|\sum_{k=-s_2}^{s_2}\sum_{l=-s_2}^{s_2}\frac{\exp\left(-\frac{k^2+l^2}{2\sigma_2^2}\right)}{\sum_{k'=-s_2}^{s_2}\sum_{l'=-s_2}^{s_2}\exp\left(-\frac{k'^2+l'^2}{2\sigma_2^2}\right)}\exp\left(-i2(kp+lq)\right)\hat{D}^1_{(p,q)}(x,y)\right| \\ &= \left|\sum_{k=-s_2}^{s_2}\sum_{l=-s_2}^{s_2}\frac{\exp\left(-\frac{k^2+l^2}{2\sigma_2^2}\right)\exp\left(-i2(kp+lq)\right)}{\sum_{k'=-N}^{N}\sum_{l'=-s_2}^{s_2}\exp\left(-\frac{k'^2+l'^2}{2\sigma_2^2}\right)}\hat{D}^1_{(p,q)}(x,y)\right| \\ &\leq \sum_{k=-s_2}^{s_2}\sum_{l=-s_2}^{s_2}\left|\frac{\exp\left(-\frac{k^2+l^2}{2\sigma_2^2}\right)}{\sum_{k'=-s_2}^{s_2}\sum_{l'=-s_2}^{s_2}\exp\left(-\frac{k'^2+l'^2}{2\sigma_2^2}\right)}\right|\left|\hat{D}^1_{(p,q)}(x,y)\right| \\ &\leq \left|\hat{D}^1_{(p,q)}(x,y)\right|. \end{aligned} \tag{5.16}$$

On the other hand from (5.5) and Plancherel-Parseval's theorem, we have

$$r_2(x,y) = \sum_{m=0}^{2a}\sum_{n=0}^{2a}\left|D^2_{(m,n)}(x,y)\right|^2 = \frac{1}{(2a+1)^2}\sum_{p=0}^{2a}\sum_{q=0}^{2a}\left|\hat{D}^2_{(p,q)}(x,y)\right|^2,$$

From (5.16), we get

$$\begin{aligned} r_2(x,y) &\leq \frac{1}{(2a+1)^2}\sum_{p=0}^{2a}\sum_{q=0}^{2a}\left|\hat{D}^1_{(p,q)}(x,y)\right|^2, \\ &\leq \sum_{m=0}^{2a}\sum_{n=0}^{2a}\left|D^1_{m,n}(x,y)\right|^2 = r_1(x,y). \end{aligned}$$

This proves that the local variability on blurred part is smaller than the local variability value on clear area.

5.2.2/ The Fusion Scheme of The Proposed Method

The fact that even though there are already many multi-focus image fusion algorithms however many researchers keep developing the multi-focus image fusion field. In this work, we develop a novel fusion method that consists of weighting each pixel of each image by exponential of local variability. This local variability at (x,y) is calculated from the quadratic difference between the value of the pixel (x,y) and the all pixel values of its neighbors as explained in the previous chapter, in equation (4.8). Consider p original source images, $I_1, I_2, \cdots, I_p$, with different focus to be fused. The images here have the same size $R \times C$ and are assumed registered. Then, the steps of image fusion with size of nieghborhood "a" are as follows:

Step 1: For each pixel of each image, we calculate the local variability of every source image, $v_{a,k}(x,y)$ defined in (5.1):

$$v_{a,k}(x,y) = \sqrt{\frac{1}{T}\sum_{m=-a}^{a}\sum_{n=-a}^{a}\left|I_k(x,y) - I'_k(x+m,y+n)\right|^2} \tag{5.17}$$

Step 2: The fusion image proposed, F, is calculated in the following model:

$$F(x,y) = \frac{\sum_{k=1}^{p} \exp\left(v_{a,k}(x,y)\right) I_k(x,y)}{\sum_{k=1}^{p} \exp\left(v_{a,k}(x,y)\right)}. \tag{5.18}$$

Obviously, this method depends on the size "a". First, we tried with a small size $(a = 1)$, we show that the NLV method is better than DWT. To improve this method and to compare with all other methods we optimize the value of "a" for having the minimum Root Mean Square Error (RMSE), where RMSE is defined in Chapter 3. For that, we show that the value of "a" depends on the blurred area.

Indeed, the choice of the size of the neighborhood "a" used in NLV method depends on variance (v) and the size(s) of the blurring filter. Our objective is to have a model that give the value of the "a" according to the "v" and "s". For that we take sample of 1000 images that we blurred using Gaussian filter with different values of v and s $(v = 1, 2, 3, \cdots, 35$ and $s = 1, 2, 3, \cdots, 20)$.

After that for each image I blurred with parameters "v" and "s", we apply our fusion method with different values of "a" ("$a = 1, 2, \quad, 17$") and determine the value of "a" that gives the minimum RMSE, denoted by $a_l(v,s)$ where l is the index of l^{th} image. Then we take the mean of the $a_l(v,s)$ for 1000 images, denoted $a(v,s)$, because the coefficient of variation is smaller than 0.1.

To propose a model, firstly, we have studied the variation of "a" in according to variance "v" for each fixed size of blurring filter "s". We remark that this variation is logarithmic. For example "$s = 8$" on Fig. 5.2., by using non linear regression we obtain model: $2.1096 \ln v + 2.8689$.

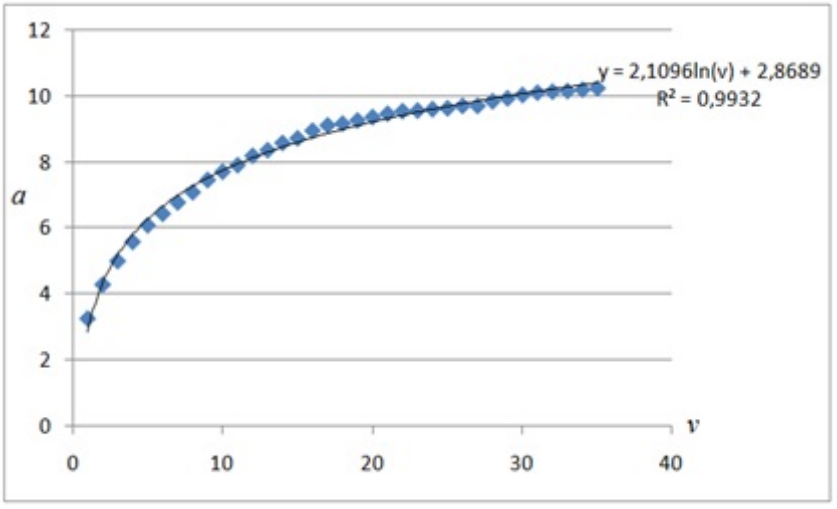

Figure 5.2: graph between "a" and variance of blurring filter where "s"=8

In general, the model is

$$a(v,s) = c_1(s) \ln v + c_2(s) \tag{5.19}$$

where c_1 and c_2 are functions that depend on "s". The graphs that describe c_1 and c_2 , respectively, Fig. 5.3 and Fig. 5.4.

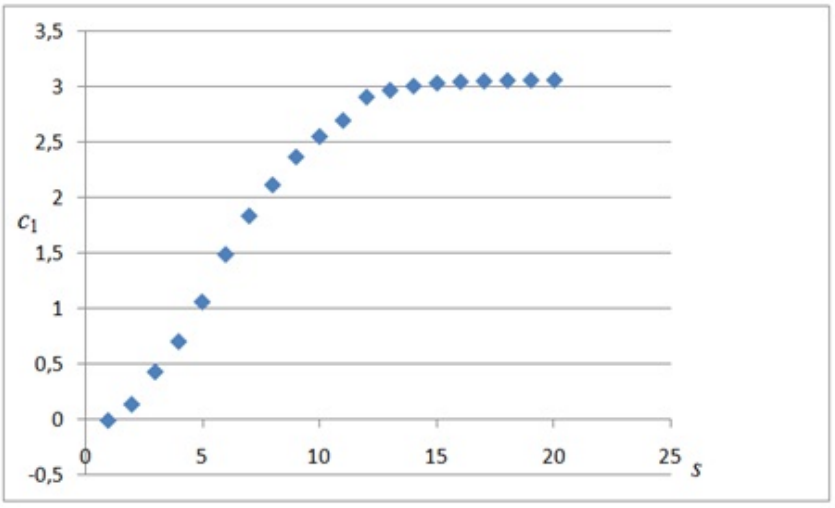

Figure 5.3: graph of $c_1(s)$

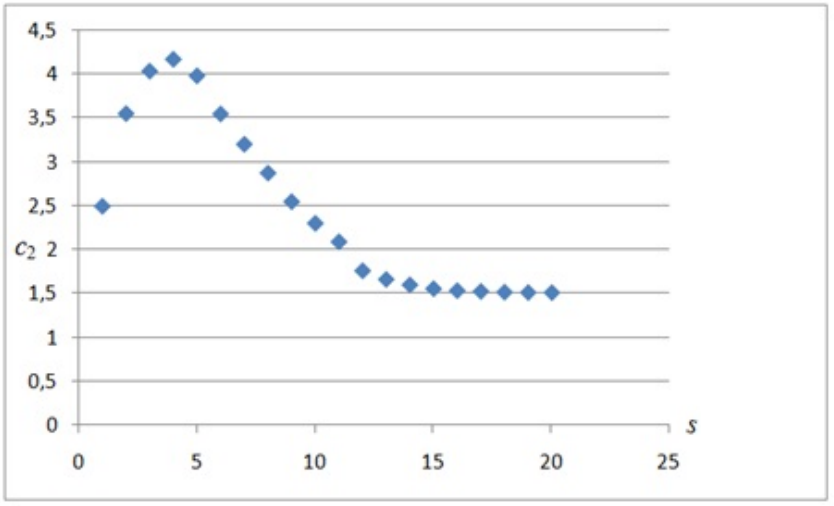

Figure 5.4: graph of $c_2(s)$

By giving a model of c_1 and c_2 and introduce the model in (5.19), we get the following model:

$$a(v,s) = \frac{3.0348761}{1 + 29.0909139\exp(-0.5324955s)} \ln(v) + 0.434\frac{75.062269}{1.225175s}\exp\left(-0.5\left(\frac{\ln(s) - 2.655551}{1.225175}\right)^2\right) \tag{5.20}$$

As "a" is integer, we have two choices of a is either floor of $a(v,s)$, denoted by$\lfloor a(v,s)\rfloor$or ceiling of $a(v,s)$, denoted by $\lceil a(v,s)\rceil$ where $\lfloor x\rfloor = \min\{n \in \mathrm{Z} | n \geq x\}$ and $\lceil x\rceil = \max\{m \in \mathrm{Z} | m \leq x\}$. Since the RMSE values of both "a" are very slightly different,

then we can choose any "a" of them. We use "a" that gives the minimum RMSE in the following of this thesis, either $\lfloor a(v,s) \rfloor$ or $\lceil a(v,s) \rceil$.

We validate our model by applying it to 150 images (we generate 150 pairs multi focus images with various values of variance and size of blurring filter) and the result is as good as expected. It shows that our method is better than DST-LV and LP(DWT) methods.

To use this NLV method, we must firstly estimate the variance and the size of blurring filter. There exists some work that give the methods to estimate variance of blurring filter and the blur detection as in [2], [22],[37],[39].

We also propose another method where we combine Laplacian pyramid method and NLV method. We use Laplacian pyramid with NLV as a selection rule, denoted by LP(NLV).

5.3/ Experimental Results

The NLV method is performed on a datasets of images [57] using Matlab2013a. We artificially produce a pair of out of-focus images, by blurring the left part of reference image to obtain the image with in focus on the right and then blurring the right part of the reference image to produce the image with in focus on the left. Blurring process is accomplished by using a Gaussian filter with many values of variance and size. We have applied these methods on a database of 150 images. Furthermore, in the appendix table A.2, we present RMSE of all the images used for the comparison of methods.

The proposed method outperforms other methods. In order not to encumber this work we chose to present only three images (image 'bird', image 'bottle', and image 'building'), all images consist of two images with different focus and one reference image as is shown in Fig 5.5. In this work the multi-focus images presented in Fig 5.5 are obtained with variance = 10 and filter size = 5.

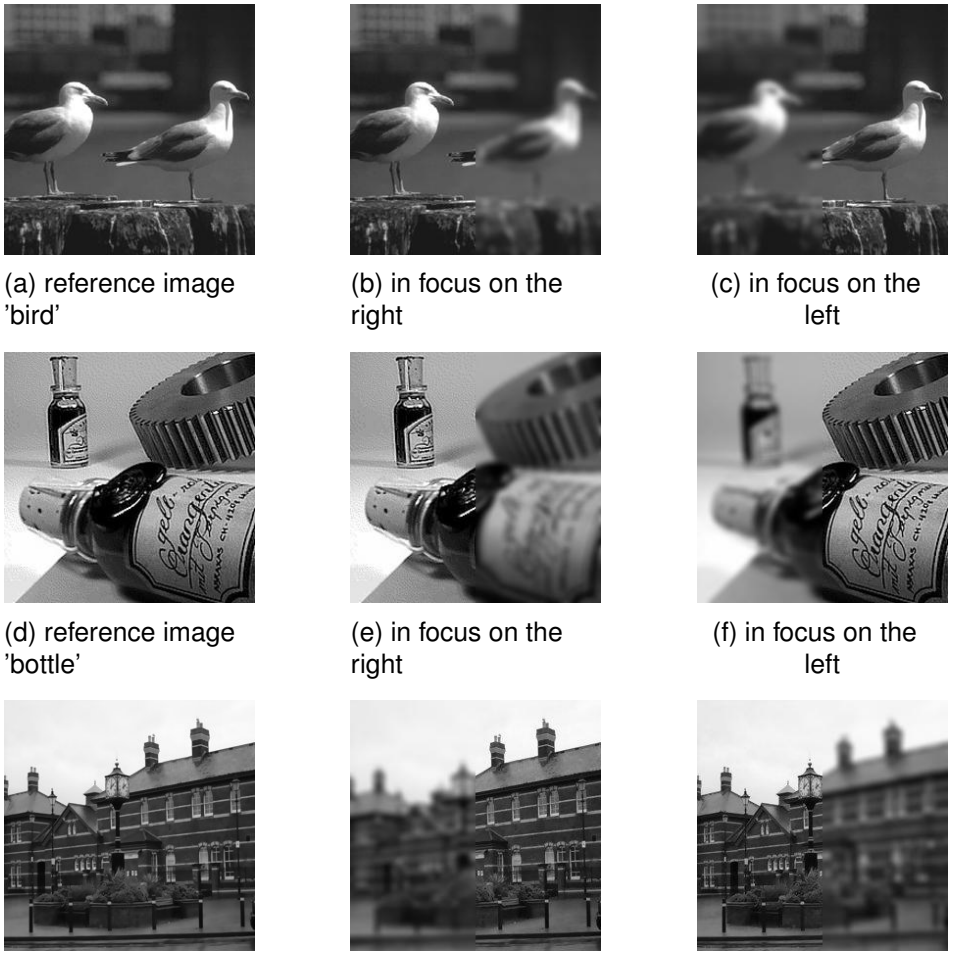

(a) reference image 'bird' (b) in focus on the right (c) in focus on the left

(d) reference image 'bottle' (e) in focus on the right (f) in focus on the left

(g) reference image 'building' (h) in focus on the right (i) in focus on the left

Figure 5.5: The images used in the experiment.

We fuse images using PCA, DWT, LP(DWT), LP-PCA, DCT+Var, Bilateral Gradient, Energy of Laplacian (EOL), MSSF, DST-LV, NLV, and LP(NLV) methods, where the value of the parameter of NLV "a" is determined by the model (5.20). For comparison purpose, four evaluation measures are used: Root Mean Square Error (RMSE), Normalized Cross Correlation (NCC), Structural Similarity (SSIM), and Mutual Information. Th figure Fig. 5.6. shows the fused results of the first example (bird image).

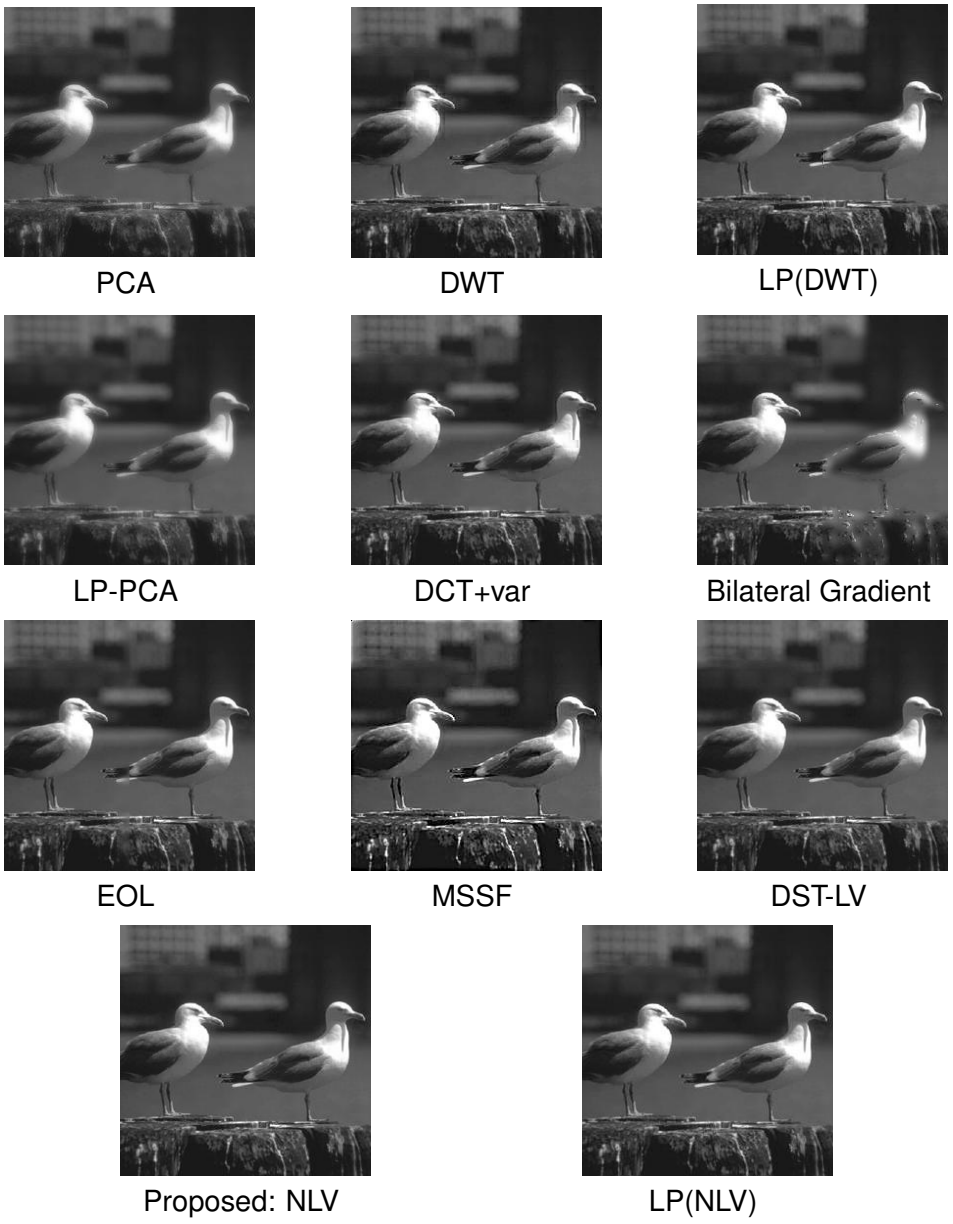

Figure 5.6: Experiment results of multi-focus image fusion image 'bird'.

A clearer comparison can be made visually by examining the differences between the fused images for different methods (Fig. 5.6) and reference images Fig. 5.5 (a). It can be seen that the fused image produced by NLV method is basically a combination of the good-focus parts in the source images. We can see blocking artifact on the result of DWT image fusion, compare with the other methods image fusion. To measure the differences between methods, we use the evaluation metrics (RMSE, NCC, SSIM, Mutual information). We have found that the NLV method performs better compared to other methods, see Table 5.1. For three images presented in this chapter and blurred with variance = 10 and size of blurring filter = 5, the model (5.20) gives the neighbor size "a" = 5 and "a" = 6. Here we use "a" = 6 because it result the smaller RMSE compared to "a" = 5 however the RMSE values of "a" = 5 and "a" = 6 are very slightly different.

	PCA	DWT	LP (DWT)	LP-PCA	DCT+ var	bilateral gradient	EOL	MSSF	DST-LV	NLV	LP (NLV)
RMSE	6.9205	3.5678	1.5190	1.4681	2.6860	8.8378	2.2792	10.4547	0.5766	**0.5466**	0.8253
NCC	0.9881	0.9965	0.9994	0.9994	0.9980	0.9784	0.9986	0.9786	0.9999	**0.9999**	0.9998
SSIM	0.9508	0.9747	0.9965	0.9966	0.9880	0.9220	0.9957	0.9477	0.9983	**0.9981**	0.9992
Mutual information	3.3233	3.7903	4.7704	4.8136	5.9425	4.5153	6.3188	3.3133	6.4519	**6.1738**	6.0114

Table 5.1: Performance evaluation image 'bird'

From the value of RMSE calculated for eleven methods in the Table 5.1., for image 'bird': the smallest is NLV method, the second smallest is DST-LV, the third is LP(NLV) and so on, as we can see on the table 5.1. NLV method is the best method among the methods and LP-NLV is better than LP-DWT.

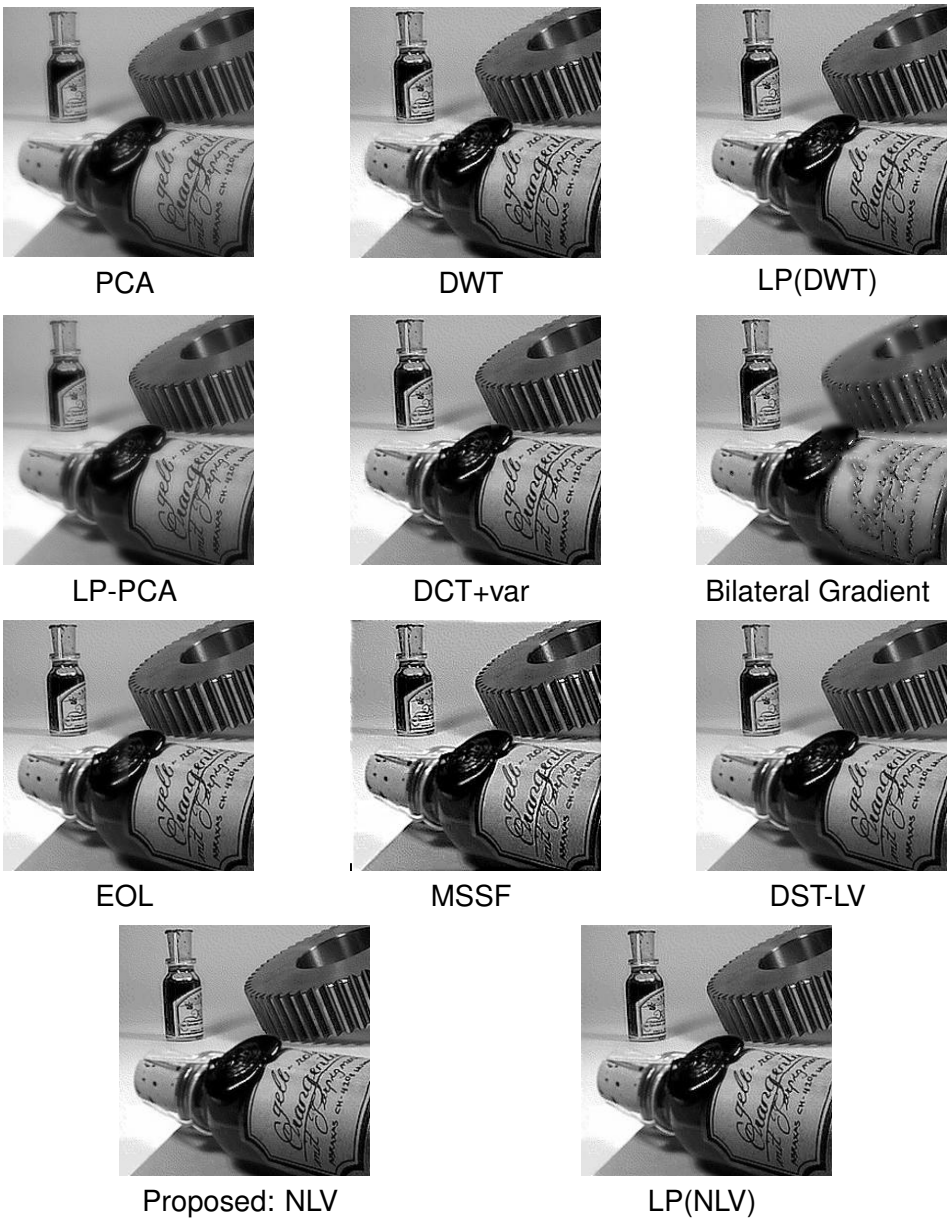

Figure 5.7: Experimental results of multi-focus image fusion image 'bottle'.

For image 'bottle', Fig. 5.7, subjectively it can be seen that the Bilateral gradient and MSSF methods does not handle the edge well compared the other method. On the other hand, the result image of NLV contains the balanced color and brightness as the original images to be fused. To confirm our result, we calculate the evaluation metrics: RMSE, NCC, SSIM and mutual information, see Table 5.2. From the value of RMSE calculated for eleven methods in the Table 5.2., we can classify these methods from smaller values of RMSE that the smallest is NLV method, the second smallest is DST-LV, the third smallest is LP(NLV).

	PCA	DWT	LP (DWT)	LP-PCA	DctVar	Bilateral gradient	EOL	MSSF	DST-LV	NLV	LP (NLV)
RMSE	15.0059	5.3846	2.5282	2.4850	2.6421	20.3804	3.6811	16.9197	0.9761	**0.9020**	1.5843
NCC	0.9792	0.9971	0.9994	0.9994	0.9993	0.9570	0.9986	0.9774	0.9999	**0.9999**	0.9997
SSIM	0.8770	0.9625	0.9905	0.9933	0.9878	0.7870	0.9915	0.9231	0.9966	**0.9968**	0.9978
Mutual information	2.9261	4.1448	5.1300	5.1502	7.3880	4.8356	7.2055	3.0480	7.5430	**7.3880**	6.9144

Table 5.2: Performance evaluation image 'bottle'

Figure 5.8: Experimental results of multi-focus image fusion image 'building'.

Figure Fig. 5.8 shows the fused image results of multi-focus images 'Building', in visual term, we can see that the fused result of PCA method is reduced in contrast and the

fused result of Bilateral gradient is not so clear compared to other methods. Moreover, to ensure that our proposed method is superior, four evaluation metrics are calculated: RMSE, NCC, SSIM, and mutual information, see Table 5.3. From Table 5.3, it shows that that NLV performed well.

	PCA	DWT	LP (DWT)	LP-PCA	DctVar	Bilateral gradient	EOL	MSSF	DST-LV	NLV	LP (NLV)
RMSE	10.2199	5.3986	2.1841	2.1426	3.9493	13.2749	2.9458	15.4439	0.6610	**0.4329**	1.1413
NCC	0.9929	0.9979	0.9997	0.9997	0.9989	0.9875	0.9994	0.9862	1.0000	**1.0000**	0.9999
SSIM	0.9065	0.9606	0.9936	0.9937	0.9838	0.8359	0.9922	0.9298	0.9981	**0.9985**	0.9995
Mutual information	3.2245	3.7195	4.5266	4.5408	6.3934	4.4457	6.6142	3.1381	6.8629	**6.8065**	6.5839

Table 5.3: Performance evaluation image 'building'

The NLV method provides better results as compared to other methods in this thesis after comparing the performance evaluation of all methods with each others.The NLV method gives significant improvement over other methods.

5.4/ CONCLUSION

In this work, we proposed image fusion method based on neighbor local variability (NLV). The precision of this fusion depends on the size of the neighborhood of local variability. The size of neighborhood is characterized by the variance and the size of blurring filter, more often that the blurring filter is Gaussian. The fused image is obtained by weighting each pixel by the exponential of the local variability. The result of experiment shows that the NLV method gives significant improvement result in both visually and quantitatively image fusion in comparison with ten other fusion methods. Laplacian pyramid with NLV as a selection rule is also applied, LP(NLV). Based on the experiment result, LP(NLV) is better than LP(DWT) and DWT.

III

CONCLUSION

6

CONCLUSION AND FUTURE WORK

The major concern of image fusion is to combine the relevant information from multiple image of a scene into a single more informative image. Image fusion methods have shown a great progress in recent years. The aim of this thesis is to study a multi-focus image fusion approach based on local variability.

In this framework, we develop three general fusion methods based respectively on the Laplacian pyramid with discrete wavelet transform (LP(DWT)), the theory of evidence of Dempster-Shafer Theory with a particular distance taking into account a local variability (DST-LV) and a model which consists of weighting the image by their local variability (NLV). These methods are applied to a database of images blurred by Gaussian filters.

The first method is to use the Laplacian pyramid as a technique of reduction and expansion then to fuse the images at each level of the Laplacian pyramid by discrete wavelet transform method. It gives a significant improvement of the two separate techniques.

We also introduce a criterion for each pixel of the image that measures the quadratic difference between this pixel and its neighbors. In this work, this quantization is called local variability at each pixel. It obviously depends on the size of the neighborhood used in image.

The second method proposed is to use the Dempster-Shafer theory by taking the local variability as a measure to calculate the mass function. This mass function allows to calculate the plausibility of each pixel that belongs to blurred part.

We show that the local variability of pixels in the blurred area is smaller than in the focus area. As we know that focus part contains more information than blurred part. This information corresponds to high value of local variability. From this result, we propose a method which consists of creating a fusion model by weighting each pixel by its local variability from each image. Then we use exponential function to boost the contribution of a pixel with higher value of local variability.

In order to optimize the results, a model is also proposed to determine the size of the neighborhood of the local variability according to the parameters of the blurring filter. A study based on several metrics of evaluation which compare the proposed methods to the different existing fusion methods shows the effectiveness of the proposed methods based on the local variability approach.

Compared to other methods given in the state of the art, all proposed methods provide a high spatial fused image, without any distortions and blocking artifacts. The experimental results show that the proposed NLV method is superior to other proposed methods in this

thesis and it greatly improves spatial resolution. Indeed, the Laplacian pyramid image fusion integrates multi-source information at the basic level and can provide more abundant, accurate and reliable detail information. It is also effective for preserving the edge. Furthermore, the DWT gives better preservation of both edge features and component information of the object in new fused image preserving in this way the detail image information. The DWT also retains the coefficients of in-focus regions within the image. So that our first proposed method, LP(DWT), which is a combination of Laplacian pyramid and DWT fusion give significant improvement.

The proposed methods based on local variability approach perform well because they work directly on each pixel by exploiting local variability that take into account the neighborhood so that it gives more detail information about the pixel.

Our proposed methods can be used in many applications, such as

- Drone is a new technology in digital imaging, it has opened up unlimited possibilities for enhancing photography. Drone can capture images on the same scene that zooms in on different objects, and at various altitudes. It will produces several images on the same scene but with different objects in-focus.
- In medical imaging, the DST-LV can be used to detect an abnormal object or cell using local variability where the behavior of each pixel with its neighborhood is given.
- For quality control in of food industry, cameras are used that take pictures. each camera targets one of several objects to detect an anomaly. The objects are on a conveyor belt. To have a photo containing all the objects in-focus, we can use our proposed methods of fusion which gives more details information.

There are several perspectives of this work:

- As many work on image fusion have implemented on grayscale images. In this thesis, all proposed methods are performed on the grayscale image. However, these proposed methods can be extended to color images as color conveys significant information.
- We are also encouraged to fuse more than two images by taking into account the local variability in each image (intra variability) and variability between image (inter variability). This inter variability can detect the 'abnormal pixels' among the images.
- Very often the blurred image can be represented as the convolution between the clear image and Gaussian filter. We will investigate that if it is possible to approach any blurred image by Gaussian filter or more generally by alpha-stable filter.
- We have built a model of the size of the neighborhood for the third proposed method (NLV). The model is a function of the parameters of Gaussian filter. The future work is to estimate the parameters of Gaussian filter from the source blurred image.
- We are motivated to extend the DST-LV method to fuse images with different objects from different sensors (multimodal).

7

Our publications

- I. S. Wahyuni, R. Sabre. Wavelet Decomposition in Laplacian Pyramid for Image Fusion. International Journal of Signal Processing Systems (IJSPS), Vol. 4, No. 1, pp.37-44, 2016.
- I. S. Wahyuni, R. Sabre. Multi-focus image fusion using Laplacian Pyramid technique based on Alpha-Stable filter (accepted on Canadian Journal of Basic and Applied Sciences).
- I. S. Wahyuni, R. Sabre. Pixel level multi-focus image fusion based on local variability (submitted on IET Image Processing).
- I. S. Wahyuni, R. Sabre. Multi-focus Image fusion using Dempster Shafer Theory based on local variability (submitted on International Journal of Approximate Reasoning)

BIBLIOGRAPHY

[1] A. H. Adelson, C. H. Anderson, J. R Bergen, P. J. Burt, J. M. Ogden. Pyramid method in image processing. RCA Engineer, vol 29(6), pp. 31-41, 1984.

[2] V. Aslantas. A depth estimation algorithm with a single image. Optic Express OSA Publishing, Vol. 15, Issue 8, 2007.

[3] A. Achim, P. Tsakalides, and A. Bezerianos. SAR image denoising via bayesian wavelet shrinkage based on heavy-tailed modeling. IEEE Transaction on Geoscience and Remote Sensing, Vol. 41, pp. 1773–1784, 2003.

[4] P. J. Burt and E. H. Adelson. The laplacian pyramid as a compact image code. IEEE Transactions on Communication, vol. 31, no. 40, Apr, 1983.

[5] D. P. Bavirisetti and R. Dhuli. Multi-focus image fusion using multi-scale decomposition and saliency detection. Ain Shams Engineering Journal. 2016.

[6] Y. Bando, H. Holtzman and R. Raskar, Near-invariant blur for depth and 2d motion via time-varying light field analysis, ACM Trans. on Graphics, vol. 32, no. 2, pp. 13, 2013.

[7] P. J. Burt and R. J. Kolezynski. Enhanced image capture through fusion. Proc. International Conference on Computer Vision, pp. 173-182, 1993.

[8] I. Bloch. Some aspects of Dempster-Shafer evidence theory for classification of multi-modality medical images taking partial volume effect into account. Pattern Recognition Letters 17, pp. 905-919, 1996.

[9] I. Bloch. Fusion of Image Information under imprecision and uncertainty: numerical methods. Data fusion and perception. G. Della Riccia et al. Springer-Verlag Wien. 2001.

[10] I. Bloch. Information Fusion in Signal and Image Processing. John Wiley and Sons, Inc. 2008.

[11] P. J. Burt. The pyramid as a structure for efficient computation. in Multiresolution Image Processing and Analysis, A. Rosenfeld, Ed., New York: Springer-Verlag, 1984.

[12] J. Chanussot, G. Mauris, P. Lambert. Fuzzy fusion techniques for linear features detection in multitemporal SAR images. IEEE Trans. Geoscience and Remote Sensing 37(3): 122-1305, 1999.

[13] Y.Q. Chen, L. Q. Chen, H. J. Gu, and K. Wang. Technology for multi-focus image fusion based on wavelet transform. Advanced Computational Intelligence (IWACI), 2010 Third International Workshop. 2010.

[14] S. Cheng, H. Chooi, Q. Wu and K. Castleman, Extended depth-of-field microscope imaging: Mpp image fusion vs. wavefront coding, in: IEEE International Conference on Image Processing, pp. 2533-2536, 2006.

[15] O. Cossairt, M. Gupta and S. K. Nayar, When does computational imaging improve performance, IEEE Trans. on Image Processing, vol. 22, no. 2, pp. 447-458, 2013.

[16] Y. Chai, H. F. Li, and Z. F. Li. Multifocus image fusion scheme using focused region detection and multiresolution. Optics Communications, 284 (19), 4376-4389, 2011.

[17] O. Cossairt, C. Zhou, and S. Nayar, Diffusion coded photography for extended depth of field, ACM Trans. on Graphics, vol. 29, no. 4, pp. 31, 2010.

[18] A. P. Dempster. Upper and lower probabilities induced by a multivalued mapping. The Annals of Mathematical Statistics 38: 325-339, 1967.

[19] A. P. Dempster. A generalization of bayesian Inference. Journal of the Royal Statistical Society, Series B (methodological) 30: 205- 247, 1968.

[20] T. Denoeux. Reasoning with imprecise belief structures. International Journal of Approximate Reasoning 20 (1): 79-111, 1999.

[21] A. Deng, Jin Wu and S. Yang, "An Image Fusion Algorithm Based on Discrete Wavelet Transform and Canny Operator," Advance Research on Computer Education, Simulation and Modelling Communication in Computer and Information Science, Vol. 175, pp. 32-38, 2011.

[22] J. H. Elder and S. W. Zucker. Local Scale Control for Edge Detection and Blur Estimation. IEEE Transactions on Pattern Analysis and Machine Intelligence, Vol. 20, No. 7, 1998.

[23] V. N. Gangapure, S. Banerjee, and A. S. Chowdhury. Steerable local frequency based multispectral multifocus image fusion. Information Fusion, vol 23 p 99–115, 2015.

[24] Q. Guihong, Z. Dali, and Y. Pingfan. Medical image fusion by wavelet transform modulus maxima. Opt. Express [Online], 9(4), pp. 184-190, 2001.

[25] A. A. Goshtasby and S. G. Nikolov. Image fusion: Advance in the state of the art. Information fusion, 8, 114-118, 2007.

[26] R. Garg, P. Gupta, H. Kaur. Survey on multi-focus image fusion algorithm. Proceedings of 2014 RAECS UIET Panjab University, IEEE. 2014.

[27] R.C. Gonzales and R.E. Woods. Digital Image Processing 2nd edition. Prentice Hall. 2002.

[28] G. Hannsgen,"Infinite-Variance, Alpha-Stable Shocks in Monetary SVAR," International Review of Applied Economics, Taylor and Francis Group, Vol. 26, pp. 755-786, 2012.

[29] M. H. Hassan. Object recognition based on Dempster-Shafer reasoning. Proc. SPIE 1002, Intelligent Robots and Computer vision VII. 1989.

[30] M. B. A. Haghighat, A. Aghagolzadeh, and H. Seyedarabi. Real-time fusion of multi-focus images for visual sensor networks. Machine vision and image processing (MVIP), 2010 6th Iranian. 2010.

[31] D. J. Heeger and J. R. Bergen. Pyramid based texture analysis/Syntesis. Proc. 22nd Annual Conference on Computer Graphics and Interactive Techniques, pp. 229-238,1995.

[32] N. Indhumadhi and G. Padmavathi. Enhanced image fusion algorithm using laplacian pyramid and spatial frequency based wavelet algorithm. International Journal of Soft Computing and Engineering (IJSCE). ISSN: 2231-2307, Vol. 1, Issue 5, 2011.

[33] D. Jiang, D. Zhuang, and Y. Huang. Investigation of image fusion for remote sensing application. 2013.

[34] G. J. Klir and T. A. Folger. Fuzzy sets, uncertainty and information. Englewood Cliffs. Prentice-Hall. 1988.

[35] G. Kaur and P. Kaur. Survey on multifocus image fusion techniques. International Conference on Electrical, Electronics, and Optimization Techniques (ICEEOT). pp. 1420-1425, 2016.

[36] K. Kalaivani and Y. A. V. Phamila. Analysis of Image Fusion Techniques based on Quality Assessment Metrics. Indian Journal of Science and Technology, Vol 9(31), pp. 1-8, 2016.

[37] A. Kumar, R. Paramesran, C. L. Lim, and S. C. Dass. Tchebichef moment based restoration of Gaussian blurred images. Applied Optics, Vol. 55, Issue 32, pp. 9006-9016, 2016.

[38] M. Kowsalya and C. Yamini. A Survey on pattern classification with missing data using Dempster Shafer theory. International Conference on Information Engineering, Management and Security (2015): 134-138, 2015.

[39] R. Liu, Z. Li, and J. Jia. Image partial blur detection and classification. Computer Vision and Pattern Recognition, 2008. CVPR 2008. IEEE Conference on 23-28 June 2008.

[40] H. Li, B. S. Manjunath, and S. K. Mitra. Multisensor image fusion using the wavelet transform. Graphical Models and Image Processing, 57 (3), 235- 245, 1995.

[41] H. Li, S. Wei, and Y. Chai. Multifocus image fusion scheme based on feature contrast in the lifting stationary wavelet domain. EURASIP Journal on Advances in Signal Processing, 2012.

[42] F. Maes. Multimodality image registration by maximization of mutual information. IEEE Transaction Medical Imaging. Vol. 16 Issue 2,1997.

[43] S. G. Mallat. Theory for multiresolution signal decomposition: The wavelet representation. IEEE Trans. Pattern Anal. Mach. Intel. 11(7), 674-9, 1989.

[44] L. Mihaylova, P. Brasnett, A. Achim, D. Bull, and N. Canagarajah. Particle filtering with Alpha-Stable distributions. IEEE Workshop on Statistical Signal Processing, pp. 381 – 386, 2005.

[45] J. B. Mena and J. A. Malpica, J. A. Color Image Segmentation Using The Dempster-Shafer Theory of Evidence for The Fusion of Texture. Proceeding ISPRS Volume XXXIV-3/W8.pp.139-144, 2003.

[46] R. Martinez-Cuenca, G. Saavedra, M. Martinez-Corral and B. Javidi, Extended depth-of-field 3-d display and visualization by combination of amplitude-modulated microlenses and deconvolution tools, Journal of Display Technology, vol. 1, no. 2, pp. 321-327, 2005.

[47] M. D. Mulla, S. Prasad, F. Pacifici, P. Gamba, J. Chanussot, J. A. Benediktsson. Challenges and opportunities of multimodality and data fusion in remote sensing. Proceeding of the IEEE 103(9): 1585-1601, 2015.

[48] S. K. Nayar. Shape from Focus System. Proc. of IEEE Conf. Computer Vision and Pattern Recognition, pp. 302-308, 1992.

[49] J. Nunez, X. Otazu, O. Fors, A. Prades. V. Pala, and R. Arbiol: Multiresolution-based image fusion with additive wavelet decomposition. IEEE Trans. on Geoscience and Remote Sensing 37(3), 1204–1211,1999.

[50] V. P. S. Naidu and J. R. Raol. Pixel-level image fusion using wavelet and principal component analysis. Defense Science Journal, vol. 58, no. 3, pp.338-352, 2008

[51] C. L. Nikias and M. Shao. Signal processing with Alpha-Stable distributions and applications (Adaptive and Learning Systems for Signal Processing, Communications and Control Series), 1995.

[52] B. Osgood. The Fourier transform and its applications. Stanford University. 2009.

[53] Z. Omar and T. Stathaki Image Fusion: An Overview. Fifth International Conference on Intelligent Systems, Modelling and Simulation. 2014.

[54] G. Pajares and J. M. Cruz. A wavelet-based image fusion tutorial. Pattern Recognition, vol. 37, 2004.

[55] A. Petland. A new sense for depth of field. IEEE Transactions on Pattern Analysis and Machine Intelligent, Vol. 9, No. 4, pp. 523-531, 1987.

[56] A. A. Pure, N. Gupta, and M. Shrivastava. An Overview of Different Image Fusion Methods for Medical Applications . International Journal of Scientific & Engineering Research, Volume 4, Issue 7, pp. 129-133, 2013.

[57] www.rawsamples.ch. Accesed: 30 November 2016

[58] O. Regniers, L. Bombrun, D. Guyon, J. C. Samalens, C. Tinel, G. Grenier, C. Germain. Wavelet based texture modeling for the classification of very high resolution maritime pine forest images. International Geoscience and Remote Sensing Symposium (IGARSS). 2014.

[59] O. Regniers, L. Bombrun, D. Guyon, J. C. Samalens, C. Germain. Wavelet-Based Texture Features for the Classification of Age Classes in a Maritime Pine Forest. IEEE Geoscience and Remote Sensing Letters. 2015.

[60] M. Rombaut and Y. M. Zhu. Study of Dempster–Shafer for image segmentation applications. Image Vision Comput., vol. 20, pp. 15–23, 2002.

[61] K. Sentz and S. Ferson. Combination of Evidence in Dempster-Shafer Theory. SAND2002-0835 Technical Report. Sandia National Laboratories, Albuquerque, New Mexico.2002.

[62] G. Shafer. A mathematical theory of evidence. Pricenton University Press. 1976.

[63] P. Shah, S. N. Merchant, and U. B. Desai. Multifocus and multispectral image fusion based on pixel significance using multiresolution decomposition. Signal Image and Video Processing, 7 (1), 95-109, 2013.

[64] J. Tian, L. Chen, L. Ma, and W. Yu. Multi-focus image fusion using a bilateral gradient-based sharpness criterion. Optic Communications, 284, pp 80-87, 2011.

[65] Y. Yang, D. Park, S. Huang, and N. Rao. Medical image fusion via an effective wavelet-based approach. EURASIP Journal an Advances in Signal Processing. 2010.

[66] S. K. Verma, M. Kaur, and R. Kumar. Hybrid image fusion algorithm using Laplacian Pyramid and PCA method. Proceeding of the Second International Conference on Information and Communication Technology for Competitive Strategies. 2016.

[67] P. Viola and III William M. Wells. Alignment by maximization of mutual information. Journal International of Computer Vision, Vol. 24 Issue 2, September 1997. Kluwer Academic Publisgers Hingham, MA, USA.

[68] Z. Wang, C. Bovik, H. R. Sheikh, and E. P. Simonchelli. Image quality assesment: from error measurement to structural similarity. IEEE Transactions on Image Processing, Vol. 13, No. 1, 2004.

[69] Walley, P. Statistical reasoning with imprecise probabilities. London: Chapman and Hall. 1991.

[70] W. Wang and F. Chang. A multi-focus image fusion method based on laplacian pyramid. Journal of Computers [Online]. 6(12), 2011.

[71] T. Wan, N. Canagarajah, and A. Achim. A statistical multi-scale image segmentation via Alpha-Stable modeling. IEEE International Conference on Image Processing, Vol. 4, pp. 357-360, 2007.

[72] T. Wan, N. Canagarajah, and A. Achim. Compressive image fusion. IEEE International Conference on Image Processing, pp. 1308-1311, 2008.

[73] C. Wang, M. Liao, and X. Li. Ship detection in SAR image based on the Alpha-Stable distribution. Sensors , Vol. 8, pp. 4948-4960, 2008.

[74] H. Wu, M. Siegel, R. Stiefelhagen and J. Yang. Sensor fusion using Dempster-Shafer theory, IEEE Instrumentation and Measurement Technology Conference Anchorage, AK, USA, 21-23 May 2002.

[75] Z. Yingshi. Remote sensing application principles and methods. Beijing: Science press, pp.253-254, 2003.

[76] Y. Yang, S. Huang, J. Gao, and Z. Qian. Multi-focus Image Fusion Using an Effective Discrete Wavelet Transform Based Algorithm. Measurement Science Review, Volume 14, No. 2, 2014.

[77] R. R. Yager and L. Liu. Classic Works of the Dempster-Shafer Theory of Belief Functions. Springer. pp.1 -34, 2007.

[78] Y. Yang, D. Park, S. Huang, and N. Rao. Medical image fusion via an effective wavelet-based approach. EURASIP Journal an Advances in Signal Processing, 2010.

[79] D. M. Yan and Z. M. Zhao. Wavelet decomposition applied to image fusion. Proc. Int. Conf. on Info-tech and Info-net, pp. 291–295. IEEE Press, New Jersey .2001.

[80] X. Yuan, J. Zhang, X. Yuan, and B. P. Buckles. Low Level Fusion of Imagery Based on Dempster-Shafer Theory. Proceedings of the Sixteenth International Florida Artificial Intelligence Research Society Conference. pp. 475-479, 2003.

[81] H. Zhu, O. Basir, and F. Karray. Data fusion for pattern classification via the Dempster-Shafer evidence theory. in Proc. IEEE Int. Conf. Syst., Man, Cybern., vol. 7, pp. 109–114, 2002.

[82] Z.R. Zhang, Y.M. Kang, and Y. Xie. Stochastic resonance in a simple threshold sensor system with Alpha Stable noise. Communications in Theoretical Physics, The Smithsonian/NASA Astrophysics Data System, Vol. 61, pp. 578-582, 2014.

[83] P. Zhao, G. Liu, C. Hu, and H. Huang. Medical image fusion algorithm on the Laplace-PCA. Proc. 2013 Chinese Intelligent Automation Conference, pp. 787-794, 2013.

[84] H. Zhao, A. Shang, Y. Y. Tang and B. Fang, Multi-focus image fusion based on the neighbor distance. International Journal of Pattern Recognition, vol. 46, no.3, pp. 1002-1011, 2013.

[85] K. Zhan, J. Teng, Q. Li, and J. Shi. A novel explisit multi-focus image fusion method. Journal of Information Hiding and Multimedia Signal Processing, vol. 6, no. 3, pp.600-612, 2015.

[86] B. H. Zhang, C. T. Zhang, Y. Y. Liu, J.S. Wu, and L. He. Multi-focus image fusion algorithm based on compound PCNN in Surfacelet domain. Optik, 125 (1), 296-300, 2014.

[87] Z. Yingshi. Remote sensing application principles and methods. Beijing: Science press, pp.253-254, 2003.

List of Figures

List of Tables

IV

APPENDICES

A

Comparison Table

A.1/ RMSE of 150 images for LP(DWT) method

Image	LP(Average)	LP(Maximum)	DWT	LP(DWT)
1	6.9008	8.6008	3.5678	**1.5190**
2	10.4622	13.2814	6.7770	**3.3991**
3	7.4398	10.1568	3.6668	**1.7530**
4	5.1192	6.7956	2.9586	**1.2994**
5	8.5383	11.6224	4.1174	**2.0467**
6	6.0003	8.1245	3.2838	**1.3721**
7	6.3186	8.5827	3.2818	**1.3427**
8	9.4100	12.6952	3.7657	**1.8426**
9	8.5444	11.4765	3.3784	**1.6162**
10	6.4576	8.5471	2.6654	**1.4705**
11	6.2681	8.3705	3.1307	**1.4953**
12	7.8582	10.4846	4.2101	**2.1434**
13	1.3905	1.8886	0.7199	**0.3354**
14	6.8797	9.2365	3.3951	**1.4722**
15	5.8954	7.8333	4.4629	**1.6287**
16	11.9543	16.3748	5.5163	**2.5516**
17	10.1952	12.5527	3.3771	**2.0591**
18	9.0674	12.0423	4.5632	**2.3655**
19	1.5731	2.3402	0.9222	**0.5219**
20	4.9178	5.9655	2.4917	**1.1739**
21	8.3875	11.6786	5.9271	**2.1197**
22	8.9952	12.4162	5.0578	**2.2345**
23	6.9439	9.0398	3.7722	**1.4146**
24	2.9413	3.8104	2.0777	**0.9389**
25	9.9915	13.6476	6.0786	**2.2316**
26	9.5174	13.3018	4.7092	**2.0839**
27	13.9819	18.2567	4.9991	**3.3709**
28	8.5602	10.8736	4.2662	**2.0033**
29	7.0418	9.3307	3.5392	**1.4915**
30	4.9011	6.7289	3.5651	**1.9504**
31	7.8913	11.3365	3.6334	**2.6702**

32	10.1898	13.6604	4.5793	**2.2625**
33	8.8881	12.1821	4.8290	**2.0955**
34	7.8437	10.7584	4.9964	**2.6051**
35	8.5966	11.5909	4.0661	**2.2392**
36	10.8929	15.2018	3.3564	**2.0723**
37	9.5998	13.4518	4.1954	**2.1335**
38	8.6468	11.6562	4.7195	**1.9451**
39	10.6487	13.9436	6.1495	**2.9069**
40	9.3320	12.7805	5.1122	**2.5685**
41	7.2232	9.3170	4.9375	**1.9237**
42	10.2378	13.6145	5.4614	**2.4884**
43	5.3643	7.8519	3.0536	**1.7742**
44	7.9835	10.1543	4.1305	**2.2643**
45	19.5453	27.5442	4.4485	**3.2854**
46	4.0351	5.6970	2.3804	**1.0079**
47	13.1851	18.1667	7.6606	**2.9364**
48	12.0602	16.3593	5.3114	**2.9674**
49	20.8035	28.5636	5.7858	**3.7103**
50	19.2403	24.0102	5.9751	**3.4326**
51	16.5298	23.3848	7.1275	**3.5002**
52	14.0186	20.0200	4.0390	**2.1493**
53	24.3286	34.5161	6.0696	**3.9630**
54	14.4370	19.4302	6.2952	**3.2444**
55	12.5555	17.5969	6.6705	**2.3117**
56	18.0852	23.6963	5.5845	**3.2907**
57	4.5241	6.0223	4.0191	**1.2848**
58	16.1951	21.9939	5.1929	**3.5729**
59	5.4837	7.2958	2.9089	**1.4565**
60	7.9028	10.1213	4.3939	**2.1251**
61	5.0079	6.8792	3.0374	**1.1602**
62	5.7917	7.8320	3.2261	**1.3899**
63	8.2907	11.5201	4.0773	**2.3910**
64	4.9196	6.7466	3.0058	**1.2506**
65	13.0116	16.1517	5.9553	**3.0731**
66	4.1926	5.5183	2.7129	**1.0907**
67	13.8608	18.8017	6.3854	**2.9530**
68	2.8480	3.7106	1.6401	**0.6886**
69	9.3169	12.4320	4.4319	**2.3495**
70	12.5429	17.1914	5.2616	**2.6204**
71	8.7515	12.4801	3.7527	**1.8593**
72	11.3966	14.7892	5.0342	**2.4471**
73	7.3066	9.7526	3.8599	**1.7523**
74	5.7888	8.8769	2.1902	**0.7701**
75	9.8673	12.7340	4.2009	**2.0868**
76	7.6384	10.1302	5.9656	**2.0094**
77	4.6718	6.3867	3.6548	**1.4770**
78	12.2918	16.6833	5.7301	**3.0534**

79	7.9995	9.9382	2.8528	**1.7552**
80	6.8417	9.5624	3.0473	**1.3381**
81	4.0207	4.9895	1.9525	**1.0203**
82	8.2122	10.6426	3.5129	**2.0774**
83	8.3914	11.0453	4.7572	**2.3047**
84	10.8539	14.3202	4.6260	**2.1802**
85	15.0220	21.0072	5.3846	**2.5282**
86	6.9737	9.0245	2.9368	**1.8748**
87	6.2544	8.5210	4.0736	**1.7742**
88	5.7366	7.5903	2.7753	**1.2944**
89	5.3297	7.1815	3.9911	**1.1222**
90	8.1571	10.8905	5.5663	**2.9682**
91	4.1625	5.3223	2.0478	**1.3271**
92	7.2665	8.9764	3.0717	**1.7610**
93	8.8042	11.5162	6.2204	**2.2511**
94	10.0124	12.1151	5.2489	**2.5357**
95	7.0702	9.6246	3.4598	**1.8000**
96	11.7297	15.7993	6.1849	**2.6361**
97	6.7897	9.0956	2.7288	**1.3402**
98	6.1836	8.0147	3.6737	**1.9123**
99	3.9789	5.3167	3.1536	**0.9927**
100	8.1449	10.8914	4.3448	**1.7107**
101	6.6673	8.6944	3.6953	**1.3463**
102	8.2980	11.1037	3.8103	**1.7678**
103	4.2581	5.8824	1.6038	**0.9118**
104	8.0299	9.1973	2.9223	**1.5283**
105	9.7437	13.4202	4.6429	**2.3445**
106	5.9441	8.1837	2.6124	**1.2630**
107	5.8366	8.4925	2.9465	**1.3157**
108	9.0363	12.0285	4.4869	**2.0450**
109	7.1553	9.4696	5.8194	**1.9990**
110	17.1678	21.2835	5.9149	**3.5258**
111	8.5015	11.6792	5.1692	**2.0261**
112	5.1580	7.3526	3.3301	**1.3613**
113	13.1864	17.0256	6.9691	**3.1263**
114	6.2225	7.9341	2.7835	**1.8634**
115	6.2225	7.9341	2.7835	**1.8634**
116	9.5225	12.1562	4.2312	**2.3683**
117	3.6057	4.5657	2.0427	**0.8051**
118	2.1182	2.8569	0.7702	**0.6275**
119	13.8796	17.8908	5.1980	**3.0429**
120	10.0776	14.3792	5.2845	**2.6140**
121	13.7939	18.5235	4.4214	**3.2627**
122	5.0833	6.7907	2.6008	**1.5426**
123	8.9952	12.4162	5.0578	**2.2345**
124	8.6138	11.1410	5.7177	**2.1486**
125	8.0834	10.5889	4.1740	**1.9516**

126	7.7982	10.5130	5.9803	**3.3464**
127	8.7562	11.6427	4.6246	**1.7986**
128	17.1037	22.4735	6.1219	**3.6793**
129	8.3532	11.5101	4.3915	**2.1682**
130	7.2792	9.9167	5.4858	**2.2774**
131	6.4475	8.4207	2.8849	**1.3849**
132	3.2537	4.6083	2.4376	**1.0017**
133	5.1697	6.9625	2.9181	**1.4530**
134	7.5748	10.0242	4.5868	**1.7555**
135	12.1422	15.7355	5.0708	**3.0527**
136	4.1710	5.7269	2.9266	**0.9563**
137	6.1089	7.8800	2.8082	**1.7942**
138	8.0650	10.9014	5.8790	**2.5846**
139	8.0450	10.8283	3.3298	**2.0040**
140	9.8665	12.5536	5.1857	**2.3660**
141	7.9449	10.9454	3.2520	**1.8440**
142	8.9358	12.0399	3.7736	**1.8936**
143	10.1926	13.1384	5.3986	**2.1841**
144	13.9200	18.9018	4.7780	**3.2559**
145	6.9487	8.9942	3.6312	**1.6082**
146	9.6435	13.5412	4.0506	**2.0575**
147	15.1067	20.2606	6.1762	**3.2957**
148	3.6152	4.7940	2.2867	**0.8807**
149	13.1864	17.0256	6.9691	**3.1263**
150	10.7505	14.0064	4.1283	**2.4296**

Table A.1: Table RMSE of 150 images for LP(DWT) method

A.2/ RMSE OF 150 IMAGES FOR DST AND NLV

Image	DST-LV	DWT	NLV	LP (DWT)	LP (NLV)	DCT +Var	Bilateral Gradient	MSSF	EOL
1	0.5766	3.5678	0.5466	1.5190	0.8253	2.6860	8.8378	10.4547	2.2792
2	0.8554	6.7770	0.8422	3.3991	1.6660	5.8342	14.7006	14.1356	3.8413
3	0.7401	3.6668	0.3834	1.7530	0.8568	2.5415	10.3027	12.8118	1.9301
4	0.2437	2.9586	0.2269	1.2994	0.2576	2.7217	5.2088	5.4510	4.1168
5	0.8392	4.1174	0.6223	2.0467	1.0089	3.4253	8.4477	12.5065	3.0234
6	0.4965	3.2838	0.4715	1.3721	0.6136	2.8205	6.8490	9.1966	1.8962
7	0.4086	3.2818	0.3592	1.3427	0.8021	1.8261	7.6890	12.2161	0.8328
8	1.3426	3.7657	0.5215	1.8426	1.0823	2.2308	13.4102	12.7320	2.2213
9	1.7216	3.3784	0.4607	1.6162	0.8784	2.4775	12.3683	12.1165	1.9937
10	2.1413	2.6654	0.2636	1.4705	0.9869	1.2905	10.5622	11.9749	2.2624
11	0.9756	3.1307	0.6026	1.4953	1.1869	2.2186	8.9969	10.4455	1.9645
12	0.6762	4.2101	0.6184	2.1434	1.3638	3.0857	10.2518	14.5641	1.2481
13	0.5303	0.7199	0.1899	0.3354	0.2091	0.6287	1.4871	5.3482	0.4459
14	0.6502	3.3951	0.4370	1.4722	1.2077	2.1175	8.2507	10.9823	1.6850

15	1.7057	4.4629	0.5481	1.6287	1.1052	4.2112	6.7201	9.8758	1.7826
16	0.7576	5.5163	0.5102	2.5516	1.5857	3.1291	15.3525	17.8907	3.4541
17	0.5317	3.3771	0.4873	2.0591	1.6408	1.8465	12.3752	16.5393	2.7365
18	0.7449	4.5632	0.6730	2.3655	0.7299	3.4793	11.6880	9.3041	4.2320
19	0.2371	0.9222	0.2325	0.5219	0.2726	0.6936	1.9063	3.7717	0.7871
20	0.4867	2.4917	0.3967	1.1739	0.8300	1.7747	6.0726	8.4616	1.6548
21	1.0509	5.9271	0.8521	2.1197	0.9780	5.0875	11.4113	9.5884	2.8874
22	0.9399	5.0578	0.6946	2.2345	0.7347	3.7339	10.9129	9.5417	2.9610
23	0.9380	3.7722	0.4518	1.4146	0.7325	3.0072	8.0140	12.4737	1.5138
24	0.7982	2.0777	0.4213	0.9389	0.5160	1.8682	3.1150	4.6310	1.5949
25	0.6315	6.0786	0.7754	2.2316	1.0477	5.1572	10.8521	11.0927	3.3117
26	0.4570	4.7092	0.4639	2.0839	1.2097	3.7234	12.7628	13.8193	2.1084
27	0.7223	4.9991	0.5954	3.3709	2.5427	1.9039	18.1974	19.9892	3.3580
28	1.1951	4.2662	0.5561	2.0033	1.0189	3.0640	10.2646	13.6351	3.3378
29	0.4330	3.5392	0.4321	1.4915	0.7810	2.2477	8.6253	12.9653	1.7949
30	2.3955	3.5651	0.7521	1.9504	1.2940	3.2176	5.1710	9.8090	1.4212
31	0.8139	3.6334	0.6020	2.6702	2.1556	2.1148	9.7981	13.2877	2.2251
32	1.5639	4.5793	0.5898	2.2625	1.6946	2.6669	13.5146	15.7897	2.7949
33	0.8677	4.8290	0.7079	2.0955	1.4841	3.1693	9.6714	14.6599	2.7325
34	0.9785	4.9964	0.8246	2.6051	1.4933	4.4465	10.2500	12.7287	2.0935
35	0.5519	4.0661	0.5396	2.2392	1.1421	2.4660	10.9568	12.8245	2.5884
36	0.4884	3.3564	0.4629	2.0723	2.2374	1.0260	12.6672	17.0313	2.2655
37	0.5977	4.1954	0.4652	2.1335	1.4856	1.8999	12.8084	14.7728	1.7152
38	0.6078	4.7195	0.6484	1.9451	1.0853	3.1984	10.8573	13.3436	2.0207
39	0.6934	6.1495	0.7511	2.9069	1.9587	5.4699	13.6390	16.6838	2.0447
40	0.6870	5.1122	0.6214	2.5685	1.4710	3.2146	11.2552	12.8992	2.3869
41	1.1781	4.9375	0.7657	1.9237	0.9830	4.5309	9.9621	13.0663	2.3916
42	0.7656	5.4614	0.6977	2.4884	1.7144	3.6305	12.7185	13.1104	4.7045
43	5.1508	3.0536	0.4612	1.7742	2.3312	1.6608	9.1044	10.1143	0.4450
44	0.8349	4.1305	0.6492	2.2643	2.2469	3.3530	10.4302	11.5939	1.6971
45	0.5916	4.4485	0.7000	3.2854	2.9196	0.0000	22.4423	23.6231	6.0015
46	0.5934	2.3804	0.4420	1.0079	0.6665	1.7282	5.4741	7.8809	0.9966
47	0.9811	7.6606	1.0529	2.9364	1.4657	5.9611	17.2135	16.2282	3.7555
48	0.6919	5.3114	0.6770	2.9674	1.9514	2.7671	14.8315	13.3398	1.8851
49	0.9064	5.7858	0.7982	3.7103	3.3422	2.1991	24.3093	22.9181	5.0594
50	0.8613	5.9751	0.8304	3.4326	2.2419	2.6743	24.5014	22.1739	5.6461
51	1.5001	7.1275	1.3016	3.5002	2.9765	4.9331	19.6468	18.9522	4.5448
52	0.3972	4.0390	0.2993	2.1493	2.2275	1.6420	19.5601	17.1296	2.8022
53	0.7739	6.0696	0.8537	3.9630	3.7473	1.4589	26.4794	23.0023	6.2324
54	0.8230	6.2952	0.7387	3.2444	2.1007	3.5080	17.7436	17.1508	4.0888
55	0.6913	6.6705	0.6392	2.3117	1.6616	6.2170	18.2523	15.3365	4.3794
56	0.7833	5.5845	0.7632	3.2907	2.7780	3.3811	22.6741	19.5367	6.1956
57	2.9408	4.0191	0.7340	1.2848	0.7641	3.6526	4.4491	9.7584	1.2363
58	0.8724	5.1929	0.8934	3.5729	3.0577	3.3331	16.4376	19.4758	5.3093
59	1.0098	2.9089	0.3911	1.4565	1.1549	1.6379	6.5375	9.7325	1.7475
60	1.8802	4.3939	0.6187	2.1251	1.3799	3.1622	8.1497	12.2144	2.1378
61	0.6746	3.0374	0.5039	1.1602	0.7287	2.4244	6.5249	7.5616	1.4657

62	1.2282	3.2261	0.3602	1.3899	1.0402	2.5323	5.9887	9.2390	1.2462
63	1.1671	4.0773	0.9956	2.3910	1.6026	2.2288	11.8693	9.4105	3.0072
64	0.8716	3.0058	0.3732	1.2506	0.6551	2.2520	7.0086	8.6464	1.7624
65	1.4664	5.9553	0.8851	3.0731	1.9290	3.0401	16.6178	17.4253	3.2712
66	0.4155	2.7129	0.3580	1.0907	0.9293	2.1263	5.4103	8.4434	0.8201
67	0.7388	6.3854	0.7102	2.9530	1.7988	4.2671	17.3117	18.2511	2.8636
68	0.4865	1.6401	0.3117	0.6886	0.3233	1.5088	3.9754	4.8035	1.1074
69	0.5930	4.4319	0.5468	2.3495	1.7171	3.2360	11.6129	12.4607	1.7920
70	0.7430	5.2616	0.5460	2.6204	1.4519	3.1350	16.2315	17.8097	1.7217
71	0.4883	3.7527	0.4079	1.8593	1.3171	2.1649	10.5771	12.6049	2.5390
72	0.7653	5.0342	0.6916	2.4471	1.7512	3.1950	14.1441	14.8117	2.6779
73	1.4035	3.8599	0.5783	1.7523	1.2394	2.4210	8.5165	12.1122	1.8232
74	0.3846	2.1902	0.4146	0.7701	0.3732	1.6981	6.3697	9.2985	0.4679
75	0.7385	4.2009	0.7531	2.0868	1.3213	2.1937	11.5892	15.1582	2.6999
76	0.7359	5.9656	0.4109	2.0094	0.5254	6.3150	9.7482	9.8887	3.4813
77	0.3776	3.6548	0.4416	1.4770	0.5028	3.8559	4.3750	7.1215	3.6482
78	0.7003	5.7301	0.7028	3.0534	1.8419	4.5155	19.1566	15.7565	2.0156
79	0.4805	2.8528	0.4596	1.7552	0.6159	1.8010	10.0959	10.8574	3.3373
80	0.3290	3.0473	0.3405	1.3381	0.9109	1.4802	8.6130	9.6944	1.6873
81	0.9216	1.9525	0.3233	1.0203	0.9261	1.3925	5.8216	10.1735	1.0934
82	0.5546	3.5129	0.6223	2.0774	1.1388	2.1469	10.5076	13.0998	2.5408
83	1.7412	4.7572	0.7178	2.3047	1.3087	3.0818	11.2322	12.0947	2.7173
84	0.7078	4.6260	0.6018	2.1802	1.4538	2.1152	12.7995	13.6753	3.2565
85	0.9761	5.3846	0.9121	2.5282	1.5843	2.6421	20.3804	16.9197	3.6811
86	0.4984	2.9368	0.4674	1.8748	1.0595	1.5780	8.9907	9.7476	2.3928
87	1.1307	4.0736	0.9023	1.7742	0.9760	3.6102	8.2387	10.8573	1.6476
88	0.6383	2.7753	0.3655	1.2944	1.1004	1.8445	6.5271	9.2677	1.0160
89	0.3089	3.9911	0.4582	1.1222	0.4421	3.4288	6.8041	7.8254	0.8455
90	0.9196	5.5663	0.8779	2.9682	1.4563	5.6468	12.7165	10.7738	2.3468
91	0.7319	2.0478	0.3319	1.3271	0.7738	1.5615	4.2419	10.4678	1.4617
92	0.7499	3.0717	0.6477	1.7610	1.2867	1.4838	9.5144	8.4111	2.5640
93	0.6924	6.2204	0.8359	2.2511	1.0501	5.9803	11.2019	8.5379	2.5079
94	0.8624	5.2489	0.8048	2.5357	1.2518	3.9238	12.0070	14.9451	2.8721
95	1.8964	3.4598	0.6421	1.8000	0.8955	2.6851	8.0037	10.7645	3.1116
96	1.9635	6.1849	1.2541	2.6361	3.6381	3.7408	15.8929	14.2708	1.8469
97	0.6749	2.7288	0.3900	1.3402	0.5344	1.3481	8.6736	10.1631	2.0565
98	0.6701	3.6737	0.6083	1.9123	1.3384	2.9634	8.1539	24.4582	3.0072
99	0.5905	3.1536	0.4703	0.9927	0.6223	2.7126	5.6868	7.6505	0.9642
100	0.6940	4.3448	0.5395	1.7107	1.0782	3.1981	10.6561	10.9843	2.0839
101	0.5918	3.6953	0.5125	1.3463	0.8251	2.4619	8.3673	11.2739	1.6386
102	0.8187	3.8103	0.5921	1.7678	1.3413	2.2278	10.8730	13.2488	2.4653
103	0.4627	1.6038	0.3502	0.9118	0.4496	0.5165	5.9926	8.2142	1.5129
104	0.3668	2.9223	0.3592	1.5283	0.6610	1.2788	8.6825	9.7011	2.1519
105	0.6112	4.6429	0.6197	2.3445	1.0972	2.5301	12.4243	13.1776	4.1080
106	0.2702	2.6124	0.3229	1.2630	0.8122	1.2452	7.9279	11.0023	1.5993
107	0.7655	2.9465	0.6142	1.3157	0.8546	2.3129	9.3074	6.0007	1.8149
108	0.9989	4.4869	0.9430	2.0450	1.5326	3.1209	12.3171	13.8210	2.5687

109	0.5128	5.8194	0.4967	1.9990	0.3572	5.5664	8.9167	9.5729	2.3895
110	0.6927	5.9149	0.7156	3.5258	2.5914	2.5687	21.8379	20.4852	5.0583
111	0.7256	5.1692	0.6795	2.0261	1.0292	4.5819	9.0432	11.2907	3.5670
112	1.0160	3.3301	0.4858	1.3613	0.6191	2.5371	7.1254	9.6119	1.3916
113	1.1404	6.9691	0.9788	3.1263	1.6375	5.3573	17.9154	16.6834	2.9859
114	0.6669	2.7835	0.5695	1.8634	2.6765	0.9890	7.8641	10.0369	1.4241
115	0.6669	2.7835	0.5695	1.8634	2.6765	0.9890	7.8641	10.0369	1.4241
116	0.8008	4.2312	0.7292	2.3683	2.0098	2.4649	11.7454	14.4906	2.9060
117	1.3346	2.0427	0.3110	0.8051	0.3776	1.4920	4.0403	5.4671	1.4263
118	0.1707	0.7702	0.2384	0.6275	0.5562	0.1570	2.7531	3.8920	0.7925
119	1.0274	5.1980	0.9574	3.0429	2.0416	2.9524	15.6404	19.3963	3.4626
120	1.0071	5.2845	0.8388	2.6140	1.9765	3.5942	11.5004	14.2650	3.5576
121	0.9641	4.4214	0.8484	3.2627	2.4222	1.4919	16.3686	20.7950	3.9966
122	0.5924	2.6008	0.4948	1.5426	1.2894	1.6394	8.1598	6.0825	3.1537
123	0.9399	5.0578	0.6946	2.2345	0.7347	3.7339	10.9129	9.5417	2.9610
124	0.9471	5.7177	0.8197	2.1486	1.1914	4.9548	9.8391	11.7000	4.4961
125	0.7839	4.1740	0.5002	1.9516	0.8636	3.0860	9.9996	10.1731	2.7429
126	0.6228	5.9803	0.5674	3.3464	1.5761	4.8900	10.8907	11.8480	1.8417
127	0.5009	4.6246	0.5002	1.7986	0.7887	3.4432	11.4172	12.3007	2.1931
128	0.6791	6.1219	0.6127	3.6793	2.7237	2.9354	22.3216	25.7554	4.4897
129	0.8770	4.3915	0.6106	2.1682	1.3482	3.0537	11.4224	11.8260	3.4229
130	0.5437	5.4858	0.5651	2.2774	1.0594	5.3505	9.8912	11.5386	2.1005
131	0.4742	2.8849	0.3390	1.3849	1.2258	2.2396	8.6000	10.4385	1.8888
132	0.5448	2.4376	0.3362	1.0017	0.8235	2.3441	4.8856	6.1257	0.8113
133	0.7206	2.9181	0.6099	1.4530	1.0132	1.1908	6.9525	9.7148	1.4669
134	0.5570	4.5868	0.6450	1.7555	1.2175	3.8647	8.1368	11.6458	1.5967
135	0.8778	5.0708	0.8778	3.0527	1.7198	3.2624	17.9502	16.3969	4.1595
136	0.4286	2.9266	0.4399	0.9563	0.4672	2.7686	5.1030	10.7264	1.7450
137	1.5104	2.8082	0.3739	1.7942	1.4660	1.7104	6.2452	14.2197	1.2148
138	0.7979	5.8790	0.9343	2.5846	1.6155	4.3638	10.1335	10.3574	2.9049
139	0.5177	3.3298	0.4843	2.0040	1.5020	1.1596	10.5161	11.9300	2.1102
140	0.9394	5.1857	0.5691	2.3660	1.2811	3.7367	14.4164	13.6176	2.5827
141	0.5344	3.2520	0.4354	1.8440	1.1598	1.5823	10.0576	13.1441	1.7679
142	0.6721	3.7736	0.6237	1.8936	1.4776	2.0583	11.8497	14.3454	2.3371
143	0.6610	5.3986	0.4329	2.1841	1.1413	3.9493	13.2749	15.4439	2.9458
144	0.6144	4.7780	0.6031	3.2559	2.5049	1.8674	17.7929	19.8430	4.1279
145	0.4066	3.6312	0.4280	1.6082	0.9659	2.6047	8.5756	12.3321	2.2493
146	0.6268	4.0506	0.6101	2.0575	1.5382	2.3871	11.8575	14.4562	3.5936
147	0.6344	6.1762	0.6022	3.2957	1.7153	4.0142	18.1177	20.7751	4.1848
148	1.1952	2.2867	0.3247	0.8807	0.6456	1.3009	4.0007	5.4225	1.0025
149	1.1404	6.9691	0.9788	3.1263	1.6375	5.3573	17.9154	16.6834	2.9859
150	0.5403	4.1283	0.4432	2.4296	1.6489	2.0153	16.0467	15.1192	2.0914

Table A.2: Table RMSE of 150 images for DST method and NLV method

B

Software Implementation

B.1/ Blurring image

```
function [ im1,im2 ] = blur_image( imr,s,v )
%input image: imr (reference image), v (variance of Gaussian filter),
%s(size of Gaussian filter)
%output: 2 blurred images (im1 and im2)

[rows, columns] = size(imr);
midColumn = ceil(columns/2);
leftHalf = imr(:, 1:midColumn);
rightHalf = imr(:, midColumn+1:end);

[x,y]=meshgrid(-s:1:s);

r=((x).^2+(y).^2).^(0.5);
ga=v/2;

t=exp(-r.^2/(4*ga))/(4*pi*ga);
tg=t/sum(sum(t));

blurryLeft = imfilter(leftHalf, tg,'replicate');
blurryRight = imfilter(rightHalf, tg,'replicate');


D1={leftHalf, blurryRight};
im1=cell2mat(D1);
figure,imshow(im1),title('blurry right')

G1={blurryLeft,rightHalf};
im2=cell2mat(G1);
figure,imshow(im2),title('blurry left')

end
```

B.2/ Laplacian Pyramid image fusion

B.2.1/ REDUCE function

```
%function reduce for the gaussian pyramid
%filter image and subsample

function [g1] = reduce(g0,w)

[C,R]=size(g0);
g1=[];
%use kernel filter with weight w
for I=2:(C+1)/2-1
   for J=2:(R+1)/2-1
      g1(I,J)=sum(sum(w.*g0(2*I-3:2*I+1,2*J-3:2*J+1)));
   end
end


%compute 4 edges of the output image
wtemp=w(:,3:5);
for I=2:(C-1)/2
   g1(I,1)=sum(sum(wtemp.*g0(2*I-3:2*I+1,1:3)));
end

wtemp=w(:,1:3);
for I=2:(C-1)/2
   g1(I,(R+1)/2)=sum(sum(wtemp.*g0(2*I-3:2*I+1,R-2:R)));
end

wtemp=w(3:5,:);
for I=2:(R-1)/2
   g1(1,I)=sum(sum(wtemp.*g0(1:3,2*I-3:2*I+1)));
end

wtemp=w(1:3,:);
for I=2:(R-1)/2
   g1((C+1)/2,I)=sum(sum(wtemp.*g0(C-2:C,2*I-3:2*I+1)));
end

%compute 4 corners of the output image
wtemp=w(3:5,3:5);
g1(1,1)=sum(sum(wtemp.*g0(1:3,1:3)));
wtemp=w(1:3,3:5);
g1((C+1)/2,1)=sum(sum(wtemp.*g0(C-2:C,1:3)));
wtemp=w(3:5,1:3);
g1(1,(R+1)/2)=sum(sum(wtemp.*g0(1:3,R-2:R)));
wtemp=w(1:3,1:3);
g1((C+1)/2,(R+1)/2)=sum(sum(wtemp.*g0(C-2:C,R-2:R)));
```

B.2.2/ EXPAND FUNCTION

```
function[gl1]=expand(gl0,w)
[C,R]=size(gl0);
gl1=zeros(2*C-1,2*R-1);

%interpolation
gl1(2:2:2*C-2,2:2:2*R-2)=4*(gl0(1:C-1,1:R-1)*w(4,4)+gl0(2:C,1:R-1)*w(2,4)+
gl0(1:C-1,2:R)*w(4,2)+gl0(2:C,2:R)*w(2,2));

gl1(3:2:2*C-3,2:2:2*R-2)=4*(gl0(1:C-2,1:R-1)*w(5,4)+gl0(2:C-1,1:R-1)*w(3,4)+
gl0(3:C,1:R-1)*w(1,4)+gl0(1:C-2,2:R)*w(5,2)+gl0(2:C-1,2:R)*w(3,2)+gl0(3:C,2:R)*w(1,2));

gl1(2:2:2*C-2,3:2:2*R-3)=4*(gl0(1:C-1,1:R-2)*w(4,5)+gl0(1:C-1,2:R-1)*w(4,3)+
gl0(1:C-1,3:R)*w(4,1)+gl0(2:C,1:R-2)*w(2,5)+gl0(2:C,2:R-1)*w(2,3)+gl0(2:C,3:R)*w(2,1));

gl1(3:2:2*C-3,3:2:2*R-3)=4*(gl0(1:C-2,1:R-2)*w(5,5)+gl0(2:C-1,1:R-2)*w(3,5)+
gl0(3:C,1:R-2)*w(1,5)+gl0(1:C-2,2:R-1)*w(5,3)+gl0(2:C-1,2:R-1)*w(3,3)+
gl0(3:C,2:R-1)*w(1,3)+gl0(1:C-2,3:R)*w(5,1)+gl0(2:C-1,3:R)*w(3,1)+gl0(3:C,3:R)*w(1,1));

%compute edges
temp=w(5,3)+w(5,1)+w(3,3)+w(3,1)+w(1,3)+w(1,1);
gl1(3:2:2*C-3,1)=(gl0(1:C-2,1)*w(5,3)+gl0(1:C-2,2)*w(5,1)+gl0(2:C-1,1)*w(3,3)+
gl0(2:C-1,2)*w(3,1)+gl0(3:C,1)*w(1,3)+gl0(3:C,2)*w(1,1));

temp=w(5,3)+w(5,5)+w(3,3)+w(3,5)+w(1,3)+w(1,5);
gl1(3:2:2*C-3,2*R-1)=(gl0(1:C-2,R)*w(5,3)+gl0(1:C-2,R-1)*w(5,5)+gl0(2:C-1,R)*w(3,3)+
gl0(2:C-1,R-1)*w(3,5)+gl0(3:C,R)*w(1,3)+gl0(3:C,R-1)*w(1,5));

temp=w(4,3)+w(4,1)+w(2,3)+w(2,1);
gl1(2:2:2*C-2,1)=(gl0(1:C-1,1)*w(4,3)+gl0(1:C-1,2)*w(4,1)+
gl0(2:C,1)*w(2,3)+gl0(2:C,2)*w(2,1));

temp=w(4,3)+w(4,5)+w(2,3)+w(2,5);
gl1(2:2:2*C-2,2*R-1)=(gl0(1:C-1,R)*w(4,3)+gl0(1:C-1,R-1)*w(4,5)+
gl0(2:C,R)*w(2,3)+gl0(2:C,R-1)*w(2,5));

```

```
36 temp=w(3,5)+w(1,5)+w(3,3)+w(1,3)+w(3,1)+w(1,1);
37 gl1(1,3:2:2*R-3)=(gl0(1,1:R-2)*w(3,5)+gl0(2,1:R-2)*w(1,5)+gl0(1,2:R-1)*w(3,3)+
38 gl0(2,2:R-1)*w(1,3)+gl0(1,3:R)*w(3,1)+gl0(2,3:R)*w(1,1));
39
40 temp=w(3,5)+w(5,5)+w(3,3)+w(5,3)+w(3,1)+w(5,1);
41 gl1(2*C-1,3:2:2*R-3)=(gl0(C,1:R-2)*w(3,5)+gl0(C-1,1:R-2)*w(5,5)+gl0(C,2:R-1)*w(3,3)+
42 gl0(C-1,2:R-1)*w(5,3)+gl0(C,3:R)*w(3,1)+gl0(C-1,3:R)*w(5,1));
43
44 temp=w(3,4)+w(1,4)+w(3,2)+w(1,2);
45 gl1(1,2:2:2*R-2)=(gl0(1,1:R-1)*w(3,4)+gl0(2,1:R-1)*w(1,4)+gl0(1,2:R)*w(3,2)+gl0(2,2:R)*w(1,2));
46
47 temp=w(3,4)+w(5,4)+w(3,2)+w(5,2);
48 gl1(2*C-1,2:2:2*R-2)=(gl0(C,1:R-1)*w(3,4)+gl0(C-1,1:R-1)*w(5,4)+gl0(C,2:R)*w(3,2)+gl0(C-1,2:R)*w(5,2));
49
50 %compute corners
51 temp=w(3,3)+w(3,1)+w(1,3)+w(1,1);
52 gl1(1,1)=(gl0(1,1)*w(3,3)+gl0(1,2)*w(3,1)+gl0(2,1)*w(1,3)+gl0(2,2)*w(1,1));
53
54 temp=w(3,3)+w(5,3)+w(3,1)+w(5,1);
55 gl1(2*C-1,1)=(gl0(C,1)*w(3,3)+gl0(C-1,1)*w(5,3)+gl0(C,2)*w(3,1)+gl0(C-1,2)*w(5,1));
56
57 temp=w(3,3)+w(3,5)+w(1,3)+w(1,5);
58 gl1(1,2*R-1)=(gl0(1,R)*w(3,3)+gl0(1,R-1)*w(3,5)+gl0(2,R)*w(1,3)+gl0(2,R-1)*w(1,5));
59
60 temp=w(3,3)+w(5,3)+w(3,5)+w(5,5);
61 gl1(2*C-1,2*R-1)=(gl0(C,R)*w(3,3)+gl0(C-1,R)*w(5,3)+gl0(C,R-1)*w(3,5)+gl0(C-1,R-1)*w(5,5));
```

B.2.3/ LP(DWT)

```
function [ f ] = fusion_laplacianwavelet( im1,im2 )
%image fusion using Laplacian wavelet
g=double(im1);h=double(im2);
imagesize1=size(g);
imagesize2=size(h);

p=0.3;
t1 = [1/4-p/2; 1/4; p; 1/4; 1/4-p/2];
t=t1*t1';
g=[g(1,1) g(1,1:imagesize1(2));g(1:imagesize1(1),1) g]; %resize the image
g=double(g);
h=[h(1,1) h(1,1:imagesize2(2));h(1:imagesize2(1),1) h]; %resize the image
h=double(h);

%-------------generate the next 3 levels of Gaussian pyramid---------------
g1=reduce(g,t);
h1=reduce(h,t);

g2=reduce(g1,t);
h2=reduce(h1,t);

g3=reduce(g2,t);
h3=reduce(h2,t);

g4=reduce(g3,t);
h4=reduce(h3,t);
%---------------interpolate images in the Gaussian pyramid-----------------
g11=expand(g1,t);
h11=expand(h1,t);

g21=expand1(g2,t);
h21=expand1(h2,t);

g31=expand(g3,t);
h31=expand(h3,t);

g41=expand(g4,t);
h41=expand(h4,t);

%--------------------generate the Laplacian pyramid------------------------
Lg0=g-g11;
Lh0=h-h11;

Lg1=g1-g21;
Lh1=h1-h21;

Lg2=g2-g31;
Lh2=h2-h31;

Lg3=g3-g41;
Lh3=h3-h41;

%-------------------------------LP ...
    DWT--------------------------------------
fw3=wfusimg(g3,h3,'haar',5,'mean','max');
fw2=wfusimg(Lg2,Lh2,'haar',5,'mean','max');
fw1=wfusimg(Lg1,Lh1,'haar',5,'mean','max');
```

```
57 fw0=wfusimg(Lg0,Lh0,'haar',5,'mean','max');
58
59 %----------------------Reconstruction LP DWT-------------------------------
60 rfw2=fw2+expand1(fw3,t);
61 rfw1=fw1+expand1(rfw2,t);
62 rfw0=fw0+expand1(rfw1,t);
63 f=rfw0;
64 end
```

B.3/ LOCAL VARIABILITY

```
function d1=local_variability (im1,a)
%input: im1 (image),  a (size of neighborhood)
%output: d1 (local variability)

image1=double(im1);

S=size(image1);
for i=a+1:S(1)-a
  for j=a+1:S(2)-a
  d1(i,j)=sqrt((sum(sum((image1(i,j)-image1(i-a:i+a,j-a:j+a)).^2))./ ((2*a+1).^2-1));
  end
end

for k=1:a
for j=a+1:S(2)-a
d1(k,j)=sqrt((sum(sum((image1(k,j)-image1(1:a+k,j-a:j+a)).^2)))/((a+k)*(2*a+1)-1));
d1(S(1)-k+1,j)=sqrt((sum(sum((image1( S(1)-k+1,j)-image1(S(1)-k+1-a:S(1),j-a:j+a)).^2)))/((a+k)*(2*a+1)-1)) ;
end
end

for k=1:a
d1(k,a)=sqrt((sum(sum((image1(k,a)-image1(1:k+a,1:a+a)).^2)))/((k+a)*2*a-1));
end

for k=1:a
d1(a,k)=sqrt((sum(sum((image1(a,k)-image1(1:a+a,1:k+a)).^2)))/((k+a)*2*a-1));
end

for k=1:a
    for j=S(2)-a+1:S(2)
d1(k,j)=sqrt((sum(sum((image1(k,j)-image1(1:k+a,j-a:S(2))).^2)))/((k+a)*(S(2)-j+a+1)-1));
    end
end

d1(1,1)=sqrt (sum(sum((image1(1,1)-image1(1:a+1,1:a+1)).^2)))/ (   (a+1)^2-1));
d1(S(1),1)=sqrt((sum(sum((image1(S(1),1)-image1(S(1)-a:S(1),1:a+1)).^2)))/  ((a+1)^2-1));
d1(S(1),S(2))=sqrt((sum(sum((image1(S(1),S(2))-image1(S(1)-a:S(1),S(2)-a:S(2))).^2)))/  ( (a+1)^2-1));

```

```
for l=1:a
for i=a+1:S(1)-a
d1(i,S(2)-l+1)=sqrt( (sum(sum((image1(i,S(2)-l+1)-image1(i-a:i+a,S(2)-l+1-a:S(2))).^2)))/ (  (2*a+1)*(l+a)-1));
d1(i,l)=sqrt  ( (sum(sum((image1(i,l)-image1(i-a:i+a,1:l+a)).^2)))/ ((2*a+1)*(a+l)-1 ));
end
end


for k=1:a
d1(k,a)=sqrt((sum(sum((image1(k,a)-image1(1:k+a,1:a+a)).^2)))/((k+a)*2*a-1));
end

for k=S(1)-a+1:S(1)
    for j=S(2)-a+1:S(2)
d1(k,j)=sqrt((sum(sum((image1(k,j)-image1(k-a:S(1),j-a:S(2))).^2)))/((S(1)-k+a+1)*(S(2)-j+a+1)-1));
    end
end

for k=1:a
    for i=S(1)-a+1:S(2)
d1(i,k)=sqrt((sum(sum((image1(i,k)-image1(i-a:S(1),1:k+a)).^2)))/((S(1)-i+a+1)*(k+a)-1));
    end
end
```

B.4/ MULTI-FOCUS IMAGE FUSION USING DST BASED ON LOCAL VARIABILITY

```
function [f_dst ] = fusion_dst( image1, image2,a )
%UNTITLED4 Summary of this function goes here
%   Detailed explanation goes here

image1=double(image1);
image2=double(image2);

S=size(image1);
d1=local_variability(image1,a);
d2=local_variability(image2,a);


%d=abs(d1-d2);
%image 1
d1max=max(max(d1));
d1min=min(min(d1));
md1=1-((d1-d1min)/(d1max-d1min));
mean_md1=mean(mean(md1));
std_md1=sum(sum((mean_md1-md1).^2))/(S(1)*S(2)-1);
m1ac1=md1.*(1-std_md1);
m1ac3=std_md1*ones([S(1) S(2)]);
m1ac2=1-m1ac1-m1ac3;

%image 2
d2max=max(max(d2));
d2min=min(min(d2));
md2=1-((d2-d1min)/(d2max-d2min));
mean_md2=mean(mean(md2));
std_md2=sum(sum((mean_md2-md2).^2))/(S(1)*S(2)-1);
m1bc1=md2.*(1-std_md2);
m1bc3=std_md2*ones([S(1) S(2)]);
m1bc2=1-m1bc1-m1bc3;

pls1=m1ac1+m1ac3;
pls2=m1bc1+m1bc3;

for i=1:S(1)
    for j=1:S(2)
        if pls1(i,j)<pls2(i,j);
                f_dst(i,j)=image1(i,j);
  elseif pls1(i,j)>pls2(i,j);
          f_dst(i,j)=image2(i,j);
  elseif pls1(i,j)==pls2(i,j);
          f_dst(i,j)=(image1(i,j)+image2(i,j))/2;
  end
end
end
end
```

```
function[y] = rmse_dst(imr,im1,im2,a)

imf=fusion_dst(im1,im2,a);
imr=double(imr);
```

```
imf=double(imf);
D=sum(sum((imr-imf).^2))/length(imr(:));
RMSE=D.^2;
y=RMSE;
```

```
for a=1:10
y(a)=rmse_dst(imr,im1,im2,a);
end

[rmse_min,a_min]=min(y)

%final fused image of DST-LV: F
F=fusion_dst(imr,im1,im2,a_min)
```

B.5/ MULTI-FOCUS IMAGE FUSION USING NLV

```
%Model of size of neighborhood (a)
function [a] = size_neighborhood( v,s )
%v = variance of blurring filter, s = size of blurring filter
a=(3.0384761/(1+29.0909139*exp(-0.5324955*s)))*log(v)+
0.434*(-75.062269/(-1.225175*s))*
exp(-0.5*((log(s)-2.655551)/-1.22175)^2);
end

%Multi-focus image fusion using NLV
function [ f ] = fusion_NLV( im1,im2,a )
%image fusion using neighborhood local variability
im1=double(im1);
im2=double(im2);

S=size(im1);
d1=local_variability(im1,a);
d2=local_variability(im2,a);

for i=1:S(1)
    for j=1:S(2)
f(i,j)=(exp(d1(i,j)).*im1(i,j)+exp(d2(i,j)).*im2(i,j))./
(exp(d1(i,j))+exp(d2(i,j)));
 end
end
end
```

Document generated with LaTeX and:
the LaTeX style for PhD Thesis created by S. Galland — http://www.multiagent.fr/ThesisStyle
the tex-upmethodology package suite — http://www.arakhne.org/tex-upmethodology/

Abstract:

In this thesis, we are interested in the multi-focus image fusion method. This technique consists of fusing several captured images with different focal lengths of the same scene to obtain an image with better quality than the two source images. We propose an image fusion method based on Laplacian pyramid technique using Discrete Wavelet Transform (DWT) as a selection rule. We then develop two multi-focus image fusion methods based on the local variability of each pixel. It takes into account the information in the surrounding pixel area. The first method is to use local variability as an information in the Dempster-Shafer theory. The second method uses a metric based on local variability. Indeed, the proposed fusion method weighs each pixel by an exponential of its local variability. A comparative study between the proposed methods and the existing methods was carried out. The experimental results show that our proposed methods give better fusions, both in visual perception and in quantitative analysis.

Keywords: Multi-focus image fusion, Laplacian pyramid, Discrete Wavelet Transform, Local variability, Dempster-Shafer theory

Résumé :

Dans cette thèse, nous nous intéressons aux méthodes de la fusion d'images multi focales. Cette technique consiste à fusionner plusieurs images capturées avec différentes distances focales de la même scène. Cela permet d'obtenir une image de meilleure qualité à partir des deux images sources. Nous proposons une méthode de fusion d'images s'appuyant sur les techniques des pyramides Laplaciennes en utilisant comme règle de sélection les transformées d'ondelettes discretes(DWT: Discrete Wavelet Transform). Nous développons, par la suite, deux méthodes de fusion d'images multi focales basée sur la variabilité locale de chaque pixel. Elle tient en compte les informations dans la région environnante des pixels. La première consiste à utiliser la variabilité locale comme information dans la méthode de Dempster-Shafer. La seconde utilise une métrique basée sur la variabilité locale. En effet, la fusion proposée effectue une pondération de chaque pixel par une exponentielle de sa variabilité locale. Une étude comparative entre les méthodes proposées et celles existantes a été réalisée. Les résultats expérimentaux démontrent que nos méthodes proposées donnent des meilleurs fusions, tant dans la perception visuelle que dans l'analyse quantitative.

Mots-clés : la fusion d'images multi focus, les pyramidales Laplaciennes, la transformée en ondelettes discrète, la variabilité locale, la théorie de Dempster-Shafer

SPIM

■ École doctorale SPIM - Université de Bourgogne/UFR ST BP 47870 F - 21078 Dijon cedex
■ tél. +33 (0)3 80 39 59 10 ■ ed-spim@univ-fcomte.fr ■ www.ed-spim.univ-fcomte.fr

UNIVERSITÉ DE BOURGOGNE